ALMA MATER STUDIORUM
UNIVERSITÀ DI BOLOGNA

DOTTORATO DI RICERCA IN

# Scienze Biotecnologiche, Biocomputazionali, Farmaceutiche e Farmacologiche

Ciclo XXXVI

**Settore Concorsuale: 05/E1- BIOCHIMICA GENERALE**

**Settore Scientifico Disciplinare: BIO/10**

# AN IN VITRO CHARACTERIZATION OF THE BIOENERGETIC EFFECTS OF A PHYTOSOME-BASED COENZYME Q10 FORMULATION AS A POTENTIAL TREATMENT FOR TROYER SYNDROME

**Presentata da:** ***Nicola Rizzardi***

**Coordinatore Dottorato**

Chiar.ma Prof.ssa
Maria Laura Bolognesi

**Supervisore**

Chiar.ma Prof.ssa
Romana Fato

**Co-supervisore**

Chiar.mo Prof.
Christian Bergamini

Esame finale anno 2024

# TABLE OF CONTENTS


**1. Introduction** ..... 1

*1.1. Coenzyme Q10 biosynthesis* ..... 1

*1.2. Coenzyme Q10 functions* ..... 6

*1.3. Coenzyme Q10 involvement in aging and diseases* ..... 10

*1.3.1. Primary CoQ10 deficiencies* ..... 11

*1.3.2. Secondary CoQ10 deficiencies* ..... 11

*1.4. Strategies on CoQ10 delivery* ..... 12

*1.5. Hereditary Spastic Paraplegia (HSP)* ..... 14

1.6. *Troyer Syndrome* ..... 15

**2. Aims** ..... 17

*2.1. Bioenergetics and delivery characterization of a new formulation of Coenzyme Q10* ..... 17

*2.2. Bioenergetics characterization and UBQ treatment efficiency on fibroblasts derived from a patient affected by Troyer Syndrome* ..... 18

**3. Material and methods** ..... 20

*3.1. Subject* ..... 20

*3.2. Next Generation Sequence analysis* ..... 20

*3.3. Cell lines culture and treatment* ..... 21

3.4. *CoQ10 determination* ..... 21

3.5. *Oxygen consumption rate* ..... 22

*3.6. Intracellular NAD(P)H Determination* ..... 23

*3.7. Nucleotides determination* ..... 24

*3.8. Radical oxygen species measurement* ..... 24

*3.9. Mitochondrial membrane potential assessment* ..... 25

3.10. *Mitochondrial respiratory chain enzymes activity* ..... 26

3.11. *Lipid droplets quantification* ..... 27

3.12. *Lipid peroxidation measurement* ..... 27

*3.13. Ferroptosis assay* ..... 28

*3.14. Coenzyme Q10 Internalization Assay* ..... 28

*3.15. Western Blot analysis* ..... 29

*3.16. Assessment of Mitochondrial Network and Morphology* ..... 30

*3.17. Mitochondrial Mass Determination* ..... 31

*3.18. Cell Proliferation assay* ..... 31

*3.19. Measurement of Intracellular Free Calcium levels* ..... 31

*3.20. Glutathione quantification* ..... 32
*3.21. Mitochondrial protein import assessment* ..... 32
*3.22. Blue Native Polyacrylamide Gel Electrophoresis (BN-PAGE) assay* ..... 33
*3.23. RNA sequencing* ..... 34
*3.24. qPCR* ..... 34
*3.25. Rescue experiments* ..... 35
**4. Results** ..... 37
*4.1. UBQ® supplementation significantly increases the endogenous CoQ10 levels in both I407 and H9c2 cell lines.* ..... 37
*4.2. Supplementation with UBQ® improves Oxygen Consumption Rate, ATP and NADH level, protein content, transmembrane potential, and citrate synthase activity* ..... 39
*4.3. CoQ10 Phytosome formulation protects against Oxidative Stress* ..... 43
*4.4. UBQ® counteracts the lipid membrane peroxidation and Ferroptosis* ..... 45
*4.5. The CoQ10 phytosome formulation uptake is promoted by micropinocytosis process* ..... 47
*4.6. Exome Sequence (ES) analysis identified a new biallelic variants in Spartin in a 5-years old patient* ..... 49
*4.7. Biallelic variants in Spartin affect the cell growth and mitochondrial functionality* ..... 51
*4.8. The mitochondria-associated membranes integrity is impaired in patient's fibroblasts and* $SY^{c.892dupA}$ *carrying a mutation in Spartin resulting in altered calcium levels and a compromised mitochondrial protein import* ..... 56
*4.9. Spartin mutations affect mitochondrial respiratory chain enzymes expression and assembly* ..... 61
*4.10. Loss of function mutation in Spartin affects the transcription of several nuclear and mitochondrial genes* ..... 65
*4.11. Impaired mitochondrial protein import leads to a diminished CoQ10 amount in e19 and* $SY^{c.892dupA}$ *cells* ..... 72
*4.12. Wild Type Spartin protein expression restored the impaired bioenergetic parameters in patient's fibroblasts and* $SY^{C.892dupA}$ ..... 73
**5. Discussion** ..... 78
*5.1. Enhanced Coenzyme Q10 Bioavailability and improved mitochondrial functionality in cultured cells through CoQ10 phytosome formulation* ..... 78
*5.2. Mutations in Spartin affect mitochondrial protein import process leading to altered bioenergetics reversed by UBQ®* ..... 83
**6. Conclusions** ..... 89
**7. Bibliography** ..... 90

# 1. Introduction

## *1.1. Coenzyme Q10 biosynthesis*

Ubiquinone or Coenzyme Q (CoQ) is a lipid-soluble molecule spread across all domains of life characterized for the first time by Crane in the 1957[1]. Its structure is constituted by an isoprenoid chain, which confers the extraordinary lipophilicity, and a benzoquinone ring which allows the canonical redox activity. In humans, the polyisoprenoid tail counts 10 isoprenoid units and its biosynthesis is a highly regulated and complex process. Recent advances in molecular biology and biochemistry have provided insights into the regulatory mechanisms governing CoQ10 biosynthesis, highlighting the dynamic nature of this essential process[2] (Figure 1). The earliest steps of CoQ10 biosynthesis are regulated by a series of enzymatic reactions that occur in the cytosol, for the hydrophobic isoprenoid units biosynthesis and head group production, and in the mitochondria for the tail polymerization and the benzoquinone modifications. The polyisoprenoid side chain biosynthesis takes place in the cytosol through the Mevalonate pathway[3,4]. The mevalonate pathway is a vital metabolic pathway that serves as the primary route for the biosynthesis of cholesterol, isoprenoids, and ultimately, coenzyme Q10 (CoQ10)[5,6]. It encompasses a series of enzymatic reactions responsible for the conversion of acetyl-CoA to isopentenyl pyrophosphate (IPP), a key precursor in the synthesis of CoQ10. The process starts with the fusion of three acetyl-CoA molecules, promoted by the enzyme acetoacetyl-CoA thiolase. Subsequently, a second condensation occurs under the influence of 3-hydroxy-3-methylglutaryl-coenzyme A (HMG-CoA) synthase, resulting in the formation of HMG-CoA. Then, HMG-CoA is reduced to mevalonate by HMG-CoA reductase, a rate-limiting enzyme that is highly regulated and often targeted in therapeutic interventions for hypercholesterolemia. The conversion of mevalonate to IPP involves a sequence of enzymatic steps, including phosphorylation and decarboxylation reactions. Key enzymes in this process include mevalonate kinase (MVK), phosphomevalonate kinase (PMK), and mevalonate pyrophosphate decarboxylase (MVD), collectively driving the synthesis of IPP. Isoprenoids, such as

geranyl pyrophosphate (GPP) and farnesyl pyrophosphate (FPP), are crucial intermediates derived from IPP. CoQ10 biosynthesis is particularly dependent on FPP, as it serves as the precursor for the polyisoprenoid tail of CoQ10.

Several studies have elucidated the intricate regulation of the mevalonate pathway and its impact on CoQ10 biosynthesis. Notably, investigations into the regulation of HMG-CoA reductase have provided insights into the control mechanisms governing the overall pathway and its implications for cellular processes.

In mammals, the benzoquinone head group of the CoQ is produced starting from the tyrosine which is converted into phenylalanine by the phenylalanine hydroxylase (PDH) and, subsequently, into 4 hydroxy-benzoate (4-HB) [7,8] but the enzymes involved in this process are still unknown. The tyrosine-4-HB conversion in yeast and bacteria, instead, is promoted *de novo* by the shikimate pathway[9]. Furthermore, yeast can directly produce the 4-HB from p-aminobenzoate (pABA), using that as an alternative head group precursor[10].

The second step of the CoQ biosynthetic pathway occurs in the mitochondria by various genes where the IPP and the 4-HB are transported by an unknown mechanism. The tail polymerization is regulated by the activity of two different polytransferases, PDSS1 and PDSS2 (Coq1p in yeast). Its attachment to the benzoquinone ring, instead, is mediated by the polyprenil transferase COQ2 (Coq2p in yeast). These two proteins are differently localised in the inner mitochondrial membrane: PDSS1 and PDSS2 are associated with the peripheral side[11], whereas COQ2 is a membrane protein integrated into the membrane[12–14]. Nevertheless, Mugoni and collaborators showed that the non-mitochondrial prenyltransferase protein UBIAD1 promotes the biosynthesis of CoQ in the Golgi's membrane inducing a protection of cardiovascular tissues from eNOS-dependent oxidative stress[15].

The latest phases of CoQ biosynthesis are allowed by several enzymes that form the "CoQ complex" or "CoQ synthome", a multi protein complex located on the matrix side of the inner mitochondrial membrane[16,17] (Figure. 2). After the tail-benzoquinone ring attachment, the head group is then subjected to different decarboxylation and a series of hydroxylations and methylations. In eukaryotes, the flavin-dependent monooxygenase COQ6 (Ubil in procaryotes) catalyzes the C5-hydroxylation using flavin adenine dinucleotide (FAD) as a cofactor and NAD(P)H as a coenzyme for

reduction of FAD[18]. The head group O-methylations is promoted by COQ3 in eukaryotes[19–21] and by UbiG in bacteria[22] but the enzymes involved in the subsequent decarboxylation and C1-hydroxylation are still undefined. The decarboxylation and the C1-hydroxylation in procaryotes, instead, are catalyzed respectively by UbiD[23] and UbiH which was demonstrated to promote the C-1 hydroxylation in *Escherichia coli*[24]. Finally, COQ5 and COQ7 regulate the C2-methylation and C6-hydroxylation respectively in eukaryotes[25,26–30] both in a NADH depend manner[25,31,32], whereas UBbiE and UbiF allow the same reactions in procaryotes[33,34]. By contrast to COQ7, UbiF it's been predicted to be a flavin-dependent monooxygenase highly similar to UbiI and UbiH[35].

As mentioned above, the CoQ biosynthesis shows several steps that are not completely clarified and the molecular function of some proteins that form the CoQ synthome is still not characterized[2]. One of the master regulator of the CoQ biosynthesis in mammals is represented by COQ4[36,37], a complex Q scaffold able to bind both lipids and proteins, which underlying mechanism it's not defined yet in any organism[38]. The humans COQ8A (or ADCK3) and COQ8B (or ADCK4) both play a key role in the CoQ biosynthesis and integrity in an obscure way. Bioinformatic analysis on the *S. cerevisiae* Coq8 elucidated the structure of this protein revealing the conserved kinase motifs in its primary structure[39]. Moreover, it's been shown that Coq3p, Coq5p, and Coq7p phosphorylation is affected in *⊿coq8* yeast[40,41]. Recent works demonstrated that five different ADCK proteins are expressed in humans but only mutations in ADCK3 and ADCK4 have been observed in several disorders related to Coenzyme Q10 biosynthesis[42]. For the other ADCK proteins, instead, no clues of their role in the CoQ10 metabolic pathway have been reported. Another protein which the role remains questioned is represented by COQ9. It's been largely demonstrated that it enhances the CoQ synthome stability[43–46] through an unknown mechanism. Lohman and collaborators, in a very elegant work[46], solved for the first time the crystal structure of COQ9 revealing a lipid-binding site which allows the bond with several lipid species. Moreover, they speculated that the conserved residues within COQ9 form a distinct surface patch surrounding the lipid-binding site which is essential for its interaction with COQ7. This observation implies that COQ9 may play a necessary role in facilitating the lipid binding to the COQ7. Finally, COQ10A, COQ10B

in mammals (Coq10p in yeast, UbiJ in procaryotes)[47–49] and Coq11p (or YLR290C) in yeast[46] (in mammal has not been characterized yet) regulate the last unknown processes of the CoQ biosynthesis. Allan and colleagues demonstrated that CoQ biosynthesis is affected in yeast with coq10 mutations [47] with a less contribution by the produced CoQ for the OxPhos. Nevertheless, yeast *ΔCoq11p* didn't show a totally CoQ deficient and didn't show any difference in the growth rate[49].

Recent studies demonstrated that the enzymes forming the CoQ complex can module their own expression and stability depending on the presence or absence of lipid substrates[50]. This group of enzymes has been found to be present on the contact spots between the mitochondria and the endoplasmic reticulum (ER)[50]. Alterations in the ER-mitochondria binding sites result, indeed, in a CoQ domain assembly defects and, as consequence, in a CoQ intermediates accumulation [50]. Interestingly, Eisenberg-Bold and collaborators identified a destabilization of CoQ enzymes in yeast null for the encounter structure (ERMES) complex with a consequential drop of the CoQ6 amount [51]. This new evidence highlighted the role of the proteins involved in the CoQ synthesis to improve the substrates availability for an efficient CoQ production and distribution through the cells.

.

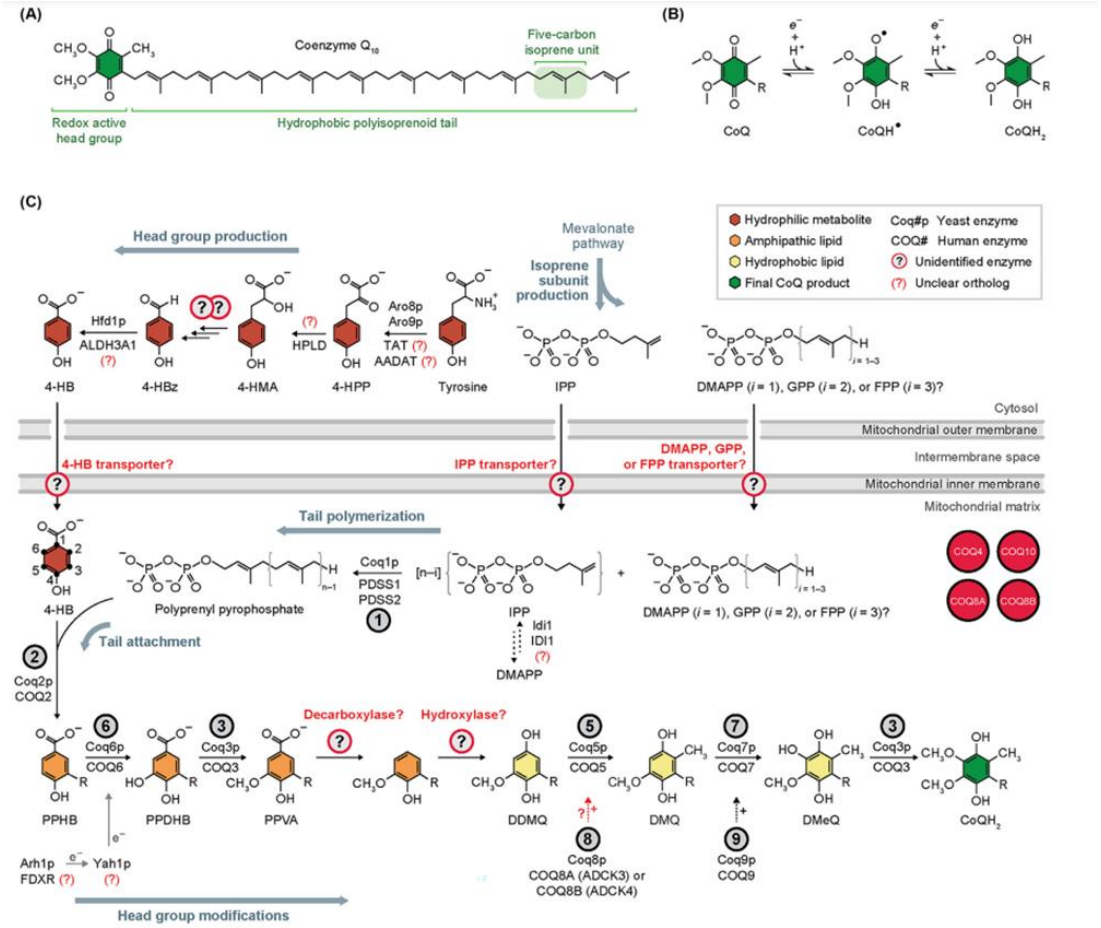


**Fig.1** Representative scheme of the ubiquinone biosynthesis in eukaryotes[52]

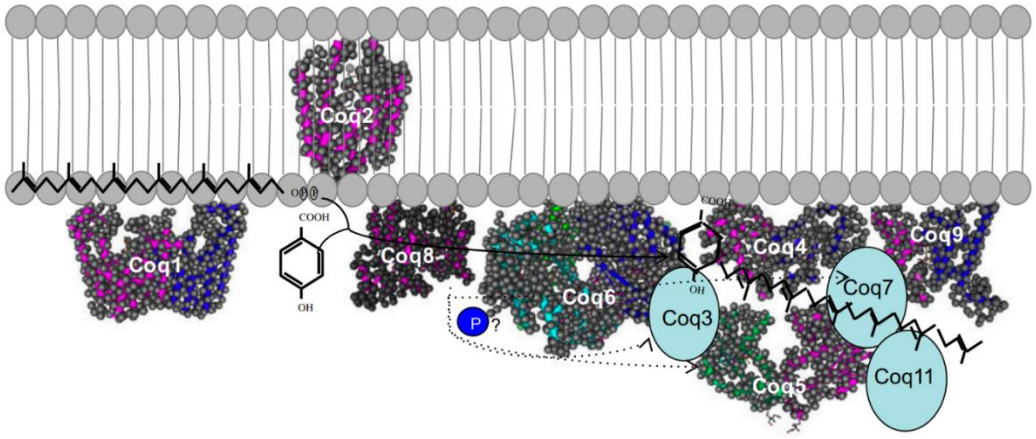


**Fig.2** Diagram of the CoQ synthome in eukaryotes[39]

Table 1. CoQ biosynthetic genes from various species.

| Function | *H. sapiens* | *M. musculus* | *C. elegans* | *A. thaliana* | *S. cerevisiae* | *S. pombe* | *E. coli* |
|---|---|---|---|---|---|---|---|
| Polyprenyl diphosphate synthase | *PDSS1 + PDSS2* | *Pdss1 + Pdss2* | *COQ1* | *SPS3* | *COQ1* | *dps1 + dlp1* | *ispB* |
| PHB-polyprenyl diphosphate transferase | *COQ2* | *Coq2* | *COQ2* | *COQ2 (PPT1)* | *COQ2* | *coq2 (ppt1)* | *ubiA* |
| *O*-methyltransferase | *COQ3* | *Coq3* | *COQ3* | *COQ3* | *COQ3* | *coq3* | *ubiG* |
| Unknown | *COQ4* | *Coq4* | *COQ4* | *COQ4* | *COQ4* | *coq4* | - |
| *C*-methyltransferase | *COQ5* | *Coq5* | *COQ5* | *COQ5* | *COQ5* | *coq5* | *ubiE* |
| Monooxygenase | *COQ6* | *Coq6* | *COQ6* | *COQ6* | *COQ6* | *coq6* | *ubiI* |
| Monooxygenase | *COQ7* | *Coq7 (Clk1)* | *COQ7* | - | *COQ7* | *coq7* | *ubiF* |
| Protein kinase | *ADCK3, ADCK4* | *Adck3, Adck4* | *COQ8* | *COQ8 (ABC1)* | *COQ8 (ABC1)* | *coq8* | *(ubiB)* |
| Unknown | *COQ9* | *Coq9* | – | *COQ9* | *COQ9* | *coq9* | – |

**Tab.1** Table of the genes involved in the CoQ biosynthesis in eukaryotes[39]

### *1.2. Coenzyme Q10 functions*

CoQ10 plays an essential role in the cell homeostasis and in a huge number of biological processes[52]. Its hydrophobic nature allows this molecule to be present in the membranes of cellular organelles (Fig.3), particularly in the inner mitochondrial membrane (IMM), where it carries electron from Complex I and Complex II to Complex III of the mitochondrial respiratory chain establishing the mitochondrial potential necessary for the adenosine triphosphate (ATP) synthesis[2] (Fig.4). The CoQ pool not involved in the electron transferring from NADH to the Complex III of the mitochondrial respiratory chain diffuses through the inner mitochondrial membrane and receive electrons from FAD-dependent enzymes improving the mitochondrial

respiratory capacity[53]. Moreover, it acts as cofactor for several dehydrogenases involved in multiple cell processes providing further ways to converge the electrons to Complex III of the electron transfer chain (ETC)[52,54]. For instance, the Electron-transfer flavoprotein:ubiquinone oxidoreductase (ETF-QO), encoded by ETFDH gene, promotes the electron transfer from electron flavoprotein (ETF) to CoQ[55]. ETF accepts electrons from a large number of mitochondrial acyl-CoA dehydrogenases involved in the beta oxidation, amino acids catabolism, sarcosine dehydrogenase and dimethylglycine dehydrogenase[56]. Furthermore, CoQ can be reduced by the Dihydroorotate dehydrogenase (DHODH), allowing the conversion of dihydroorotate to orotate and, as consequence, the pyrimidine biosynthesis[57]. CoQ can also participate to the detoxification of $H_2S$ to thiosulphate accepting two electrons from the Sulfide:quinone oxidoreductase (SQOR)[58] resulted from oxidation of sulfide to sulfane sulfur. Two more dehydrogenases capable to bind quinone promoting its reduction are the mitochondrial glycerol-3-phosphate dehydrogenase (mGPDH) and the Proline dehydrogenase (PRODH) both anchored to the inner mitochondrial membrane. The mGPDH is a flavin-linked dehydrogenase faced to the intermembrane space side and induces the oxidation of the glycerol-3-phosphate to dihydroxyacetone phosphate transferring the electrons to the CoQ[59]. The PRODH is oriented to the mitochondrial matrix and converts the proline to pyrroline-5-carboxylate[60] which is further hydrolyzed in a non-enzymatic reaction to glutamic semialdehyde and, finally, oxidized to glutamate by the aldehyde dehydrogenase 4 (ALDH4A1). These two products that come from the proline oxidation can be metabolized by the urea and the tricarboxylic acids (TCA) cycle contributing to the energy production (30 molecules of ATP are produced from the oxidation of one molecule of proline)[61]. It has been largely demonstrated that, beyond its pivotal role in the oxidative phosphorylation and energy production, CoQ10 has important antioxidant properties and potential health benefits. For instance, the reduced form of CoQ ($QH_2$) protects against the oxidative damage caused by the radical oxygen species (ROS)[62,63]. In addition to its role in the free radicals neutralization and antioxidant regeneration, such as vitamin E from the α-tocopheroxyl radicals [64 65], the $QH_2$ prevents the modifications of mitochondrial proteins and DNA and interferes with the formation and propagation of the membrane lipid peroxidation. CoQ has an

extraordinary antioxidant role outside the mitochondria thank to distinct plasma membrane oxidoreductases (Fig.5). The NAD(P)H:quinone oxidoreductase 1 (NQO1) and NADH-cytochrome b5 reductase (Cyb5Red) are two most characterized plasma membrane oxidoreductases. NQO1 plays a key antioxidant role promoting the CoQ reduction through the two electrons transferring[66,67] and Vitamin E quinone (α-tocopherol quinone) generation[68]. Furthermore, the NQO1 enzyme shows scavenging superoxide dismutase proprieties functioning as a superoxide reductase[69,70]. In the recent years, the attention has been focused on the capacity of NQO1 to maintain a right NAD(P)H/NAD(P)$^+$ balance through the reduction of β-lapachone, a 1,2-naphthoquinon. Indeed, the reduction of β-lapachone by NQO1 leads to a futile cycling between the quinone and hydroquinone forms with a decrease of NADH and NADPH level and a concomitant increase of NAD$^+$ and NADP$^+$[71]. Cyb5, expressed in both plasma membrane and ER, is activated under stress conditions and contributes to the antioxidant role protection reducing CoQ through the electron flux from the NADH[72,73]. Recent woks evidenced the implication of CoQ on the protection against the synthesis of the lipid peroxides induced by ferroptosis. Ferroptosis is an intracellular iron dependent nonapoptotic cell death characterized for the first time by Dixon and colleagues in the 2012 which is morphologically, biochemically, and genetically distinct from the other kinds of cell death (apoptosis, necrosis, and autophagy) [74]. The two main defence mechanisms against the lipid peroxidation, in mammals, are represented by the phospholipid hydroperoxide glutathione peroxidase (GPX4)[75] and FSP1[76]. This oxidoreductase is able to reduce the plasma membrane CoQ that in turn inhibits the spread of the lipid peroxidation.

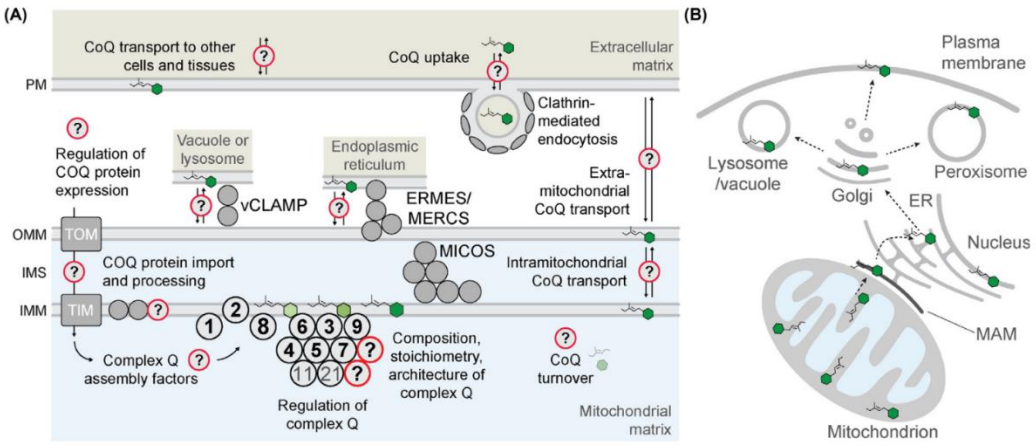


**Fig.3** Schematic imaging of the CoQ distribution and organization inside the cell[52]

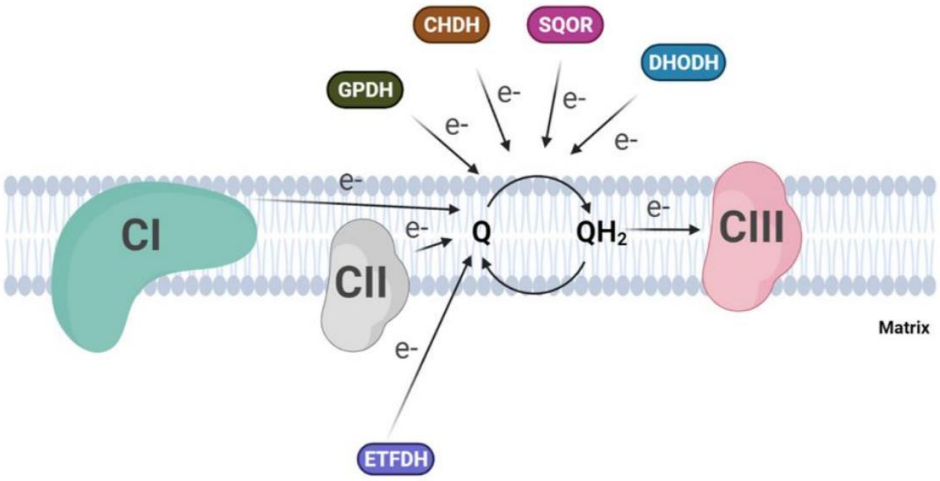


**Fig.4** CoQ contribution in the mitochondrial electron transport chain[77]

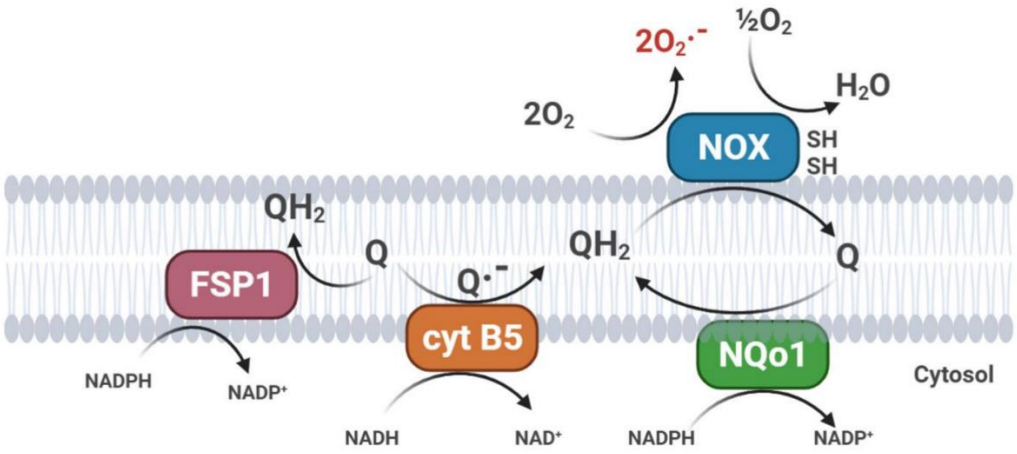


**Fig.5** Model of the cytoplasmatic dehydrogenases involved in the protection against the oxidation insults through the CoQ reduction[77]

### *1.3. Coenzyme Q10 involvement in aging and diseases*

Deficiencies in CoQ10 biosynthesis have been linked to a large spectrum of human disorders, including mitochondrial diseases, neurodegenerative conditions, cardiovascular dysfunctions and aging[78–80]. Since its essential role in the mitochondrial potential maintenance and ROS protection, a drop in the CoQ10 level affects the mitochondrial activity linked to the related diseases and aging. This molecule is also involved in the regulation of several genes related to the signalling pathways of G-protein coupled receptors, JAK/STAT, integrin, and beta-arrestin[81]. Remarkably, a low amount of CoQ10 has been observed to be linked with an increase of the transcription of different markers connected with the inflammation [82]. The diseases associated with a decrease in the CoQ10 level can be divided into two different categories depending on which genes the mutations occur.

### *1.3.1. Primary CoQ10 deficiencies*

The primary CoQ10 deficiencies are rare autosomal recessive disorders that encompass cerebellar ataxia, encephalomyopathy, infantile multisystemic form, nephropathy, and isolated myopathy[77]. These diseases occur in organs with a high energy demand and are caused by mutations in genes encoding enzymes directly involved in the CoQ10 biosynthesis. Ten genes have been identified to have pathogenic variants so far and they differ for the presence in distinct tissues and for the age of onset[83]. Indeed, while mutations in COQ2 and COQ4 genes may affect many organs, pathogenic variants in COQ8A and COQ8B have been showed to have more a specific phenotype. Furthermore, alterations in PDSS1, PDSS2, COQ2, COQ4, COQ5, COQ6, COQ7 and COQ9 are mostly present in a range from birth to early childhood, while COQ8A andCOQ8B mutations have been observed generally from the early childhood to the adolescence. Finally, pathogenic variants for COQ2[84], COQ8A[85,86] and COQ8B[87] have reported in some adult patients.

### *1.3.2. Secondary CoQ10 deficiencies*

Despite the primary one, the secondary CoQ10 deficiencies occur in mitochondrial disorders where the genes involved in the CoQ10 biosynthesis are not affected in any way. The clinical manifestations closely resemble symptoms observed in various mitochondrial disorders. Secondary CoQ10 deficiency may arise from OXPHOS defects, impaired non-OXPHOS mitochondrial processes, or dysfunction in non-mitochondrial functions[88,89]. The precise mechanisms through which these defects lead to CoQ10 deficiency remain unknown, and multiple contributing factors are considered. These factors encompass the biological functions and metabolic pathways involving CoQ10 both inside and outside the mitochondria, as well as various mechanisms that can influence CoQ10 levels by regulating its biosynthesis or turnover[90,91]. Given the wide range of disorders associated with secondary CoQ10 deficiency, establishing genotype–phenotype correlations is challenging and largely dependent on the specific etiological condition and the mutated gene involved.

Patients with secondary CoQ10 deficiency exhibit a clinical spectrum closely tied to the underlying pathology. Within these disorders, muscular impairments are present as in myopathies, featuring muscular weakness, hypotonia, exercise intolerance, or myoglobinuria[92,93]. Additionally, the central nervous system (CNS) can be affected in secondary CoQ10 deficiencies, leading to ataxia and neurological decline[94]. Furthermore, a CoQ10 deficiency has been observed in specific genetic disorders associated with lipid metabolism, including Familial Hypercholesterolemia and Multiple Acyl-CoA Dehydrogenase Deficiency (MAAD)[94]. The importance of CoQ10 it has been demonstrated also in different chronic pain syndromes, such as the fibromyalgia. A drop in CoQ10 levels together with an increase in ROS production, indeed, has been reported in blood mononuclear cells from patients [95]. However, there is considerable variability in the presence of secondary CoQ10 deficiency among individuals with the same disorders, indicating diverse susceptibility to CoQ10 deficiencies. Furthermore, genetic factors, such as additive hypomorphic mutations or specific polymorphisms, may play a role.

### *1.4. Strategies on CoQ10 delivery*

As the CoQ10 balance is affected in a large spectrum of disorders, the exogenous CoQ10 supplementation has been proposed as therapeutic approach. The oral assumption of the native molecule has been relieved to be highly ineffective due to its poor bioavailability[96]. Therefore, a plenty of different formulations of CoQ10 have been reported during the last years[97,98] and the finding of new delivery strategies represents one of the main goal to improve its uptake and distribution. Concerning the oral intake, various physiological factors influence compound bioavailability, including genetic phenotype, various disorders, sex, age, administration route, gastrointestinal tract health and food interactions. Difficulties in achieving therapeutic levels of CoQ10 drive efforts to design new oral preparations, especially given the widespread use of CoQ10 as a complementary approach in older individuals. Pravst and colleagues demonstrated that a water-soluble CoQ10 syrup preparation exhibited a 2.4-fold higher bioavailability compared to a ubiquinone

capsule preparation though CoQ10 appeared in the blood predominantly as ubiquinol, even when consumed as ubiquinone[99]. Moreover, a water soluble formulation of CoQ10 encapsulated in β-cyclodextrin inclusion complexes has been demonstrated to increase its stability and bioavailability[100]. CoQ head group analogues have been also proposed as efficient compounds to restore the CoQ levels in cells and increase the lifespan in mice[101–103]. These molecules, in fact, can be integrated into the native biosynthetic pathway leading to proper cellular distribution. Further strategies have been developed to bypass the biophysical barriers associated with the CoQ10 delivery. For instance, MitoQ, an ubiquinone derived covalently attached to a lipophilic triphenylphosphonium cation designed for mitochondrial targeting, exhibited evident antioxidant and antiapoptotic proprieties[104]. However, it was unable to restore the CoQ's electron transport chain function, likely due to the hindered membrane incorporation caused by the bulky TPP group[98]. Alternative methods involve linking TPP to the surface of CoQ-encapsulated nanoparticles[105] but the efficacy of these agents in restoring respiration has yet to be investigated. An emerging strategy involves encapsulating CoQ in mitochondria targeted liposomes, such as the MITO-Porter system, designed to fuse directly with the mitochondrial membrane[106]. Despite advancements, these delivery systems remain highly lipophilic and are subject to biophysical delivery barriers. Trying to avoid these issues, Wang and colleagues micellized CoQ10 with the fungicide caspofungin enhancing its water solubility and tissue uptake. Despite the lifespan improvement observed in CoQ deficient mice, the need to perform multiple rounds of the intravenous injection might represent a limit to propose it as a potential therapy[107]. Interestingly, the most recent scientific findings underscore the efficacy of a new food-grade delivery system of CoQ10 based on lecithin, called CoQ10 phytosome (Ubiqsome®, UBQ) providing compelling evidence of its enhanced bio-absorption and functionality in cells, plasma and human tissues[108–110,110].

### *1.5. Hereditary Spastic Paraplegia (HSP)*

Neurodevelopmental disorders (NDDs) represent a group of diseases which affect more than 3% of children around the whole world[111]. Symptoms are typically characterized by cognitive and motor developmental delay and are associated with the disruptions in the intricately coordinated processes governing brain development. With a diverse etiology, NDDs result in compromised communication, adaptive behaviour, and psychomotor skills. The most common conditions encompass by NDDs include autism spectrum disorder (ASD), intellectual disability (ID), attention deficit hyperactivity disorder, and epilepsy[111]. Several types of mutations have been identified to be correlated with NDDs, including some involved in the hereditary spastic paraplegias (HSP) onset[112]. HSP encompasses a large spectrum of neurological disorders with an estimated prevalence of two to five cases per 100000 individuals worldwide[113] identified for the first time in the early 1980s by Harding[114]. All kind of HSP are characterized by degeneration of the corticospinal tract and dorsal columns in a length-dependent manner [115] which leads to specific core clinical features, including bilateral spasticity in the lower limbs, heightened reflexes, and extensor plantar responses[113]. Onset age varies widely, ranging from early childhood to late adulthood. Reported modes of inheritance include autosomal dominant, autosomal recessive, or X-linked, with sporadic cases (i.e., lacking a family history) accounting for 13–40% of occurrences[116]. Notably, some forms of HSP can be classified in pure or complex forms depending on the clinical phenotype[117]. Patients affected by pure forms manifest pyramidal signs, accompanied by muscle weakness and bladder dysfunction. The complicated forms show several neurological signs including cerebellar manifestations, neuropathy, cognitive impairment, epilepsy, extrapyramidal and retinal signs. Beyond neurological manifestations, patients may also present with extra neurological signs, such as gastroesophageal reflux, cataracts, and abnormal skin pigmentation[113]. Moreover, some phenotypes related to mitochondrial disorders have been observed in some complicated forms of HSP since a maternal mitochondrial inheritance can rarely occur[118]. The overall functional handicap and lifespan in complex forms are contingent upon the comprehensive

clinical presentation[119]. The HSP genetic classification is quite complex due to the bunch of genes discovered to be involved on the onset of the disease. Indeed, up to 79 spastic paraplegia genes (SPGs) have been documented so far but many of these have been identified only in individual families suggesting them as HSP candidate genes[114].

### 1.6. *Troyer Syndrome*

Troyer syndrome [Online Mendelian Inheritance in Man (OMIM 275900;www.omim.org)] is an autosomal-recessive form of HSP firstly described in 1967 in the Old Order Amish with 20 individuals affected by muscle wasting in childhood[120] . Starting from then, Troyer syndrome has undergone further characterization, particularly within populations characterized by a high degree of consanguinity. Although the precise incidence remains elusive, estimates propose a frequency of 1 in 10,000,000 individuals[121]. Although the developmental delay is usually described in patients at 1-2 years old[122], Liang and collaborators have recently reported that the average age of diagnosis of Troyer Syndrome is 20 years old[121]. All previously documented patients display progressive spastic paralysis in the legs and dysarthria. Other prevalent manifestations encompass distal skeletal abnormalities, muscle atrophy, learning disabilities, drooling, and emotional lability[123–125]. Neurological manifestations in this condition emerge later in childhood, progressing insidiously and exerting a significant impact on mobility in adulthood[122].The short stature typically correlated with the Troyer Syndrome [121,126,127] is commonly accompanied by relative macrocephaly, although instances of microcephaly[127,128]. Additionally, abnormalities visible on brain MRI, notably T2 hyperintensity affecting the periventricular white matter, are well-documented in the literature[121,122,129]. It was firstly demonstrated by Patel and collaborators that Troyer Syndrome is caused by biallelic missense variants in SPART gene (or SPG20)[130]. SPG20, composed by 68,543 bases and located on chromosome 13q13.3, encodes for Spartin, a multifunctional protein composed of 666 amino acids which exhibits a complex

predicted structure with distinct alpha helix domains. Spartin consists of three known domains: the MIT (Microtubule Interacting and Trafficking molecule) domain, the C-terminal plant-related senescence domain, and the Pro-rich polypeptide binding motif (PPXY) domain[131–134]. The MIT domain forms an asymmetric three-helix bundle at the N-terminus, while the C-terminal plant-related senescence domain functions as an AAA ATPase domain housing an α/β nucleotide-binding domain (NBD) and a smaller four-helix bundle domain (HBD). The Spartin's PPXY domain, finally, binds motif facilitating the recruitment of ubiquitin ligases[131,135]. As its presence in almost all cell compartments, Spartin plays a key role in several cell functions. For instance, is implicated in the endocytosis pathway, bone morphogenetic protein (BMP) signalling, cellular response to growth stimulus (specifically EGFR intracellular trafficking), regulation of mitochondrial membrane potential, cytokinesis, microtubule-associated transport, negative regulation of cellular response to growth factor stimulus, and negative regulation of the transmembrane receptor protein serine/threonine kinase signalling pathway[134,136,137]. Moreover, Spartin plays as a ubiquitin protein ligase binder, interacting with WWP1 (AIP5) through Pro-rich polypeptide (PY motifs), a multifunctional protein predominantly localized in endosomes[131]. Spartin is mostly monoubiquitinated and exists in a steady state within a cytosolic pool, where it can be recruited to endosomes or lipid droplets (LDs)[137]. Few works have reported that SPG20 mutations can also occur in specific type of cancer but no correlation with the tumour predisposition it's still unclear so far[138,139]. Recent research has highlighted the importance of the noteworthy finding indicating that STAT3, a crucial transcriptional regulator in cancer, exerts its role by binding upstream of SPART exon 1 suppressing its expression[140].

# 2. Aims

## *2.1. Bioenergetics and delivery characterization of a new formulation of Coenzyme Q10*

Coenzyme Q10 is a lipophilic molecule which plays a pivotal role in multiple cell functions. Particularly, it acts as the main electron carrier of the ETC retaining the membrane potential and a correct ATP synthesis. Moreover, the CoQ10 is the most important hydrophobic antioxidant produced by the cells: when reduced, indeed, avoids the membranes and lipoproteins peroxidation[141]. Since its ubiquitous presence, it been largely reviewed that a drop in the CoQ10 level encompasses a massive variety of medical conditions. The CoQ10 deficiency occurs in primary or secondary forms. Primary deficiencies, arising from mutations in genes involved in its biosynthetic pathway or its regulatory processes, lead to diverse clinical conditions such as encephalomyopathy, severe infantile multisystemic disease, and cerebellar ataxia. Secondary deficiencies may result from mutations in genes not directly linked to CoQ10 biosynthesis, often due to dietary inadequacy or the use of certain drugs and medications , such as statins[142]. Despite the strong rationale for CoQ10 supplementation, contradictory results have been reported, attributed to the molecule's high lipophilicity, light sensitivity, and thermolability[143]. To address these challenges, several formulations have been developed to enhance CoQ10's oral bioavailability, including the Self-Nanoemulsifying Delivery System (SNEDDS)[144], oleogels[145] micellar nanoparticles[107], liposomes[146], cyclodextrin inclusion compounds[147], and lipid-free nanoformulations[97]. For this reason, we investigated the delivery system of a new CoQ10 formulation based on lecithin, termed CoQ10 phytosome (Ubiqsome®, UBQ) [109,148,149], on a human epithelial intestine cell line (Intestine 407, I407) and a rat cardiomyoblast cell line (H9c2). Specifically, we focused our attention on the cellular uptake and mitochondrial distribution of UBQ, highlighting the CoQ10 redox state after the cell internalization. Furthermore, we

assessed the bioenergetic effects of UBQ treatment and its protective role against oxidative stress and ferroptosis.

### *2.2. Bioenergetics characterization and UBQ treatment efficiency on fibroblasts derived from a patient affected by Troyer Syndrome*

The secondary deficiencies are more common than the primary ones and they may be associated with defects in oxidative phosphorylation (OXPHOS), compromised non-OXPHOS mitochondrial processes, or alteration in non-mitochondrial functions[150]. Patients affected by secondary CoQ10 deficiency manifest a large spectrum of disorders that are directly correlated with the underlying pathology from which it originates. However, the muscular manifestations observed in the CoQ10 deficiencies but not in the primary ones, manifest myopathies characterized by muscular weakness, hypotonia, exercise intolerance, or myoglobinuria[93,151]. Furthermore, the central nervous system can be affected in the secondary CoQ10 deficiencies leading to a progressive neurological and cognitive decline[94,152]. Establishing a molecular and genotype–phenotype association in cases of secondary CoQ10 deficiency is challenging due to the broad range of disorders associated with it. Correlations will predominantly hinge on the nature of the underlying etiological condition and the specific mutated genes. For instance, patients affected by Troyer Syndrome show peculiar symptoms associated with CoQ10 deficiencies, particularly in the alteration of energy metabolism and mitochondrial efficiency. Indeed, Ring and colleagues demonstrated that *Drosophila Spartin* expressed extends the lifespan concurrently diminishing age related ROS production, necrosis and apoptosis. In the same work, the results indicate that Spartin establishes physical interactions with proteins associated with the mitochondrial respiratory metabolism. Moreover, Spartin interacts with glycolysis enhancing the phospho-fructo-kinase-2,6 (Pfk26) and, intriguingly, is sufficient to complement for PFK26-deficiency, particularly in the early stages of aging[134]. Spartin, additionally, localizes on the outer mitochondrial membrane binding the cardiolipin allowing a correct calcium homeostasis and the

mitochondrial potential maintenance[153]. Finally, Diquigiovanni and collaborators, emphasized the role of Spartin on the mitochondrial functionality in a very elegant work. They showed, in fact, that a homozygous loss of function mutation in SPART gene leads to a sever mitochondrial dysfunction marked by increase in ROS production and affected Complex I activity[154]. Given this evidence and since correlation between Troyer syndrome and CoQ10 deficiency it's been poorly studied, we investigated the mitochondrial parameters in fibroblasts derived from a 5-years old patent carrying biallelic missense variants in SPART and in a genome-edited neuronal cell model carrying a homozygous protein-truncating mutation. We elucidated the bioenergetic status of the patient's fibroblasts and mutated cells with a particular attention on the ETC complexes activity and energy production. Moreover, we demonstrated that mutations in SPART affect the expression of the proteins involved in mitochondrial associated membranes (MAMs) integrity leading to an altered calcium homeostasis and a mitochondrial nuclear-encoded proteins import with a significative decrease of the CoQ10 level. Supplementation with UBQ compound was able to partially restore some affected parameters suggesting this molecule as potential cotreatment for Troyer syndrome patients.

# 3. Material and methods

## *3.1. Subject*

A young male patient (5 years old) was referred due to global developmental delay and muscular hypotonia, primarily affecting proximal muscle groups. He also reported leg pain after walking. The patient was born spontaneously after an uneventful pregnancy, and the postnatal period was without complications. The patient achieved the ability to sit and walk by the age of 2 and began speaking single words at 2.5 years, with speech development lagging significantly behind the normal trajectory. By the age of 6, he could construct simple sentences. He has one younger and two older reportedly healthy siblings. Clinical examination revealed brisk reflexes in the lower extremities bilateral and pes planovalgus, hypotrophic calves. He exhibited mild conductive hearing loss without the need for hearing aids. Physical measurements indicated a height of 109 cm (4th percentile), weight of 17 kg (4th percentile), and a head circumference of 51 cm (20th percentile). Metabolic screening in blood and urine yielded normal results. A Snijders–Oomen non-verbal intelligence test (SON-IQ) conducted at 5 years and 8 months indicated an IQ of 50. Additionally, the patient presented with epilepsy characterized by absences, managed with levetiracetam, and hyperopia. No facial dysmorphisms were observed.

## *3.2. Next Generation Sequence analysis*

Exome sequencing (ES) was conducted on genomic DNA extracted from the index patient and his healthy parents, following Falb and colleagues[155]. Briefly, coding genomic regions were enriched using the SureSelectXT Human All Exon Kit V7 (Agilent Technologies, Santa Clara, CA, USA) and subsequently sequenced as 2 × 100 bp paired-end reads on a NovaSeq6000 system (Illumina, San Diego, CA, USA). Variant

calling was executed using the megSAP pipeline (https://github.com/imgag/megSAP), with variant prioritization including filtering for rare variants (minor allele frequency less than 1% in gnomAD) associated with autosomal recessive, de novo, or X-linked inheritance patterns. Carrier testing for additional family members was performed using Sanger sequencing.

### *3.3. Cell lines culture and treatment*

Intestine 407 cells (I407), embryonic epithelial cells from the human intestine, were cultured in Roswell Park Memorial Institute (RPMI) 1640 medium supplemented with 10% fetal bovine serum (FBS) and 1% penicillin/streptomycin (Millipore Sigma, Burlington, MA, USA). H9c2 cells, embryonic cardiomyoblasts from rats, and dermal fibroblasts derived from both control individuals (cnt) and patients (e19), obtained from skin biopsies, along with SH-SY5Y cell models (including wild-type and genome-edited cells with the insertion of SPART c.892dupA[154]), were cultured in High Glucose Dulbecco's modified Eagle's medium (DMEM, Euroclone, Milan, Italy) supplemented with 10% FBS and 1% penicillin/streptomycin. All cell lines were maintained at 37 °C in 5% CO2 with saturating humidity. Where indicated, cells were incubated for 24 hours in complete culture medium supplemented with either 100 nM CoQ10 Phytosome® (UBIQSOME®, UBQ) or 100 nM native CoQ10, provided by Indena S.p.A Milan, Italy [108,109,148,156]. A control group was treated with the Phytosome® carrier alone (sunflower lecithin matrix).

### 3.4. *CoQ10 determination*

The total cellular CoQ10 content was determined using HPLC with a two-pump system equipped with a photodiode array detector (Agilent, Santa Clara, CA, USA, 1100 series), following the methodology reported by Liparulo et al.[157] with slight modifications. In brief, CoQ was extracted from cultured cells as described by Takada

et al[158]. Subsequently, CoQ was resuspended in 0.05% $Fe3^+$ in ethanol and subjected to chromatography on a C18 Column (Kinetex, Phenomenex, Torrance, CA, USA, 2.6 µm, 100 × 4.6 mm) using an ethanol: water (97:3, v/v) mobile phase at a flow rate of 0.6 $mL \cdot min^{-1}$. Identification of the CoQ peak at λ = 275 nm was achieved through comparison and co-elution with a standard. Quantification of CoQ was performed by measuring peak area and comparing it with standard curves, normalized based on cell number. Cell counting was conducted using an inverted microscope with a Burker chamber. For the determination of mitochondrial CoQ10 content, the same HPLC procedure was applied to mitochondria isolated from cultured cells, following the method outlined by Spinazzi et al[159]. The mitochondrial CoQ10 amount was normalized to mitochondrial protein content determined by the Lowry method[160]. The determination of cellular oxidized and reduced CoQ10 was performed using HPLC system, following the protocol by Rakusa and colleagues[161] with some modifications. Specifically, for simultaneous determination of reduced and oxidized forms, CoQ10 was extracted as described above. A portion of the hexane solution was then dried on nitrogen flux and reconstituted in acetonitrile (ACN) in the presence of 100 mg/L of butylhydroxytoluene (BHT), followed by 1 min of sonication at 4 °C and vortex mixing. The samples were transferred into a vial and immediately analyzed by HPLC, as described earlier. Identification of the oxidized CoQ10 peak at λ = 275 nm and the reduced CoQ10 peak at λ = 290 nm was achieved through comparison with standards and comparison with standard curves. As a control for total oxidized CoQ, a portion of the hexane solution was dried on nitrogen flux and resuspended in 0.05% $Fe3^+$ in ethanol, followed by sonication (2 min) and vortex mixing (30 s). The samples were then transferred into a vial and analyzed at 275 nm by HPLC. Coenzyme Q7 was used as the internal standard in all determinations.

### 3.5. *Oxygen consumption rate*

Oxygen consumption rate (OCR) was assessed following Liparulo at al.[157]. Between 0.75-1 x $10^6$ cells were seeded in Petri dishes 24 hours before the analysis to allow a

correct adhesion. Then, cells were harvested (80% of confluence) through trypsinization, washed with PBS, and resuspended in DMEM for oxygen consumption assays at 37 °C, utilizing a thermostatically controlled oxygraph chamber (Instech Mod. 203, Plymouth Meeting, PA, USA). Endogenous respiration was assessed in DMEM and compared with the minimal and maximal ones after the injection of 1 µM oligomycin A (minimum respiration) and 0.5-1 µM FCCP (carbonyl cyanide 4-trifluoromethoxy phenylhydrazone) respectively. To calculate the specific mitochondrial oxygen consumption, 5 µM antimycin A was injected to completely inhibit mitochondrial respiration[154]. The data were normalized based on cellular protein content, determined by the Lowry method, and expressed as nmoles $O2 \cdot min^{-1} \cdot mg^{-1}$.

### *3.6. Intracellular NAD(P)H Determination*

Intracellular NAD(P)H autofluorescence was assessed in intact cells using a Jasco FP-770 spectrofluorometer (Jasco, Japan), equipped with a stirring device and thermostatic control as reported by Bartolomè et al.[162]. To conduct the experiment, cells were detached through trypsinization, washed with phosphate buffer, and resuspended in HBSS buffer (156 mM NaCl, 3 mM KCl, 2 mM $MgSO_4$, 1.25 mM $KH_2PO_4$, 2 mM $CaCl_2$, 10 mM glucose, and 10 mM HEPES; pH adjusted to 7.4 with NaOH) in a 3 mL quartz cuvette at 30 °C. Following a 5-minute stabilization period, NAD(P)H spectra were recorded at $\lambda_{exc}$ 340 nm and $\lambda_{em}$ 380–500. To block the Complex I (NADH:decylubiquinone oxidoreductase) and enhance NAD(P)H content at the end of the experiments, 10 µM rotenone was introduced. Standard NADH and NAD(P)H were used for system calibration.

### *3.7. Nucleotides determination*

Adenosine triphosphate (ATP) and diphosphate (ADP) content was analyzed as reported by Joens et collaborators [163]. Briefly, 0.150 x $10^6$ cells were seeded in 6 well plate (Costar®, Corning) and treated as previously described. Subsequently, cells were detached by trypsinization, and cell pellet washed twice in PBS. After 5 minutes of centrifuge at 800 g, the cell pellet was resuspended in perchloric acid (PCA) 1M and potassium hydroxide (KOH) 600 µM. Then, samples were centrifuged at 14,000 for 30 minutes and intracellular ATP and ADP were measured by HPLC two-pump system equipped with a photodiode array detector (Agilent, Santa Clara, CA, USA, 1100 series) using a C18 column (250 × 4.6 mm, 100 Å, 5 µm; Phenomenex). Nucleotide peaks were identified at λ = 260 nm, and quantification was obtained by peak area measurement compared with standard curves. Raw data were normalized on cells number.

### *3.8. Radical oxygen species measurement*

Oxidative stress in intact cells was assessed using the specific reactive oxygen species indicator 2',7'-dichlorodihydrofluorescein diacetate (DCFDA, Thermo Fisher Scientific, Waltham, MA, USA), as reported in the method outlined by Bergamini et al.[147] with slight modifications. Briefly, cells were plated at a density of 4 × $10^4$ cells/well in 96-well plates (Optiplate, Perkin Elmer) and incubated for 24 hours to allow the adhesion. Then, for some experiments, cells were exposed to different concentrations (ranging from 6.25 nM to 100 nM) of native CoQ10, UBQ®, or phytosome vehicle dissolved in complete medium for 24 hours at 37 °C in 5% CO2. Following this incubation period, cells were washed with Hank's Balanced Salt Solution (HBSS) and treated with 10 µM DCFDA (2',7'-dichlorofluorescein diacetate, DCFH-DA, Thermo Fisher) in DMEM for 30 minutes. Subsequently, cells were washed with HBSS and treated for an additional 30 minutes with 130 µM tert-butyl hydroperoxide (TBH) in

HBSS. Finally, cells were washed again with HBSS, and the fluorescence values in each well were measured ($\lambda_{exc}$ = 485 nm; $\lambda_{em}$ = 535 nm) using a plate reader (Enspire, Perkin Elmer). Fluorescence emission was normalized to protein content measured by the Lowry method.

### *3.9. Mitochondrial membrane potential assessment*

For the mitochondrial membrane potential, two different fluorescence dyes were utilized. I407 and H9c2 cells were cultured in µ-Slide 8 well plate (Ibidi, Germany) and treated as detailed earlier. Subsequently, cells were stained with the fluorescent carbocyanine dye JC-1 (ThermoFisher Scientific) as described in the protocol outlined by Bergamini et al.[147] Shortly, cells were incubated with 5 µM JC-1 at 37 °C, 5% CO2 for 30 minutes in culture medium and then washed twice with HBSS. Images were acquired using a Nikon C1si confocal microscope (Nikon, Tokyo, Japan). Fluorescence intensity was measured using the ImageJ software standard tool (National Institutes of Health, Bethesda, MD, USA). For some experiments, cells were instead loaded with the mitochondrial potential sensor tetramethylrhodamine methyl ester (TMRM) following Kirk and colleagues with slight modifications[164]. Images were acquired using a Nikon C1si confocal microscope (Nikon, Tokyo, Japan). Fluorescence intensity was measured using the ImageJ software standard tool (National Institutes of Health, Bethesda, MD, USA). Subsequently, cells were incubated for 30 minutes using 50 nM of TMRM ($\lambda_{exc}$=544 nm, $\lambda_{em}$=590 nm; Thermo Fisher Scientific) and 125 nM of MitoTrackerGreen (MTG; $\lambda_{exc}$=490 nm, $\lambda_{em}$=516 nm; Thermo Fisher Scientific) at 37°C and 5% of $CO_2$ in DMEM. After two washes with HBSS, TMRM and MTG fluorescence intensities were recorded using a multiplate reader (Enspire, PerkinElmer) and data expressed as TMRM fluorescence intensity normalized to MTG signal.

### 3.10. *Mitochondrial respiratory chain enzymes activity*

Enzymatic activities of the ETC complexes were analyzed following Spinazzi et al.[159] with minor adjustments. Cell pellets underwent three cycles of freeze-thawing in a 20 mM hypotonic potassium phosphate buffer (pH 7.5), followed by spectrophotometric analysis of mitochondrial complexes activity at 37°C using a Jasco-V550 spectrophotometer (Jasco, Easton, MD, USA) equipped with a stirring device and thermostatic control. Complex I (NADH:decylubiquinone oxidoreductase) activity from 100 µg of isolated mitochondria was assessed in 50 mM phosphate buffer at 340 nm (ε NADH = 6.22 $mmol^{-1}$ $cm^{-1}$) added by 300 µM potassium cyanide (KCN), 10 µM antimycin A, 2.5 mg $ml^{-1}$ fatty acid-free BSA, 100 µM NADH, and 60 µM decylbenzoquinone (DB). Complex I specific activity was determined by inhibiting it with 10 µM rotenone. Complex II (Succinate dehydrogenase) activity was assessed in potassium phosphate buffer (25 mM, pH 7.5) at λ= 600 nm (ε DCPIP = 19.1 $mmol^{-1}$ $cm^{-1}$) after the addition of 150 µg of cell lysate, 1 mg $ml^{-1}$ fatty acid–free BSA, 300 µM KCN, 20 mM succinate, 80 µM 2,6-Dichlorophenolindophenol sodium salt hydrate (DCPIP; Sigma), and 50 µM DB. The specific activity of Complex II was determined by adding 10 µM of the specific inhibitor carboxine (Sigma). Complex II+III (Succinate cytochrome c reductase) activity was measured in potassium phosphate buffer (50 mM, pH 7.5), with 120 µg of cell lysate, 300 µM KCN, and 10 mM succinate. After 10 minutes of incubation, the reaction was started adding 50 µM of cytochrome c. The absorbance increase was monitored for 3 minutes at 550 nm (ε cytochrome c = 18.5 $mmol^{-1}$ $cm^{-1}$). The Complex II+III specific activity was determined by adding 18 µM antimycin A. The activity of the citrate synthase (CS) was performed measuring at 412 nm in a 100 mM Tris buffer with 0.1% Triton X-100 (ε = 13,600 $M^{-1}$ $cm^{-1}$). This analysis was conducted after introducing 30 µg of cell lysate, along with 0.1 mM acetyl-CoA, 0.5 mM oxaloacetate, and 0.1 mM 5,5'-dithiobis-2-nitrobenzoic acid (MilliporeSigma). Data were normalized to protein content assessed by the Lowry method.

### 3.11. *Lipid droplets quantification*

The staining and analysis of lipid droplets was conducted using the selective fluorescent probe Nile red[165]. Cells were initially seeded on a coverslip in complete DMEM and allowed to adhere over a 16-hour incubation period. Subsequently, cells were rinsed with NaCl 0.9% and fixed using 3.7% paraformaldehyde in PBS for 60 minutes at room temperature. After two washes with NaCl 0.9%, the paraformaldehyde was neutralized with 50 mM glycine in PBS. Following this, cells were stained with Nile Red 1 ng/ml in PBS for 10 minutes. Coverslips were mounted on microscope slides, and images were captured using a Nikon C1si confocal microscope (Nikon, Tokyo, Japan). For the quantification of lipid droplets, 30 random fields were analyzed by the ImageJ software tool (Fiji). Data were presented as the number of lipid droplets per cell.

### 3.12. *Lipid peroxidation measurement*

Lipid peroxidation was measured by the lipid peroxidation sensor BODIPY® 581/591 C11 (Thermo Fisher Scientific), as described by Pap et al[166]. In brief, cells were seeded in ibiTreat µ-Slide 8 well (Ibidi) at a density of 5 x $10^3$ cells/well in complete DMEM and incubated for 16 hours to ensure adhesion. Subsequently, cells were washed with NaCl 0.9% and stained for 30 minutes with 1 µM of BODIPY® 581/591 C11. Upon oxidation, the polyunsaturated butadienyl moiety of the dye leads to a shift of the fluorescence emission peak from red (~590 nm) to green (~510 nm). Finally, cells were washed with HBSS. Imaging was performed using a Nikon C1si confocal microscope (Nikon, Tokyo, Japan), and ImageJ software was employed for analysis. Data were expressed as the ratio of green to red fluorescence intensity.

### *3.13. Ferroptosis assay*

Almost 5 x $10^5$ cells were cultured in 96-well plates and treated with Coenzyme Q as described above. Ferroptosis was induced by incubating cells with varying concentrations of RSL3 ((1S,3R)-RSL3), an inhibitor of glutathione peroxidase 4 (GPX4). Alternatively, cells were treated with Erastin, an inhibitor of the system xc- cystine/glutamate antiporter, for 24 hours in complete medium. Following this incubation period, cell viability was assessed using an MTT ((3-(4,5-dimethylthiazol-2-yl)-2,5-diphenyltetrazolium bromide) assay. Specifically, cells were washed with HBSS and incubated for 60 minutes with 300 µM of MTT in DMEM. Afterward, cells were washed with phosphate buffer, and the formazan salts were dissolved in DMSO. Absorbance was measured at 570 nm using a multi-plate reader (EnSpire; PerkinElmer).

### *3.14. Coenzyme Q10 Internalization Assay*

Cells were previously cultured in a Petri dish. At 80% of confluence, I401 and H9c2 cells underwent a 30-minute treatment with the most common endocytosis inhibitors: 2 mM amiloride (AM)[167], known for inducing the micropinocytosis inhibition; 10 µg/mL Chlorpromazine (CPZ)[168] which inhibits clathrin-mediated endocytosis; and 200 µM genistein (GN)[169], known for inhibiting the caveolae-mediated uptake mechanism. Following this incubation period, the cells were supplemented for three hours with 100 nM UBQ, 100 nM native CoQ10, and the phytosome carrier (Vehicle). Subsequently, cells were meticulously washed with a phosphate buffer, and CoQ10 was extracted and quantified using the previously described method. Data were normalized to cells number.

### *3.15. Western Blot analysis*

Cell lysis was conducted in ice-cold RIPA buffer comprising 50 mM HEPES (Euro-Clone, Milan, Italy), 1 mM EDTA (Millipore Sigma, Burlington, MA, USA), 10% glycerol (Thermo Fisher Scientific, Waltham, MA, USA), 1% Triton X-100 (Millipore Sigma), and 150 mM NaCl, supplemented with protease (Sigma-Aldrich, 11697498001) and phosphatase inhibitors (NaF 100 mM, Na3VO4 100 mM, Pyrophosphate 100 mM, Imidazole 200 mM, pH 7) . Total protein content was quantified using the Lowry Protein Assay Kit (Bio-Rad DC Protein Assay; Bio-Rad, Hercules, CA, USA) following the manufacturer's protocol. Subsequently, protein samples (30-50 µg) were incubated for 30 min on ice and then, suspended in Laemmli buffer (BioRad, #1610737) containing β-mercaptoethanol. After that, samples were separated on 10%, 15% or Any kD Mini-Protean TGX protein gels (BioRad, #456-8124), and the separated proteins were electro-transferred onto nitrocellulose membranes utilizing the Trans-Blot Turbo Transfer System (Bio-Rad). Membranes were blocked in Tris-buffered saline with 1% Casein (Bio-Rad) or Intercept Blocking Buffer (LI-COR Biosciences, #927-60001) for 1 h at room temperature, followed by an overnight incubation at 4°C with primary antibodies. Afterward, membranes were subjected to three washes in Tris Buffered Saline buffer (Bio-Rad) and then incubated with peroxidase-conjugated secondary antibodies for 45 min at room temperature. The primary antibodies used included vinculin (mouse, 1:10,000, Millipore Sigma), γ-tubulin (mouse, 1:10,000, Millipore Sigma), β-actin (mouse, 1:10000, Millipore Sigma), β-tubulin (mouse, 1:10000, Thermo Fisher), SPART (rabbit, 1:1,000, ProteinTech, Rosemont, IL, USA), glucose-regulated protein 75 (mouse, GRP75; 1:500; Santa Cruz Biotechnology, Dallas, TX, USA), COQ7 (mouse, 1:500, Santa Cruz Biotechnology), COQ9 (mouse, 1:500, Santa Cruz Biotechnology), VDAC (mouse, 1:500, Santa Cruz Biotechnology), TIM23 (mouse, 1:100, Santa Cruz. Biotechnology), MCU (mouse, 1:100, Santa Cruz. Biotechnology), TOM70 (mouse, 1:250, Santa Cruz. Biotechnology), TOM20 (rabbit, 1:1000, Abcam), NDUFA9-CI (mouse, 1:1000, Invitrogen), COXI-COIV (mouse, 1:1000, Invitrogen), SDHA-COII, (mouse. 1:1000, Invitrogen), subunit-β-ATPase-CV (mouse, 1:1000, Invitrogen), UQCRC2 core II subunit-COIII (mouse, 1:1000, Molecular Probes),

PGC1-α (rabbit, 1:1000, Novus Bio), TFAM (mouse, 1:500, Santa Cruz), OGDH (rabbit, 1:1000, ProteinTech). Peroxidase-conjugated secondary antibodies employed were anti-mouse IgG (1:8,000; Millipore Sigma) and anti-rabbit IgG (1:8,000; Millipore Sigma). For the detection of some proteins, membranes were incubated for 1 hour at room temperature with anti-mouse (LI-COR Biosciences, #926-32212) or anti rabbit (LI-COR Biosciences, #926-68073) IgG secondary fluorescent antibodies (1:15000 dilution). Bands were visualized using WESTAR SUPERNOVA (Cyanagen, Bologna, Italy) and detected by the ChemiDoc XRS+ system (Bio-Rad) or LI-COR CLx imaging system. Densitometric analysis was carried out using ImageLab (Bio-Rad) or Image Studio™ software.

### *3.16. Assessment of Mitochondrial Network and Morphology*

To visualize the mitochondrial network, cells were seeded in ibiTreat µ-Slide 8 well plates (Ibidi, Martinsried, Germany) at a density of 5 x $10^3$ cells/well in 300 µl of complete medium and maintained at 37°C in a humidified atmosphere of 95% air, 5% CO2. After 24 hours, cells were stained with 130 nM of MitoTracker Green dye following the manufacturer's instructions (MitoTracker™ Green FM; Thermo Fisher Scientific). Subsequently, images were captured using a Nikon C1 confocal microscope (Nikon, Tokyo, Japan), and mitochondrial network morphology was evaluated using ImageJ software, as described by Bonora et al.[170]. In brief, the green channel underwent background subtraction with a radius of 10 pixels and a median filter to reduce noise. An automatic threshold value was then applied to delineate the particles. Lastly, images were analyzed using Mitochondrial Network Analysis (MiNA) software[171].

### *3.17. Mitochondrial Mass Determination*

Firstly, cells were plated in 96-well plates (OptiPlate Black; Perkin Elmer, Inc., Shelton, CT, USA) at a density of 15,000 cells per well and incubated overnight to facilitate adhesion. Subsequently, cells were treated with 200 nM of the mitochondria-specific fluorescent probe Mitotracker Green FM (MTG, Molecular Probes) in complete culture medium for 30 minutes at 37°C and 5% CO2. After treatment, cells were washed twice with PBS and fluorescence was measured using a multiplate reader (Enspire, Perkin Elmer, Waltham, MA, USA) ($\lambda_{exc}$=485 nm and $\lambda_{em}$ =530 nm)[172]. Fluorescence intensity for each mitochondria was analyzed using ImageJ software.

### *3.18. Cell Proliferation assay*

Control and mutant cells (2.5 x $10^3$ cells per well) were cultured into 48-well flat-bottomed plates. A Real-time cell proliferation was monitored for 96 hours using the IncuCyte® S3 Live Cell Analysis System (Roche Applied Sciences, Indianapolis, IN, USA) and the doubling time calculated using the GraphPad Prism 8 software.

### *3.19. Measurement of Intracellular Free Calcium levels*

Intracellular free calcium levels were evaluated in live cells using the Fluo-3 (Fluo-3, AM) probe (Thermo Fisher Scientific), following the manufacturer's instructions. Cells were plated in an ibiTreat µ-Slide 8 well at a density of 5 x $10^3$ cells/well, and the emission of the calcium-free fluorescent probe was measured using a Nikon C1si confocal microscope (Nikon) ($\lambda_{exc}$=488 nm; $\lambda_{em}$= 530 nm). Fluorescence intensity was quantified using ImageJ software standard tools for, at least, 50 different cells for each experimental condition.

### *3.20. Glutathione quantification*

Control and mutant cells were plated in 96-well plates (OptiPlate Black; PerkinElmer) at a density of 7 x $10^3$ cells/well in complete DMEM and incubated for 16 hours to allow adhesion. Following this incubation period, the medium was removed, and total glutathione was quantified using the GSH/GSSG-Glo™ kit (Promega, Madison, WI, USA) according to the manufacturer's instructions. Luminescence was measured using a multiplate reader (Enspire, Perkin Elmer). The data are presented as the mean ± standard error of at least three independent experiments.

### *3.21. Mitochondrial protein import assessment*

Control and mutant cell lines were seeded in ibiTreat µ-Slide 8 well at a density of 3.5 x $10^3$ cells per well and incubated for 16 hours to ensure adhesion. Then, cells were concurrently transfected with a mitochondria-targeted RFP (CellLight Mitochondria-RFP, BacMam 2.0) and stained with MitoTracker Green (ThermoScientific). CellLight Mitochondria-RFP, BacMam 2.0 (Life Technologies, Grand Island, NY) was introduced into the cells at a concentration of 40 particles per cell, following the manufacturer's instructions. After 48 hours, cells were stained with MitoTracker Green and observed using a Nikon C1si confocal microscope (Nikon) and the relative fluorescence for each channel was plotted to assess signal co-distribution of a region of interest (ROI) delineated along a single cell profile. For some experiments, cells were transfected with a plasmid encoding for the mitochondrial protein HyPer7[173] and then stained with MitoTracker RED. Imaged were acquired using a Confocal Microscope (Leica Microsystems).

### *3.22. Blue Native Polyacrylamide Gel Electrophoresis (BN-PAGE) assay*

Mitochondria were extracted from a 2.5 x $10^6$ as described by Ugalde[174] et al. Then, 50 ug of mitochondria were resuspended in 50 uL of Resuspension Buffer composed by 1.5 M aminocaproic acid (Sigma), 50 mM Bis-tris (Sigma) pH 7.0 at 4°C with 2 uL of 20% Lauryl maltoside (Sigma). After 5 minutes incubation in ice, samples were centrifuged at 20,000 x g for 30 min at 4C and the supernatant was transferred into a new tube. Finally, 10 uL of 10X sample Buffer (750nM aminocaproic acid, 50 mM Bis-Tris, 0.5mM EDTA, pH 7.0 at 4C, 5% Brilliant Blue G (Sigma b0770-5g)) were added and 25 µl of mitochondria loaded onto NativePage 4-16% Bis-Tris Gel (Invitrogen). Samples were run in anode and Dark Blue Cathode Buffer at 100 V for 15 minutes at 4°. After this time, the voltage was increased to 150 V for 90-120 minutes. Dark Blue Cathode Buffer was replaced with Light Blue Cathode Buffer when the dye front migration was 1/3 of the gel. Once the run was over, gel was rinsed 3 times with bi distilled water and stained by SimplyBlue™ SafeSolution (Cat. number #LC6060, Invitrogen) for 1 hour. Subsequently, gel was rinsed with a large volume of water for 1 hours and washed overnight in a solution 4% NaCl. The day after, images were acquired using LI-COR CLx imaging system and proteins were transferred to a PVDF membranes following the typical transfer protocol. Membranes were then blocked with 5% BSA in TBS-Tween for several hours and incubated overnight at 4℃ with specific primary antibodies against the proteins of interest (anti-NDUFA9 1:2000, anti-70KDa-CoII 1:2000 and anti-COX1-CoIV 1:2000, Thermofisher; anti-core 2 subunit-CIII 1:2000, anti-ATPase βsubunit-CV 1:2000, Molecular Probes). For proteins detection, the membranes were incubated for 1 h anti-mouse HRP-conjugated secondary antibodies (Jackson Immunoresearch, #115-035-146) and imaged by chemiluminescence on a ChemiDoc system (BioRad). Band intensities were quantified using Image Studio software (vs3.1, LI-COR Biosciences).

### *3.23. RNA sequencing*

RNA extraction from cell pellet was performed using TRIzol (Thermofisher #15596026) using the SV Total RNA isolation System (Promega, #Z3100). Subsequently, 30 RNAseq libraries were generated from 200 ng of RNA per sample utilizing the Lexogen QuantSeq 30 mRNA-Seq Library Prep Kit FWD designed for Illumina. To minimize run variability, these libraries were pooled. The sequencing was carried out with single-end 86 bps on an Illumina NextSeq500 sequencer (Cornell Genomics Facility). For data preprocessing, raw sequence reads underwent processing with the BBDuk program within the BBMap package. Trimmed reads were aligned to the human genome hg38 using the STAR aligner. SAM files were then converted to BAM to read overlapping reads per gene using HTSeq-count (version 0.6.1)[175]. Subsequently, the transcripts quantification was calculated through Salmon tool[176] and the Differential Expression Genes (DEGs) analysis obtained by Enrichr software tool[177].

### *3.24. qPCR*

RNA was extracted from cell pellet using Trizol-chloroform precipitation and the SV Total RNA isolation System (Promega, #Z3100). RNA concentration was measured with NanoDrop1000. Then, 0.2-1µg of total RNA were converted into cDNA by ImProm II™ Reverse Transcription System (Promega, #A3800) following the manufacturer's instructions. Quantitative real-time PCR (qPCR) amplification of cDNA was performed with the SYBR Green PCR Master Mix (ThermoFisher Scientific) on a QuantStudio 6 Flex Real-Time PCR system (ThermoFisher Scientific). Standard cycling parameters were used, and relative expression was normalized to the endogenous control (beta-actin) using the $\Delta\Delta^{Ct}$ comparative method. The quantification of mRNA expression levels was carried out using the following primers: *MT-ATP6* forward: 5'-CGCCACCCTAGCAATATCAA-3' reverse: 5'-TTAAGGCGACAGCGATTTCT-3'; *MT-ND3:*

forward:5’-GCGGCTTCGACCCTATATCC-3’, reverse: 5’-AGGGCTCATGGTAGGGGTAA-3’; *MT-CO2*: forward: 5’-CTGAACCTACGAGTACACCG-3’: reverse: 5’-TTAATTCTAGGACGATGGGC-3’; *MT-CO3*: forward: 5’-ACCAATGATGGCGCGATGTA-3’, reverse: 5’-GGCTGGAGTGGTAAAAGGCT-3’; *TIMM13*: forward 5’-GTATAGGGAAACCTGGGGGC-3’, reverse: 5’-GTGTTCCAGGCGTCCATGTAG-3’; β-Actin: forward 5’- CCTGGCACCCAGCACAAT-3’, reverse: 5’- GGGCCGGACTCGTCATACT-3’.

### *3.25. Rescue experiments*

For the rescue experiments, 4 × $10^5$ control and mutant cells were plated 24 hours before transfection with a plasmid carrying wild-type SPART (pcDNA3.1-SPART) or an empty vector, following established procedures[154]. Briefly, the human SPART coding sequence was amplified from SH-SY5Y-derived cDNA using KAPA HiFi HotStart Taq Polymerase (Kapa Biosystems, Roche Diagnostic, Mannheim, Germany) following the manufacturer's guidelines. The resulting fragment was digested with XhoI and HindIII (New England Biolabs, Hitchin, UK), cloned into the pcDNA3.1 vector, and subsequently sequenced to confirm accurate insertion. The plasmid expressing wild-type SPART and pcDNA3.1 empty vector (3 µg/experiment) were transfected into the mutated and control cells respectively. The transfection efficiency was enhanced using Lipofectamine 3000 following the manufacturer’s instructions. Forty-eight hours post transfection, cells were harvested and subjected to two washes with PBS. Spartin overexpression was detected through Western blot analysis as previously detailed. The ATP and ADP levels determination, as well as the evaluation of intracellular free $Ca^{2+}$, were conducted following the procedures described before. The rescue of the cell growth after CoQ10 treatment, 2.5 x $10^3$ cells/well were seeded in a 48-well flat-bottomed plate (Corning, Sigma) at a density of in complete DMEM and allowed to attach overnight. Subsequently, both control and mutant cells were treated for 96 hours with 100 nM of UBQ® (Indena S.R.L, Milan, Italy), and cell growth was quantified as previously outlined. For ATP and ADP determination, control and mutant cells were seeded in a 6-multiwell plates (Corning, Sigma) at a density of 5 x

$10^4$ cells/well in complete DMEM and incubated for 16 hours to facilitate the adhesion. Cells were cultured in complete DMEM supplemented with 100 nM of UBQ® for 24 hours. Following the incubation period, cells were collected, and ATP and ADP determination were carried out as described above.

# 4. Results

## *4.1. UBQ® supplementation significantly increases the endogenous CoQ10 levels in both I407 and H9c2 cell lines.*

Firstly, we evaluated the UBQ® uptake capacity in I407 and H9c2 cell lines. The cultured cells were treated with 100 nM of UBQ®, native CoQ10 (CoQ10) and phytosome alone as vehicle (vehicle) for 24 hours in culture medium. The CoQ10 extraction by HPLC and the following quantification revealed a marked increase in both cell lines treated with the UBQ®, particularly noticeable in the cardiomyoblasts. The I407 showed a significantly increase of the CoQ10 content after incubation with the UBQ® (Fig.6A) from 0.01 nmoles/$10^6$ cells to 0.05 nmoles/$10^6$ cells, whereas no differences have been observed in I407 cells treated with the native formulation of CoQ10 (CoQ10) in comparison with control cells. Likewise, the UBQ® supplementation significantly raised the total CoQ10 amount from 0.013 nmoles/$10^6$ cells to 0.41 nmoles/$10^6$ cells (Fig.6B) in H9c2 cells. Instead, the CoQ10 treatment didn't significantly alter the CoQ10 level in these cells. Furthermore, also the mitochondrial content of CoQ10 remarkably increased in both cell lines after UBQ® supplementation (Fig.6C and 6D). Indeed, we observed a 33% and a 99% increase of mitochondrial CoQ10 in I407 (0.28 nmoles/mg to 0.44 nmoles/mg) and H9c2 cells respectively compared to samples treated with vehicle and native CoQ10. Then, to deeper investigate the beneficial role of UBQ® treatment, we assessed the redox state of CoQ10 in cultured cells following supplementation with UBQ®, native CoQ10, and vehicle. As shown, in I407 cells the supplementation with UBQ® but not with CoQ10 and vehicle statistically increased the amount of the oxidized CoQ10 by threefold without affecting the levels of the reduced form (Fig.6E). The H9c2, instead, manifested an increase of oxidized CoQ10 by 20 times along with a 13-fold increase in the reduced form (Fig.6G). The H9c2, being a rat cell line, predominantly contains coenzyme Q as a CoQ9 analogue. Consequently, we conducted HPLC analysis to evaluate the CoQ9 content. The results demonstrated that supplementation with

UBQ®, CoQ10, or the vehicle did not induce any change in the level or redox state of CoQ9 (Fig. 6F).

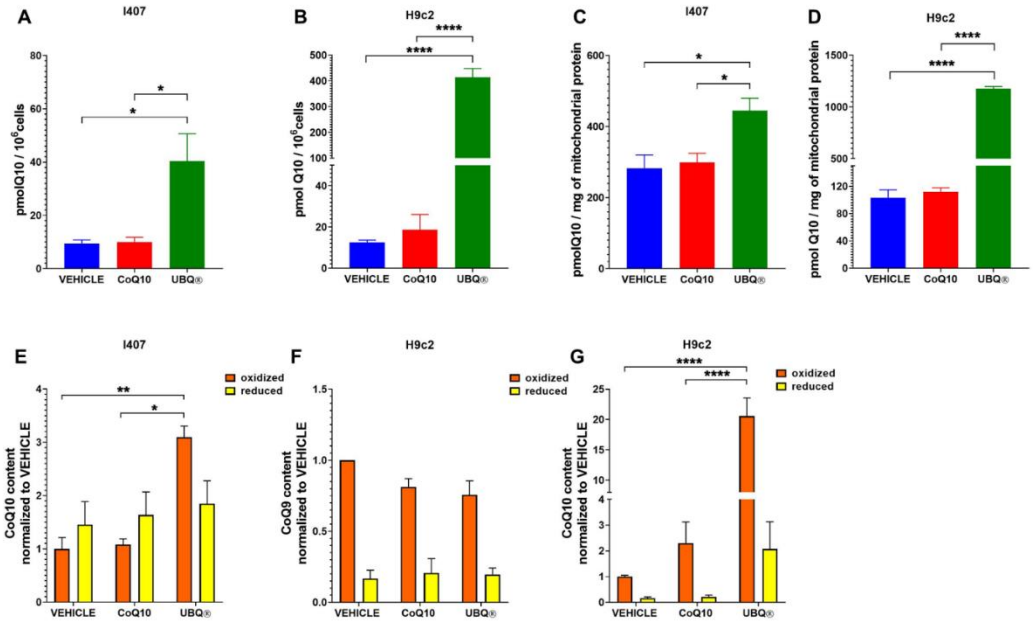


**Fig.6 Determination of Coenzyme Q10 in various cell lines following incubation with vehicle, native CoQ10 and UBQ®**. Total CoQ10 content in I407 cells (A) and H9c2 cells (B) treated for 24 hours with 100 nM of phytosome (Vehicle), 100 nM of native CoQ10 (CoQ10) and 100 nM of CoQ10 phytosome (UBQ®) (n = 3). Mitochondrial CoQ10 amount in I407 cells (C) and H9c2 cells (D) treated for 24 hours with phytosome (Vehicle), 100 nM of native Q10 (CoQ10) and 100 nM UBQ (UBQ®) (n = 3). Data were normalized to mitochondrial protein content (n = 3). (E) Reduced and oxidized CoQ10 content in I407 cells treated as above. Data are presented as a fold increase over the oxidized CoQ10 content of the vehicle-treated sample (n = 3). (F) Reduced and oxidized CoQ9 content in H9c2 cells treated as above. (G) Reduced and oxidized CoQ10 content in H9c2 cells treated as above. Data are presented as a fold increase over the oxidized CoQ9 or CoQ10 content of the vehicle-treated sample (n = 3). For all panels, data are presented as the mean ± s.e.m, * $p \leq 0.05$; ** $p \leq 0.01$; **** $p \leq 0.0001$. Statistical analysis was performed using one-way ANOVA followed by Tukey's honest significant difference test.

### *4.2. Supplementation with UBQ® improves Oxygen Consumption Rate, ATP and NADH level, protein content, transmembrane potential, and citrate synthase activity*

Since it has been largely reported that exogenous CoQ10 treatment improves several mitochondrial functions[147],we investigated the effect of vehicle, native CoQ10 and UBQ® supplementation in H9c2 and I407 cells on different bioenergetic parameters, such as oxygen consumption, ATP and NADH level, protein content, transmembrane potential, and citrate synthase activity. The oxygen consumption rate (OCR) was determined in intact cells using polarographic techniques under basal conditions (endo), in the presence of the ATPase inhibitor oligomycin A (oligo), and in the presence of the uncoupler carbonyl cyanide 4-(trifluoromethoxy) phenylhydrazone (FCCP). As reported in the Fig. 7A and 8A, the incubation for 24 hours with UBQ® markedly increased the uncoupled rate of oxygen consumption in both I407 (1.55 nmoles O2 $min^{-1}/10^6$ cells in controls; 3.12 nmoles O2 $min^{-1}/10^6$ cells in UBQ®) and H9c2 cells (4.44 nmoles O2 $min^{-1}/10^6$ cells in controls; 9.72 nmoles O2 $min^{-1}/10^6$ cells in UBQ®). At contrary, treatment with native CoQ10 showed no effect in I407 and H9c2 either. As the oxidative phosphorylation is supported by the mitochondrial NADH oxidation, we measured its level by fluorometric analysis in I407 and H9c2 cells supplemented with UBQ® and native CoQ10. UBQ® treatment significantly decreased NADH levels compared to vehicle treatment in I407 (−20.8%) and H9c2 (−17.7%) cells, respectively (Figure 7C and Figure 8C). Moreover, effects on ATP and protein content were assessed in both cell lines after supplementation with 100 nM of CoQ10 and UBQ®. HPLC analysis demonstrated that the ATP amount improved in I407 and H9c2 after 24 hours of treatment with UBQ® whereas no differences were detected in native CoQ10 treated cells (Fig.7B and 8B). Notably, the ratio between protein amount and cells number increased in I407 (1.62 fold change) and in H9c2 (1.415 fold change) in comparison to vehicle treated cells (Fig.7D and 8D). Considering that the ubiquinone plays a crucial role in the mitochondrial transmembrane potential (ΔΨm) establishment, we analyzed it in intact cells through the fluorescent dye 5,5,6,6'-tetrachloro-1,1',3,3' tetraethylbenzimi-dazoylcarbocyanine iodide (JC-1). The JC-1

probe is a lipophilic cationic dye which enters within the mitochondria in a potential dependent manner[178]. In its monomeric form, JC-1 has a green fluorescence emission at approximately 529 nm. When accumulated, the dye produces reversable complexes called J-aggregates which exhibit both excitation and emission in the red spectrum, with a maximum at around 590 nm. Consequently, in healthy cells with a normal ΔΨM, JC-1 enters and accumulates in the energized and negatively charged mitochondria, rising the red fluorescent J-aggregates. At contrary, in unhealthy and less negative mitochondria, the dye maintains its green fluorescence since it's not able to achieve the sufficient concentration to induce the formation of the J aggregates. For this reason, the red/green fluorescence ratio of the dye into the mitochondria can be regarded as a direct measure of mitochondrial polarization. The ΔΨM in I407 and H9c2 cells supplemented with UBQ® showed an increase by 1.92 and 1.26 times respectively in comparison to vehicle treated cells. Conversely, no changes in the red/green fluorescence were identified in both cell lines. Finally, we measured the Citrate synthase (CS) activity, one of the most commonly used biomarker for the mitochondrial content[179,180], in both cell lines treated with vehicle, native CoQ10 and UBQ®. As indicated in Fig. 7E, the CS activity in I407 cells incubated for 24 hours with UBQ® was significantly improved compared to the cells treated vehicle (1.42 fold chain). Notably, the supplementation with native CoQ10 didn't induce any effect on the enzyme activity.

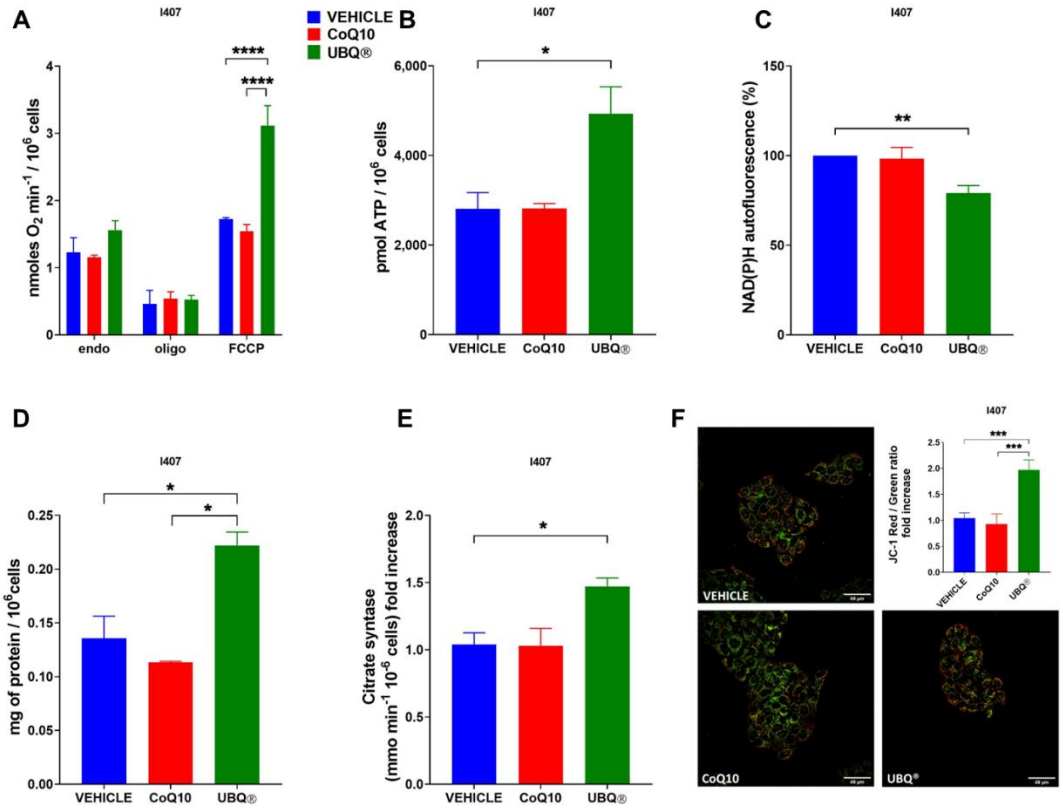


**Fig.7 UBQ® treatment beneficials on bioenergetic functions on I407 cell line**. Cells were subjected to incubation with 100 nM of phytosome (vehicle), 100 nM of native CoQ10 (Q10) and 100 nM of CoQ10 phytosome (UBQ®). (A) Mitochondrial Oxygen consumption rate in intact cells was assessed for endogenous respiration (endo), in the presence of 1 µM oligomycin A (oligo), and 0.25–1 µM carbonyl cyanide 4-(trifluoromethoxy) phenylhydrazone (FCCP). The data are expressed as nanomoles of oxygen per minute and normalized to the cell number (n = 3). (B) Total cellular ATP quantification in cell lysate (n = 3). (C) NAD(P)H autofluorescence determination in intact cells. The data were normalized to the cell number and expressed as a percentage of the vehicle-treated sample fluorescence signal; (n = 3). (D) Cellular protein content determination (n = 3). (E) Citrate synthase activity determination normalized to cell number. The data are shown as a fold increase over the vehicle-treated sample; (n = 3). (F) Representative micrographs of intact cells stained with the fluorescent dye JC-1. Quantitative analysis of the Red/Green fluorescence ratio was assessed using ImageJ software. For each condition, at least two randomly chosen fields were analyzed. Data are presented as a Red/Green fluorescence ratio fold increase over the vehicle-treated sample; (n = 5). For all panels, the data are presented as the mean ± s.e.m, * $p \leq 0.05$; ** $p \leq 0.01$; *** $p \leq 0.001$; **** $p \leq 0.0001$. Statistical analysis was performed using one-way ANOVA followed by Tukey's honest significant difference test.

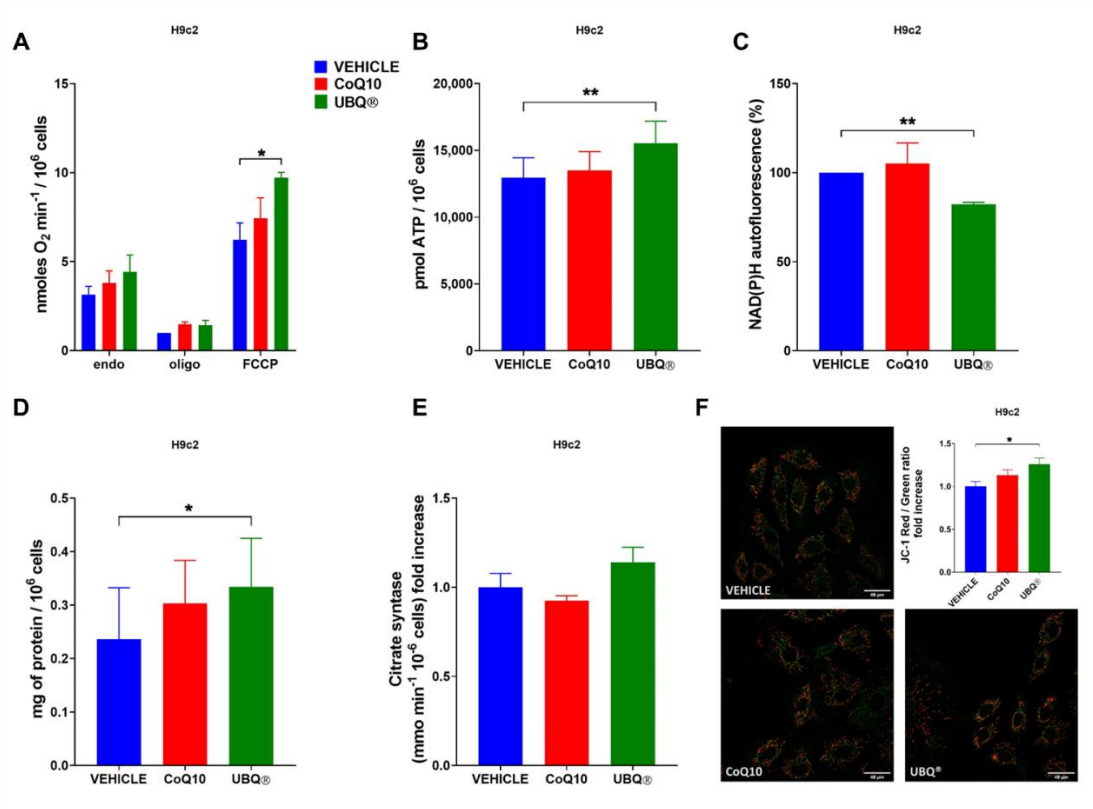


**Fig. 8: Beneficial Effects of UBQ® Treatment on Bioenergetic Functions in the H9c2 Cell Line**. Cells were incubated with 100 nM of 100 nM of phytosome (vehicle), 100 nM of native CoQ10 (Q10) and CoQ10 phytosome (UBQ®). (A) Assessment of mitochondrial oxygen consumption rate in intact cells, including endogenous respiration (endo), in the presence of 1 µM oligomycin A (oligo), and 0.25–1 µM carbonyl cyanide 4-(trifluoromethoxy) phenylhydrazone (FCCP). Data are expressed as nanomoles of oxygen per minute and normalized to the cell number (n = 3). (B) Quantification of total cellular ATP in cell lysate (n = 3). (C) Determination of NAD(P)H autofluorescence in intact cells, normalized to the cell number and expressed as a percentage of the vehicle-treated sample fluorescence signal (n = 3). (D) Measurement of cellular protein content (n = 3). (E) Assessment of citrate synthase activity normalized to cell number, presented as a fold increase over the vehicle-treated sample (n = 3). (F) Representative micrographs of intact cells stained with the fluorescent dye JC-1. Quantitative analysis of the Red/Green fluorescence ratio was performed using ImageJ software. For each condition, at least two randomly chosen fields were analyzed. Data are presented as a Red/Green fluorescence ratio fold increase over the vehicle-treated sample (n = 5). All data are presented as the mean ± s.e.m, * $p \leq 0.05$; ** $p \leq 0.01$; *** $p \leq 0.001$; **** $p \leq 0.0001$. Statistical analysis was performed using one-way ANOVA followed by Tukey's honest significant difference test.

### *4.3. CoQ10 Phytosome formulation protects against Oxidative Stress*

Given that Coenzyme Q10 is recognized as the principal endogenous lipid-soluble antioxidant, we investigated the protective role of UBQ® against the generation of reactive oxygen species (ROS). Initially, cells were treated with varying concentrations of CoQ10 and UBQ® ranging from 6.25 to 100 nM. Following a 24-hour incubation, ROS production was induced by tert-Butyl hydroperoxide (TBH), a radical polymerization initiator. The generation of ROS was assessed using the intracellular hydrogen peroxide ($H_2O_2$) sensor 2',7'-dichlorodihydrofluorescein diacetate (DCFDA), a widely employed probe for detecting intracellular $H_2O_2$ and oxidative stress. The cell-permeable H2DCFDA, commonly employed for measuring cellular H2O2[181], undergoes deacetylation by cellular esterases upon entry into cells to form 2',7'-dichlorodihydrofluorescein (H2DCF). In the presence of reactive oxygen species (ROS), predominantly $H_2O_2$, H2DCF undergoes rapid oxidation to produce 2',7'-dichlorofluorescein (DCF), characterized by high fluorescence with excitation and emission wavelengths of 498 and 522 nm, respectively. ROS levels were measured under both culture conditions, reflecting endogenous ROS, and after 30 minutes of TBH treatment, representing induced ROS. The results (Fig. 9) indicated that low concentrations of UBQ® effectively countered both endogenous (ranging from 6.25 to 25 nM) and induced ROS (from 5.25 to 50 nM) in the I407 cell line (Fig. 9A and 9B). In H9c2 cells, however, UBQ® appeared to protect only against induced ROS without exerting any effects on endogenous ROS (Fig. 9E and Fig. 9F). Importantly, treatment with native CoQ10 did not demonstrate an effective protection in both cell lines (Fig.9C, D, G and H).

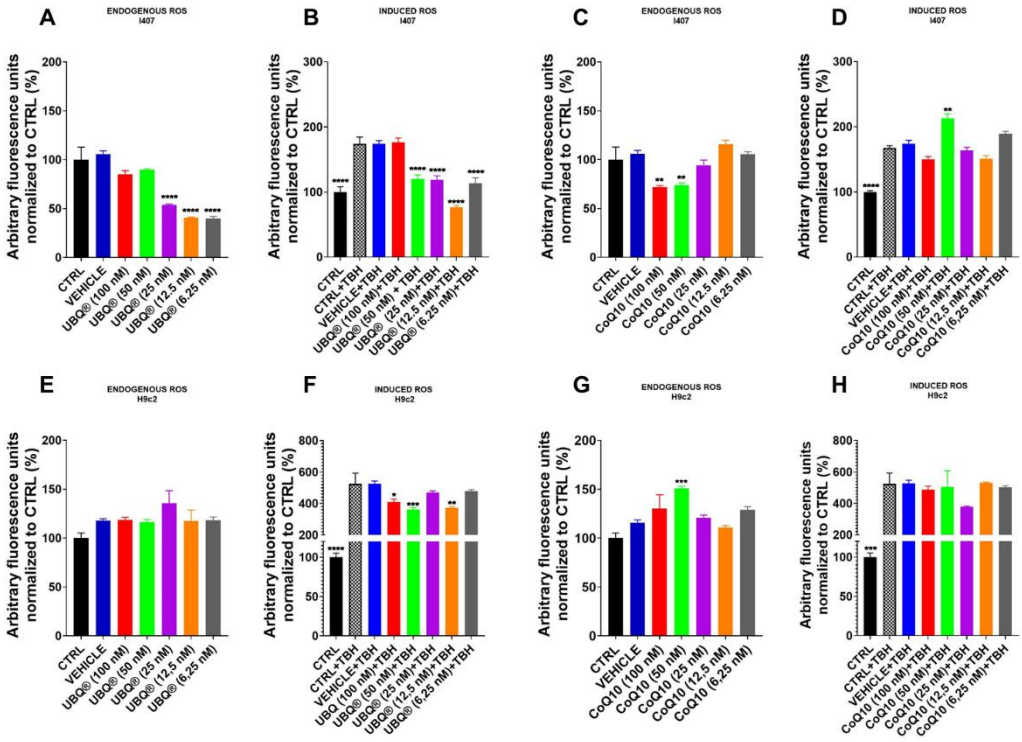


**Fig.9 Oxidative stress evaluation in I407 and H9c2 cells**. Determination of oxidative stress in I407 and H9c2 cells was conducted following a 24-hour incubation with varying concentrations of phytosome (vehicle), native CoQ10 (CoQ10), and CoQ10 phytosome (UBQ®). Endogenous oxidative stress was assessed in intact cells of I407 (A, C) and H9c2 (E, G) using the fluorescent probe 2',7'-dichlorodihydrofluorescein diacetate (DCFDA). Additionally, oxidative stress induction was carried out in intact I407 (B, D) and H9c2 (F, H) cells using 130 µM of tert-butyl hydroperoxide (TBH). The data, normalized to protein content, are presented as a percentage of the untreated control fluorescence signal (n = 48). In all panels, the results are presented as the mean ± s.e.m, with statistical analysis conducted using one-way ANOVA followed by Tukey's honest significant difference test.

### *4.4. UBQ® counteracts the lipid membrane peroxidation and Ferroptosis*

Coenzyme Q10 protects membranes from oxidative damage by directly interrupting the lipid peroxidation chain and maintaining the redox system of the plasma membrane[76,182,183]. To assess its protective role, we utilized the fluorescent fatty acid analogue BODIPY™ 581/591 C11[166,184,185]. Upon free radical-induced oxidation, the fluorescent properties of BODIPY™ 581/591 C11 transition from red to green, enabling ratio imaging of oxidant activities at the cellular level. Staining with BODIPY™ 581/591 C11 revealed that UBQ® treatment was the only treatment capable of reducing lipid peroxidation in both I407 and H9c2 cell lines compared to vehicle and native CoQ10 treatments (Fig. 10A and 10D). Specifically, UBQ® supplementation in I407 and H9c2 cells led to a significant increase in the red/green signal (1.70 and 3.89-fold change, respectively) compared to vehicle-treated cells. In contrast, supplementation with native CoQ10 had no significant effects in I407 cells. Interestingly, H9c2 cells treated with native CoQ10 exhibited a notable protection against lipid peroxidation comparable to UBQ® supplementation. Ferroptosis is a recently identified form of cell death characterized by iron-dependent lipid peroxidation, resulting in a decline in the cellular glutathione (GSH) levels[76]. Recognizing the reduction in lipid peroxidation following UBQ® treatment, we investigated the potential protective role of phytosome CoQ10 in I407 and H9c2 cells pretreated with Erastin (a selective inhibitor of the cysteine uptake that leads to a severe reduction in intracellular GSH levels) and 1S,3R-RSL3 (RSL3), a specific inhibitor of GPX4 activity. MTT assay data, showed in Fig. 10B and 10E, illustrate the percentage of viable cells at various Erastin concentrations. Notably, a 24-hour supplementation with 100 nM UBQ® increased the $IC_{50}$ in I407 cells from 29 µM (vehicle) to 42 µM (Fig. 10B). Similarly, UBQ® treatment in H9c2 cells exhibited a comparable trend, elevating the IC50 from 4.4 µM in the vehicle-treated cells to 7.7 µM (Fig. 10E). Conversely, native CoQ10 demonstrated no protective effect against cell death in both I407 and H9c2 cell lines. Furthermore, UBQ® demonstrated a partial recovery of ferroptosis induced by RSL3 treatment in both I407 (44.2% viable cells with Vehicle + RSL3 vs. 63.1% viable cells with UBQ + RSL3) and H9c2 cells (30.5% viable cells with Vehicle + RSL3 vs. 47.28% viable cells with UBQ + RSL3). As expected, no protection against

ferroptosis was observed in cells treated with 100 nM native CoQ10. These results collectively suggest that UBQ® treatment robustly counteracts oxidative stress during ferroptosis.

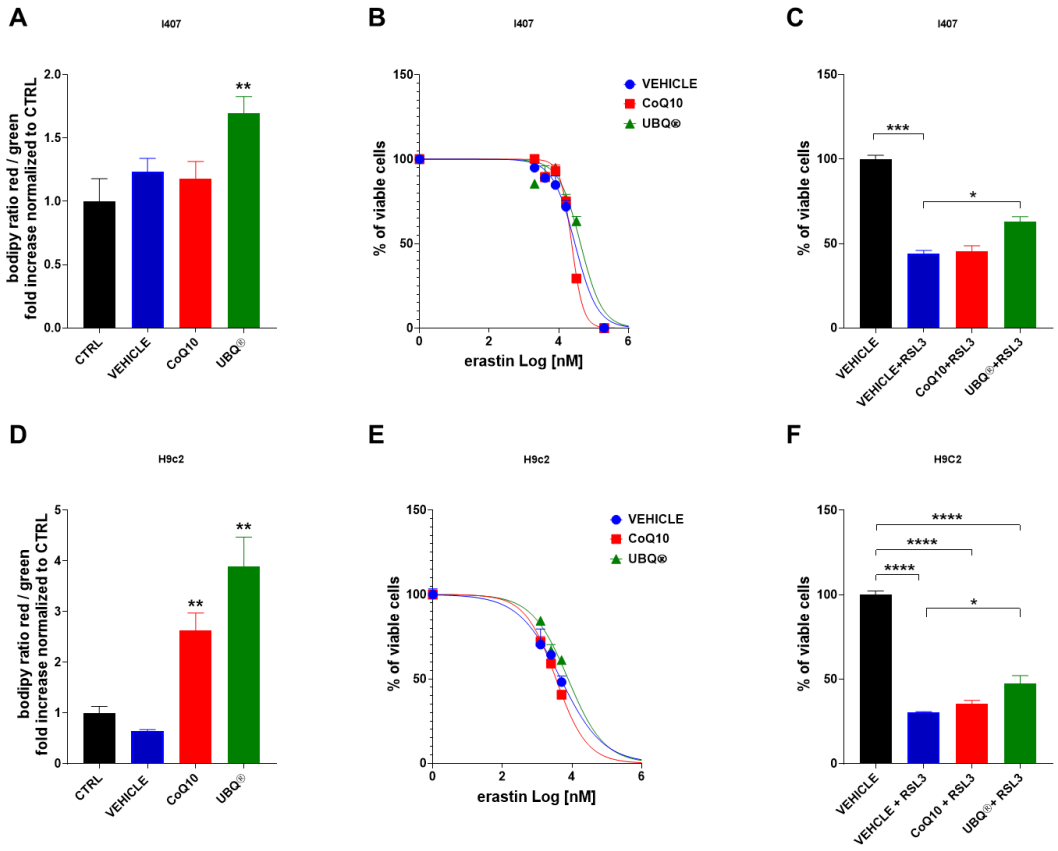


**Fig.10 Evaluation of UBQ® efficiency against lipid membrane peroxidation and ferroptosis**. Evaluation of lipid membrane peroxidation in I407 and H9c2 cells was conducted by treating them with 100 nM phytosome (vehicle), native CoQ10 (Q10), CoQ10 phytosome (UBQ®) or leaving them untreated as controls. The peroxidation status of membrane lipids was assessed using the fluorescent dye BODIPY™ 581/591 C11 in fixed I407 (Fig. A) and H9c2 (Fig. D) cells through confocal microscopy. Quantitative analysis of the Red/Green fluorescence ratio was performed using ImageJ software, and the data are presented as a fold increase over untreated controls (n = 5). Viability assays were carried out for I407 (Fig. B and C) and H9c2 (Fig. E and F) cells under different conditions. For Erastin-induced ferroptosis, cells were treated with various concentrations of Erastin, and viability was assessed by MTT assay after 24 hours of incubation (n = 3). Similarly, the viability of cells treated with the GPX4 inhibitor RSL3 (1 µM for I407 and 300 nM for H9c2) was evaluated by MTT assay after 24 hours (n = 3). Data are presented as a percentage of vehicle-treated viable cells. For all panels, the mean ± s.e.m is shown, and statistical analysis was performed using one-way ANOVA followed by Tukey's honest significant difference test.

### *4.5. The CoQ10 phytosome formulation uptake is promoted by micropinocytosis process*

The uptake mechanism of Coenzyme Q10 has been a fascinating topic for decades. Understanding how it is absorbed by different cells and tissues could provide valuable insights to enhance its incorporation. In this study, we explored three potential pathways for UBQ® internalization by exposing cells to three different endocytosis inhibitors: amiloride (AM) for micropinocytosis inhibition, chlorpromazine (CPZ) for clathrin-mediated endocytosis inhibition, and genistein (GN) for caveolae-mediated uptake mechanism inhibition. Subsequently, cells were incubated with 100 nM of UBQ® for three hours and the total Coenzyme Q10 amount was extracted and quantified as described in the material and methods section. As indicated in Fig.11A and 11B, the treatment with the AM promoted a 46% decrease and 63% decrease of the UBQ® uptake in both I407 and H9c2 cell lines respectively. Furthermore, we explored the presence of intracellular lipid droplets after UBQ®, native CoQ10 and vehicle supplementation by employing the fluorescent dye Nile red, which selectively stains neutral lipids within cells. Fig.11C and 11D revealed a significant increase in the number of lipid droplets in cells treated with UBQ®, CoQ10, and the vehicle. This observation implies that both Coenzyme Q10 and lipids from the phytosome are, to some extent, internalized in the form of lipid aggregates.

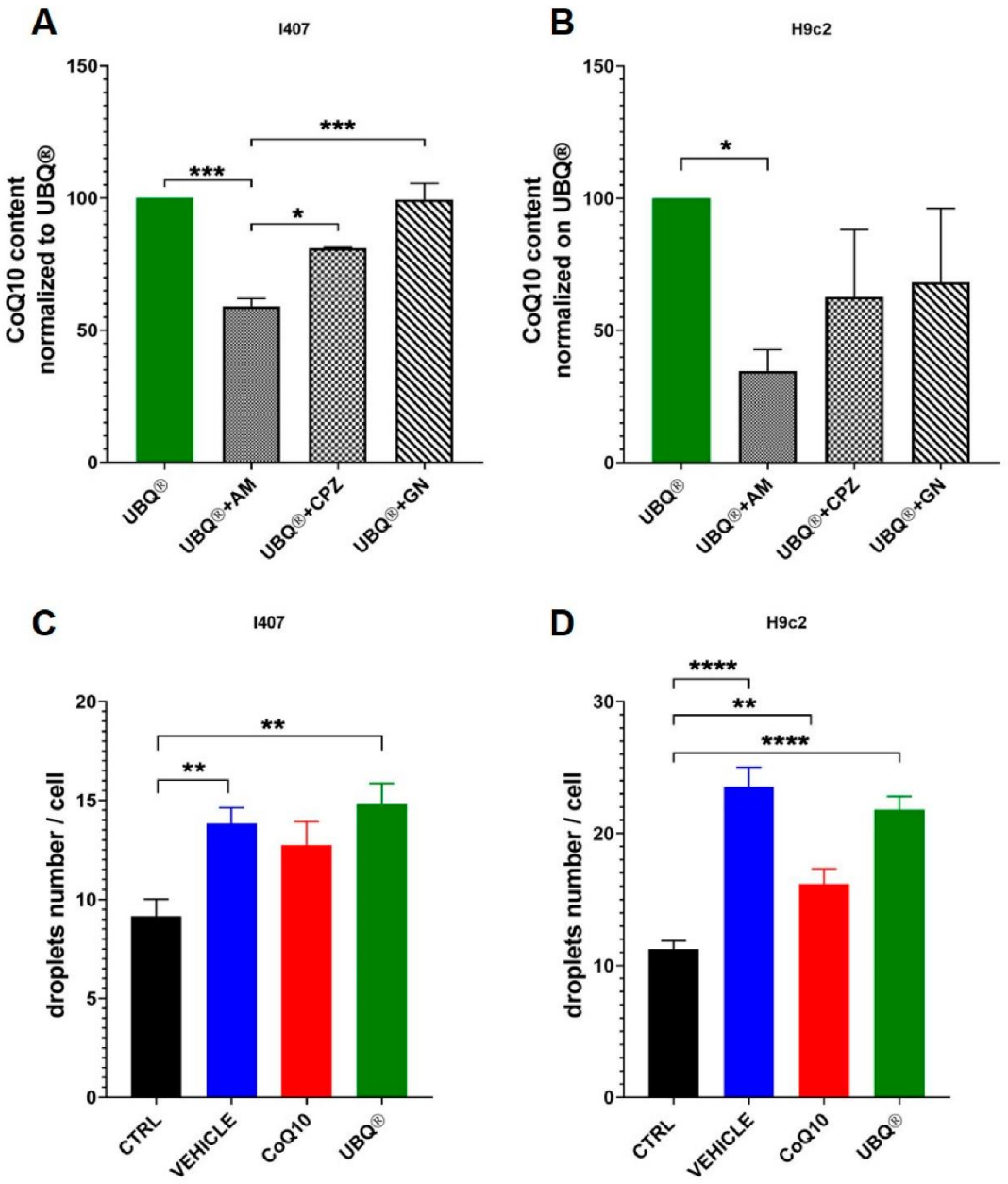


**Fig.11 Assessment of UBQ® incorporation in I407 and H9c2 cell lines**. Cellular Uptake of UBQ® Formulation: I407 (A) and H9c2 (B) cells were pre-treated for 30 minutes with 2 µM amiloride (AM), 10 µg/mL chlorpromazine (CPZ), and 200 µM genistein (GN), followed by a three-hour incubation with 100 nM CoQ10 phytosome formulation (UBQ). The total Coenzyme Q10 amount was quantified using HPLC. Data are reported as a percentage of cellular Coenzyme Q10 content compared to control samples treated with UBQ®. (n = 3). The presence of lipid droplets after product incubation was detected in fixed I407 (C) and H9c2 (D) cells through confocal microscopy using the fluorescent dye Nile Red. For each condition, at least three randomly selected fields were quantified for the number of positive Nile red spots per single cell using ImageJ software. In all panels, data represent the mean ± s.e.m, * $p \leq 0.05$; ** $p \leq 0.01$; *** $p \leq 0.001$; **** $p \leq 0.05$. Statistical analysis employed one-way ANOVA followed by Tukey's honest significant difference test.

### *4.6. Exome Sequence (ES) analysis identified a new biallelic variants in Spartin in a 5-years old patient*

We conducted a Trio ES (father–mother-index) on a young patient affected by muscular hypotonia with exercise intolerance, global developmental delay, and periventricular white matter changes at brain MRI. Two compound heterozygous variants in Spartin (OMIM*607111) inherited from his unaffected parents were detected filtering data for autosomal recessive, de novo or X-linked variants (Fig.12A). The two variants were segregating in three healthy siblings and none of whom exhibited both variants. However, all were heterozygous for one of the variants (Fig.12A). The v*a*riant c.184A > G, p.Lys62Glu (maternally inherited), had a very low minor allele frequency (MAF) of 0.00004 in gnomAD, and the paternally inherited variant c.1093T > C, p.Ser365Pro, also had a very rare MAF of 0.000008 in gnomAD. Following the American College of Medical Genetics and Genomics (ACMG) guidelines, both variants were categorized as variants of uncertain significance (VUS) posing challenges for genetic counselling in the absence of other functional evidence. Nevertheless, the patient's clinical features suggested Troyer Syndrome, prompting further investigations. Firstly, in silico analysis was performed to assess the potential fold changes induced by the two missense variants using the AlphaFold program[186]. The p.Lys62Glu variant, located in the N-terminal MIT domain, was predicted by AlphaFold to affect the exposed Lysine 62 residue within a MIT-interaction site (Fig. 13) leading to a charge change due to the Glu62 substitution. Serine 365, predicted to be an exposed residue by PSIPRED, was also analyzed by DeepREX prediction[187], indicating its potential as a terminal residue in an alpha helix within a highly flexible region. The substitution of Serine 365 with Proline was predicted to structurally alter the alpha helix. Altogether, these findings suggested a potential impact on protein folding. Subsequently, in vitro functional studies were conducted on primary skin fibroblasts from the affected patient (e19), healthy donors (cnt), and a previously characterized Spartin cell model, the SH-SY5Y cell line carrying the homozygous variant c.892dupA, to evaluate the effects of the biallelic Spartin variants. Western blot analysis revealed no significant differences in Spartin expression between patient (e19) and control fibroblasts (Fig.12B and C).

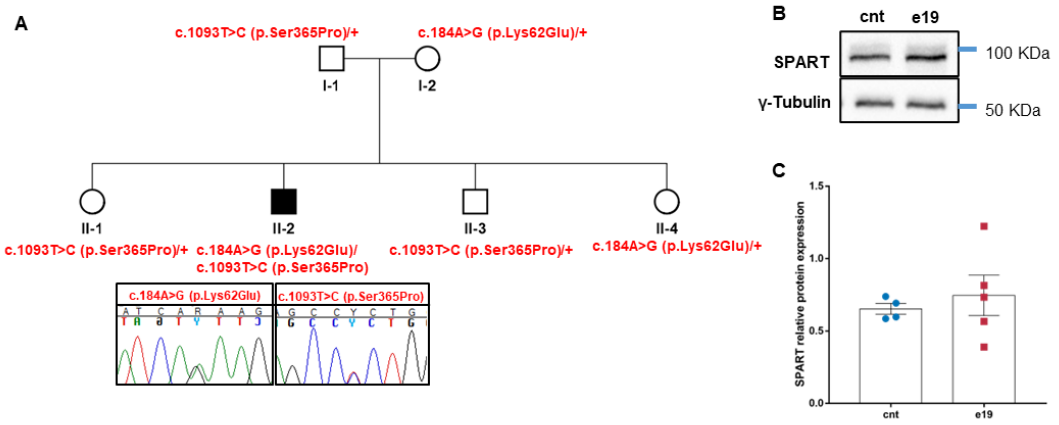


**Fig.12 Identification of new biallelic missense variants in SPART gene**. (A) Family pedigree featuring mutations in SPART. Individuals I-1, I-2, and II-I underwent ES analysis, revealing two heterozygous variants, namely c.184A > G, p.(Lys62Glu) and c.1093T > C, p.(Ser365Pro). The maternal inheritance of the p.Lys62Glu variant and paternal inheritance of the p.Ser365Pro variant are indicated. The three unaffected siblings were found to be heterozygous for one of the two variants, as depicted in the pedigree. (B) Exemplary Western blot depicting Spartin expression in total cell lysates derived from human control (cnt) and patient (e19) fibroblasts. Immunoblotting for Spartin and γ-Tubulin (utilized as an endogenous control) proteins was conducted on the same blot. Cropped images are presented. (c) Spartin expression levels normalized to γ-Tubulin (quantified through Western blot analysis). A minimum of three independent experiments were carried out. Unpaired t-test with Welch's correction, revealing non-significant differences (means ± standard error of the mean).

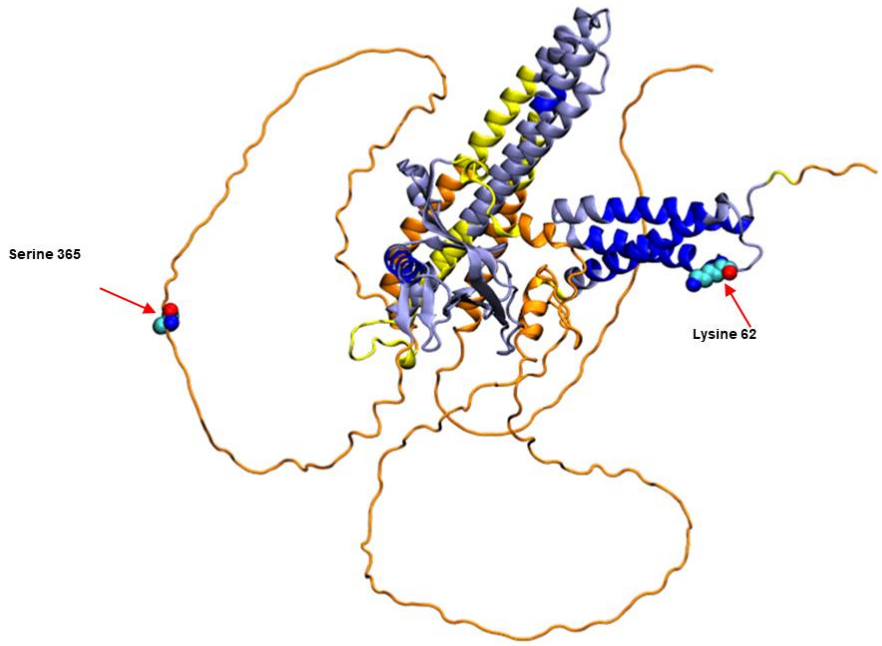


**Fig.13 Structural Representation of Spartin**. Predicted protein structure of Spartin using Alphafold. The mutated amino acids in the patient, specifically lysine at position 62 and serine at position 365 of the protein sequence, are highlighted with red arrows

### *4.7. Biallelic variants in Spartin affect the cell growth and mitochondrial functionality*

The cellular proliferation was evaluated using the IncuCyte Live-Cell Analysis System over a 96-hour period. Mutant cells exhibited a reduced proliferation rate compared to controls, with a doubling time of 38.8 hours for e19 fibroblasts and 28.9 hours for control fibroblasts (Fig. 14A). To assess the impact of mutant Spartin on mitochondrial activity, we measured the OCR in intact e19 and control cells under basal conditions and after the addition of oligomycin A and the uncoupler FCCP. As illustrated in Fig.14B, e19 cells displayed a significantly decreased uncoupled respiration rate compared to controls ($p = 0.0029$). To deeply investigate the role of Spartin in the

OXPHOS process, we measured the specific activities of mitochondrial respiratory complexes. The activity of Complex I in isolated mitochondria showed a significant decrease of 60% in e19 cells compared to controls (p = 0.0356; Fig.15D). Similarly, the activity of Complex II in e19 fibroblasts was significantly reduced by 52% compared to controls (p = 0.0397; Fig.15A), consistently with observations in the cell model carrying the c.892dupA variant (Fig.15B). Additionally, the activities of Complex II+III were significantly diminished by 65% in e19 cells compared to controls (p = 0.0385; Fig.15). Accordingly with the impaired OCR and the altered ETC complex activity, HPLC analysis on e19 cells revealed a significant decrease in the ATP/ADP ratio compared to controls (p = 0.0483; Fig.14C) as we previously observed in the SH-SY5Y cells homozygous for the c.892dupA variant in Spartin[154]. To assess the generation of mitochondrial ROS in living cells, we utilized the fluorogenic probe MitoSox Red, specifically designed to detect mitochondrial superoxide production[188]. Notably, e19 cells exhibited a significantly heightened signal in comparison to control cells (p = 0.0002; Fig. 14D). In parallel, cellular staining with the ROS indicator DCFDA, did not reveal significant differences between e19 and control cells (Fig.15E). These findings suggest that the mutant Spartin induces oxidative stress primarily within the mitochondria. As lipids are susceptible to ROS damage, we employed the lipid peroxidation sensor BODIPY C11 to stain the cells. Remarkably, e19 cells exhibited a diminished red/green ratio compared to controls, signifying heightened lipid membrane peroxidation (p = 0.0008; Fig. 14E). Several studies recognizes the tight association between ROS production and mitochondrial membrane potential hyperpolarization[189–191]. Therefore, we assessed the mitochondrial transmembrane potential using the fluorescent TMRM probe. The results revealed a significantly higher mitochondrial transmembrane potential in e19 cells compared to controls (Fig.15F*)*. To better elucidate the impact of Sparitn on oxidative stress, we evaluated the levels of reduced (GSH) and oxidized (GSSG) glutathione in e19 cells compared to control cells. GSH is a potent hydrophilic antioxidant crucial for scavenging reactive oxygen species (ROS) through non-enzymatic reduction, producing GSSG, which acts as a robust defence against lipid peroxidation. Our findings revealed a significant and pronounced reduction in the total glutathione content in e19 cells, consequently affecting both the reduced and oxidized forms (p = 0.0016, Fig. 14F; p = 0.0426, Fig.

15G; p = 0.0080, Fig. 15H). This indicates a noteworthy decrease in the cellular antioxidant capacity of e19 cells, suggesting a potential link between Spartin and heightened oxidative stress. Alterations in the mitochondrial metabolism are usually linked to an enhanced accumulation of lipid droplets[192,193]. Therefore, amount of lipid droplets per cells in e19 and control fixed cells was assayed using the Nile red fluorescent dye. As shown in Fig.14G, the cells carrying the biallelic variants in Spartin exhibited a significant rise in the lipid droplets content. Moreover, mitochondria of control and patient's fibroblasts were stained with the peculiar mitochondrial probe MitoTracker Green (MTG) (Fig.14H). Obtained results evidenced an altered mitochondrial organization in e19 cells (right panel) compared to control one (left panel). Specifically, analysis performed via Mitochondrial Network Analysis (MiNA) ImageJ toolset allowed us to observe an impairment in the branch length in Spartin mutated fibroblasts (p = 0.0138, Fig.14I). Interestingly, the mitochondrial mass obtained analyzing the MTG signal intensity, was unaltered in both control fibroblasts versus e19 cells and $SY^{wt}$ versus $SY^{892dupA}$ (Fig.15I and L).

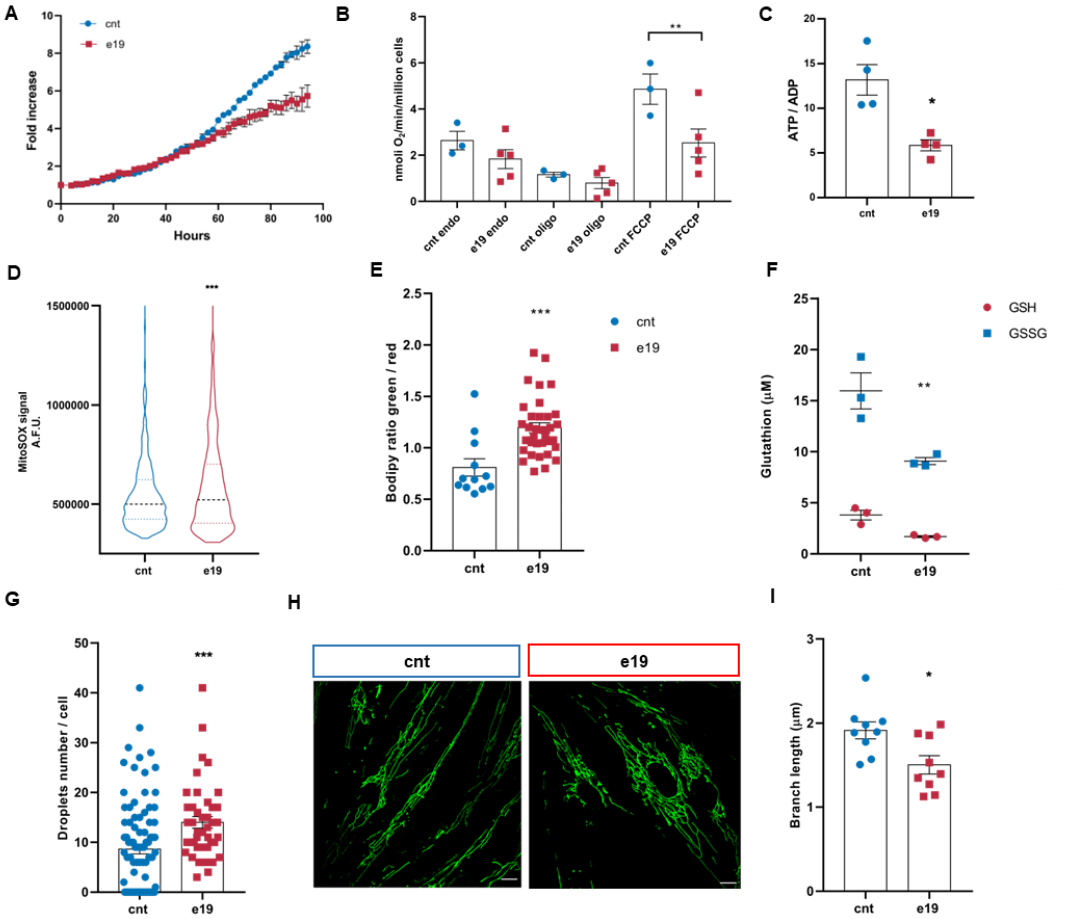


**Fig.14 Cell proliferation and mitochondrial functionality are impaired in cells carrying a Spartin biallelic variants**. (A) Analysis of cell proliferation was conducted through the IncuCyte Live-Cell Assay. Proliferating cells were imaged and analyzed every hour over a 96-hour period. The e19 cells (depicted as red squares) exhibited a lower proliferation rate compared to controls (cnt, represented by blue dots). The doubling time for e19 and control fibroblasts was 38.8 hours and 28.9 hours, respectively. (B) Mitochondrial oxygen consumption was evaluated under endogenous and uncoupled conditions. Respiration was measured in DMEM (basal respiration), in the presence of oligomycin A (non-phosphorylative respiration), and in the presence of FCCP (uncoupled respiration). In comparison with controls (cnt, blue dots), e19 fibroblasts (red squares) showed significantly reduced respiration in the presence of FCCP. Multiple independent experiments were conducted; ANOVA for multiple comparisons; **p = 0.0029 (means ± s.e.m.). Endo: endogenous basal respiration, oligo: cells treated with oligomycin A. (C) The ATP/ADP ratio in cellular extracts from control (cnt, blue dots) and e19 cells (red squares) revealed a significant difference. Paired t-test, *p = 0.021 (means ± s.e.m., n = 4). (D) Oxidative stress determination in live cells using MitoSOX demonstrated higher superoxide production in mutant cells (e19, red violin plot) versus controls (cnt, blue violin plot). Multiple independent

experiments were performed. Unpaired t-test with Welch's correction; ***p = 0.0002. (E) Membrane peroxidation determination using BODIPY 581/591 C11 showed that mutant cells (red squares) had a higher green/red ratio fluorescence intensity signal, indicating an increased membrane peroxidation status compared to controls (blue dots). Multiple independent experiments were performed. Unpaired t-test with Welch's correction, ***p = 0.0008 (means ± s.e.m.). (F) Determination of oxidized and reduced glutathione levels in control (cnt, blue dots) and e19 (red squares) cells revealed lower levels in e19 cells. Three independent experiments were performed. Two-way ANOVA with Sidak's multiple comparison test, GGSH cnt versus e19, **p = 0.0016. (G) Lipid droplets determination using Nile red dye showed that e19 cells (red squares) had an increased number of lipid droplets per cell compared to controls (cnt, blue dots). Multiple independent experiments were performed. Unpaired t-test with Welch's correction, ***p = 0.0006 (means ± s.e.m.). (H) Representative micrographs of control and e19 live fibroblasts stained with MitoTracker Green. (I) Morphology analysis performed with ImageJ MINA software revealed that mutant fibroblasts displayed a perinuclear distribution of mitochondria with significantly shorter branch length compared to controls. Multiple independent experiments were performed. Unpaired t-test with Welch's correction, *p = 0.0138 (means ± s.e.m.).

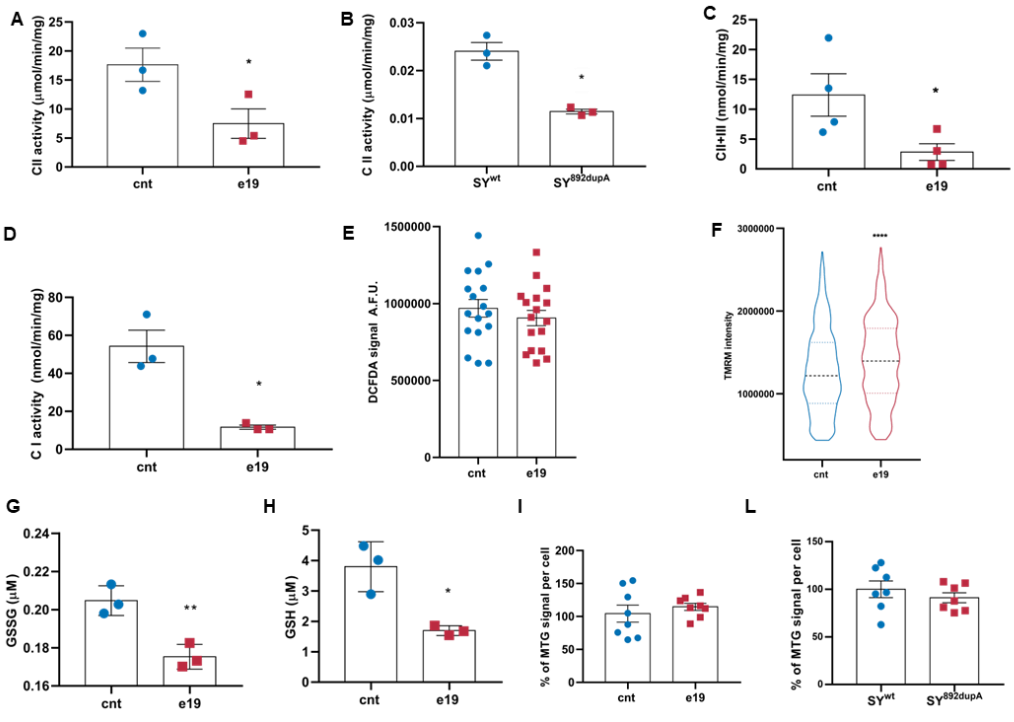


**Fig.15 Mitochondrial respiratory chain enzymes activity and oxidative stress evaluation in cnt and e19 cells**. (A) The activity of Complex II (Succinate: DCPIP reductase) was measured in cell lysates from control (blue dots) and e19 cells (red squares). An unpaired t-test with Welch's correction indicated a significant distinction, *P = 0.0397 (means ± sem, n = 3). (B) Complex II activity was assayed in cell lysates from $SY^{wt}$ (blue dots) and $SY^{892dupA}$ (red squares) cells. An unpaired t-test with test with Welch's

correction showing a significant difference, *P = 0.0155 (means ± sem, n = 3). (C) The combined activity of Complex II+III (Succinate:cytochrome c reductase) was measured in cell lysates from control (blue dots) and e19 cells (red squares). Three independent experiments were conducted, and an unpaired t-test with Welch's correction indicated a significant difference, *P = 0.0385 (means ± sem). (D) Complex I activity (NADH-DB oxidoreductase) in mitochondria isolated from control (cnt, blue dots) an e19 cells (red squares). Unpaired t-test with Welch's correction, *P=0.0356 (means±sem, n=3). (E) Oxidative stress determination in e19 and control cells using DCFDA showed no significant difference in at least three independent experiments. The Kolmogorov-Smirnov test was applied; P=ns (means ± sem). (F) Mitochondrial membrane potential was determined using tetramethylrhodamine methyl ester (TMRM) in intact e19 (red violin plot) and control fibroblasts (blue violin plot). At least three independent experiments were performed, and the Kolmogorov-Smirnov test indicated a highly significant difference, ****P < 0.0001 (means ± sem). (G) Quantification of reduced glutathione (GSH) content in control (blue dots) and e19 (red squares) cells revealed a significant difference. Unpaired t-test with Welch's correction; *P=0.0426 (means ± sem, n=3). (H) Quantification of oxidized glutathione (GSSG) content in control (blue dots) and e19 (red squares) cells also showed a significant difference. Unpaired t-test with Welch's correction; **P=0.0080 (means ± sem, n=3). (I) Mitochondrial mass determination in control fibroblasts versus e19 cells (means ± sem, n=7). (L) Mitochondrial mass determination in $SY^{wt}$ versus $SY^{892dupA}$ cells (means ± sem, n=7).

### *4.8. The mitochondria-associated membranes integrity is impaired in patient's fibroblasts and* $SY^{c.892dupA}$ *carrying a mutation in Spartin resulting in altered calcium levels and a compromised mitochondrial protein import*

It has been well established that calcium homeostasis plays a crucial role in several functions, including the regulation of mitochondrial metabolism, ATP production, and cell death[194]. Thereby, we measured the free calcium level in cnt and e19 cells using the specific Fluo-3 AM fluorescent probe. Consistent with previous findings in $SY^{892dupA}$ [154], the fluorescent signal detected in e19 cells was significantly lower compared to control fibroblasts ($p < 0.0001$; Fig.16A) . To gain insights into a potential alteration in calcium uptake by mitochondria, we measured free calcium levels after pretreatment with ruthenium red, a specific inhibitor of the mitochondrial calcium uniporter (MCU). Interestingly, we noted a significant decrease in Fluo-3AM

fluorescence in control fibroblasts treated with ruthenium red compared to untreated fibroblasts (cnt versus cnt + ruthenium, $p < 0.0001$; Fig. 16B). However, no such alteration was observed in patient cells after incubation with ruthenium red implying an impairment in the MCU activity (e19 versus e19 + ruthenium, $p = 0.01$; Fig.16B). The calcium transport into the mitochondria from the endoplasmic reticulum (ER) is promoted by a physically connection between the two organelles. This tight junctions are termed Mitochondrial Associated Membranes (MAMs)[195] and their stabilization is regulated by a different proteins including Glucose-regulated protein 75 (GRP75), the inositol 1,4,5-trisphosphate receptor (IP3R), TOM70 (one of the translocase of the outer mitochondrial membrane), the voltage-dependent anion channel 1 (VDAC1) and MCU. As Spartin is located on the outer mitochondrial membrane (OMM)[153] and interacts with GRP75[196], we assessed the expression of the protein group GRP75-VDAC-TOM70-MCU in control and mutant cells. This analysis aimed to thoroughly investigate whether alterations in Spartin expression and folding could impact this regulatory mechanism. The Western Blot analysis showed a significant expression decrease of all analyzed proteins in e19 and SY$^{c.892dupA}$ in comparison with related controls ($p = 0.0337$ for e19, $p = 0.030$ for SY$^{c.892dupA}$, Fig.16C and 17A; $p = 0.0089$ for e19, $p = 0.0020$ for SY$^{c.892dupA}$, Fig.16D and 17B; $p = 0.0467$ for e19, $p = 0.0149$ for SY$^{c.892dupA}$, Fig.16E and 17C ; $p = 0.0010$ for e19, $p = 0.0367$ for SY$^{c.892dupA}$, Fig.16F and Fig.17D). The TOM70 translocase, also playing a pivotal role in the MAMs stabilization, is associated with TIM23 subunit in the TIM-TOM complex[197] to allow a correct translocation of the nuclear encoded mitochondrial proteins. As observed for TOM70, TIM23 expression was downregulated as well in all mutant cells comparing to the respective controls ($p = 0.0006$ for e19 cells and $p = 0.0179$ for SY$^{c.892dupA}$ Fig.16G and 17E). Since we observed in mutant cells a reduced activity of Complex II, which is entirely nuclear-encoded, and a diminished expression of both crucial components in the mitochondrial import machinery, TOM70 and TIM23, we performed cell transfections with a Mitochondria-RFP probe followed by staining with MitoTracker Green (MTG). The merge of the signals from these two probes allowed us to evaluate whether the cells were proficient in transferring the protein into the mitochondria. Fig.18A evidenced that in the patient's fibroblasts (three lower panels), the green and red channels did not colocalize when compared with fibroblasts from healthy

individuals. Likewise, overlapping signals were observed only in the $SY^{WT}$ (Fig.18B, three upper panels) indicating a lack of the import of the RFP. Taken together, this data suggests that mutations in Spartin act as a critical checkpoint for the accurate import of mitochondrial proteins.

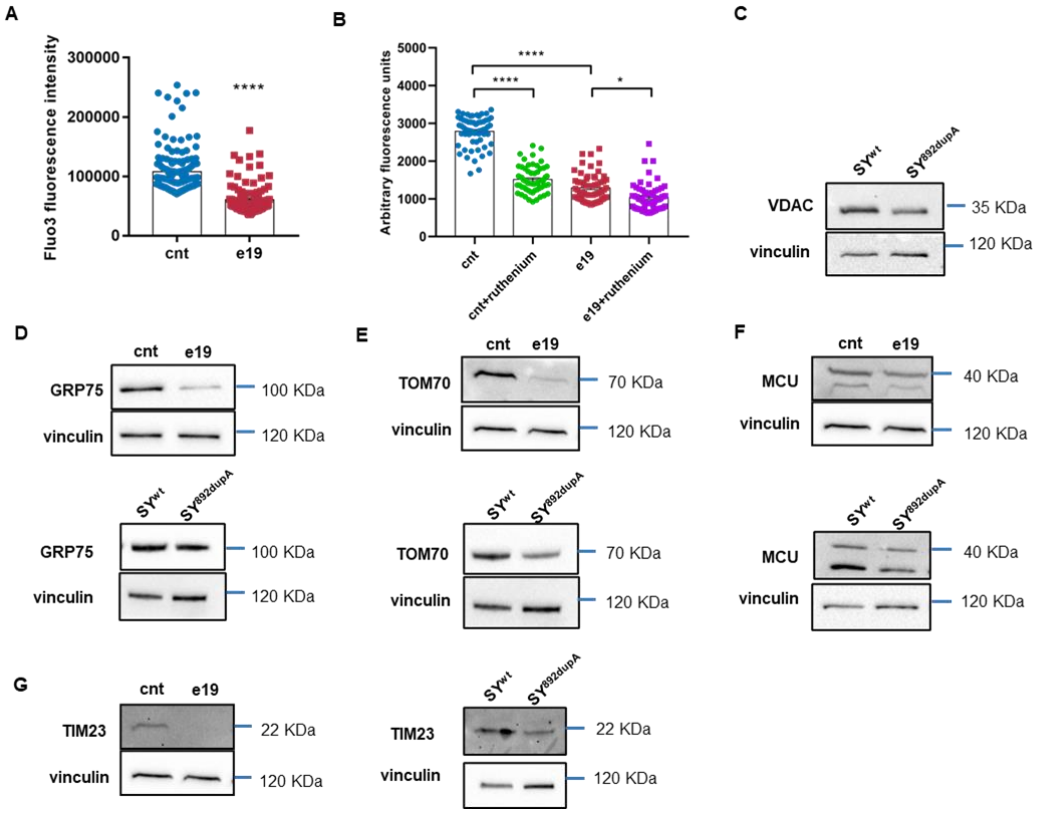


**Fig.16. Mitochondria-associated membrane (MAMs) integrity is impaired in e19 and $SY^{892dupA}$ cells.** (A) Measurement of intracellular free calcium in live control (cnt, blue dots) and mutant (e19, red squares) fibroblasts revealed a significant difference. Unpaired t-test with Welch's correction, *p = 0.001 (means ± s.e.m.). (B) Determination of intracellular free calcium in control (cnt) and mutant (e19) cells in the presence and absence of the mitochondrial calcium inhibitor ruthenium red demonstrated significant variations. Dunn's multiple comparisons test, cnt versus e19 ****p < 0.0001; cnt versus cnt + ruthenium ***p < 0.0001; e19 versus e19 + ruthenium *p = 0.01 (means ± s.e.m.). Cnt, blue dots; cnt + ruthenium, green dots; e19, red squares; e19 + ruthenium, purple squares. (C–G) Western blot analysis for VDAC, GRP75, TOM70, MCU, and TIM23 in e19 (upper panels) and $SY^{892dupA}$ (lower panels) versus corresponding control cells. Immunoblotting for the different proteins and vinculin (used as endogenous control) was performed on the same blot. Cropped images are presented. The immunoblots are representative of at least three independent experiments.

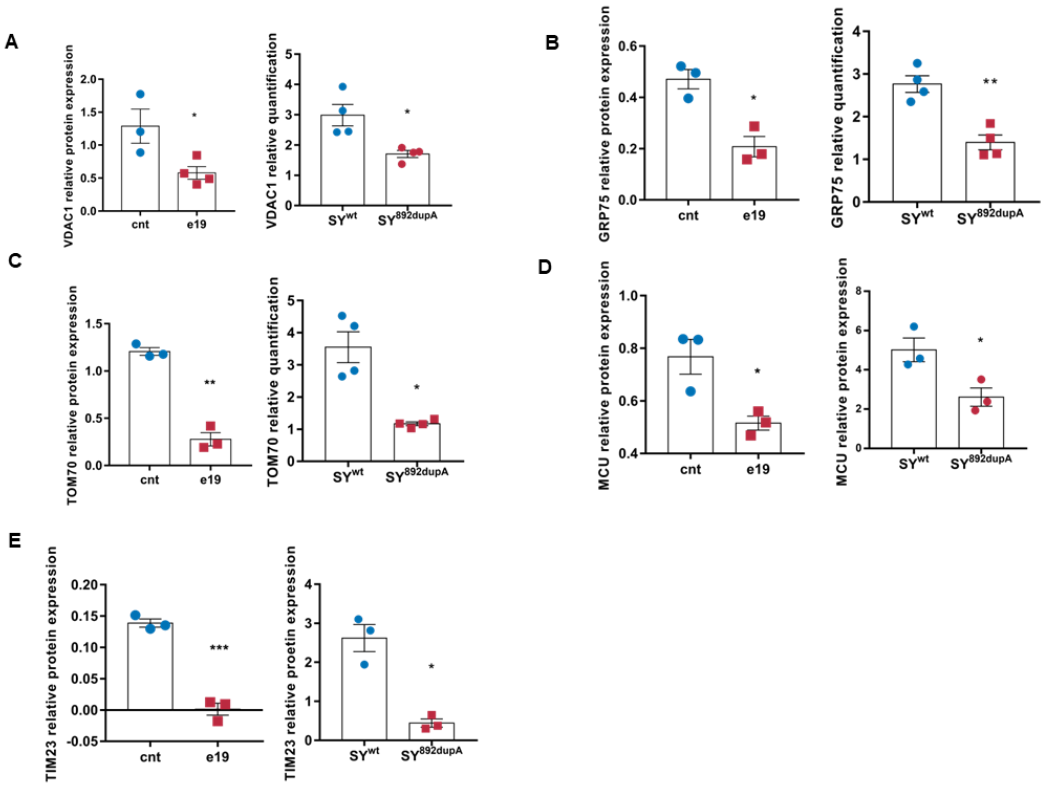


**Fig.17.Quantification of MAMs subunits and TIM23 expression in control and mutant cells.** (A) Quantification of VDAC expression in Western blot analysis, normalized to vinculin. Three independent experiments were conducted. An unpaired t-test with Welch's correction revealed a significant difference, *P=0.0337 (means ± sem). (B) Quantification of GRP75 expression in Western blot analysis, normalized to vinculin. An unpaired t-test with Welch's correction demonstrated a significant difference, *P=0.0490 (means ± sem, n=3). (C) Quantification of TOM70 expression in Western blot analysis, normalized to vinculin. An unpaired t-test with Welch's correction indicated a significant difference, **P=0.0010 (means ± sem, n=3). (D) Quantification of MCU expression in Western blot analysis, normalized to vinculin. An unpaired t-test with Welch's correction showed a significant difference, *P=0.0467 (means ± sem, n=3). (E) Quantification of TIM23 expression in Western blot analysis, normalized to vinculin. An unpaired t-test with Welch's correction revealed a significant difference, ***P=0.0006 (means ± sem, n=3).

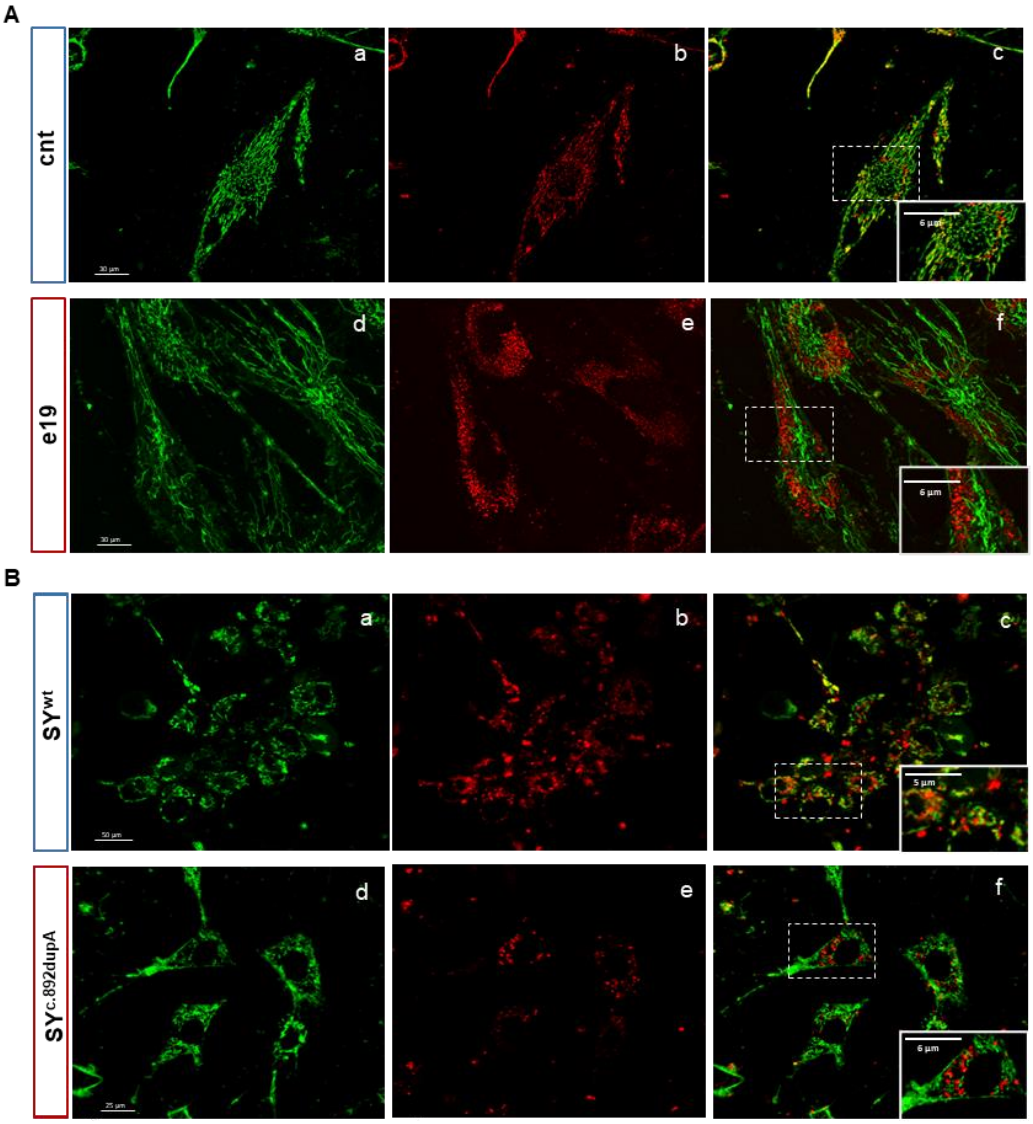


**Fig.18.Mutations in Spartin affect the import of the nuclear encoded mitochondrial protein.** (A) Fibroblasts from both control and e19 conditions were firstly transfected with a RFP targeting the mitochondria (CellLight Mitochondria-RFP, b and e) and then stained with MitoTracker Green (a and d). Merged images are shown in panels c and f. Insets in c and f provide magnified views of the regions outlined with dashed lines, with a scale bar representing 6 µm; scale bars in a and d indicate 30 µm. (B) $SY^{wt}$ and $SY^{c.892dupA}$ samples stained with MitoTracker Green (a and d) and an RFP for mitochondrial targeting (CellLight Mitochondria-RFP, b and e). Merged images are displayed in panels c and f. Insets in c and f offer enlarged views of the regions outlined with dashed lines, with scale bars representing 5 and 6 µm, respectively. Scale bar in a represents 50 µm, and scale bar in d represents 25 µm. Colocalization of green and red signals was observed in the mitochondria of control cells, while the signals did not colocalize in mutant cells e19 and $SY^{c.892dupA}$, indicating a lack of mitochondrial RFP import.

### *4.9. Spartin mutations affect mitochondrial respiratory chain enzymes expression and assembly*

Since we demonstrated an evident impairment in the nuclear encoded mitochondrial protein import and an alteration in the mitochondrial OXPHOS, we assessed the expression of the ETC enzymes in isolated mitochondria extracted from fibroblasts derived from patients, $SY^{c.892dupA}$ and respective controls. Western Blot analysis (Fig.19A-E, left panel) and related bands quantification (Fig.20A) revealed a significant downregulation of NDUFA9 (NADH:ubiquinone oxidoreductase subunit A9, complex I), SDHA (subunit A of the succinate dehydrogenase), UQCRC2 (ubiquinol-cytochrome c reductase core protein 2, complex III), COXI (cytochrome c oxidase 1) and the ATPase-β subunits (complex V) in cells carrying the c.892dupA variant compared to controls . Conversely, only a decrease in NDUA9 and SDHA subunits was observed in e19 cells compared to control fibroblasts (Fig.19A-E, right panel) (Fig.20B). Based on these results, we evaluated the assembly of the OXPHOS enzymes from isolated mitochondria of control and patient's fibroblasts and in $SY^{wt}$ and $SY^{c.892dupA}$ using the Blue Native Polyacrylamide Gel Electrophoresis (BN-PAGE) followed by immunoblotting for specific ETC enzymes subunits. (Fig.21A-D). Immunoblots and related graphs showed that the cells carrying the c.892dupA mutated variants presented an increased assembling of the Complex III followed by a diminished of the Complex IV (Fig.21A and C). In contrast, no alterations between control and patient's fibroblasts were observed in cnt and e19 cells (Fig.21B and D). To better understand whether the shift in metabolism from glycolytic to more oxidative conditions has a more pronounced impact on the alteration of ETC complex assembly, we evaluated the mitochondrial respiratory chain complexes in mitochondrial isolated from $SY^{WT}$ and $SY^{c.892dupA}$ cells cultured under starved conditions for 24 hours. Differently to what we identified in cells grown in DMEM High Glucose, the assembling capacity of Complex III+IV markedly decreased in Spartin mutant cells. Furthermore, as observed in High glucose conditions, $SY^{c.892dupA}$ exhibited an affected Complex IV assembly suggesting that Spartin might directly regulate the cytochrome c oxidase assembly.

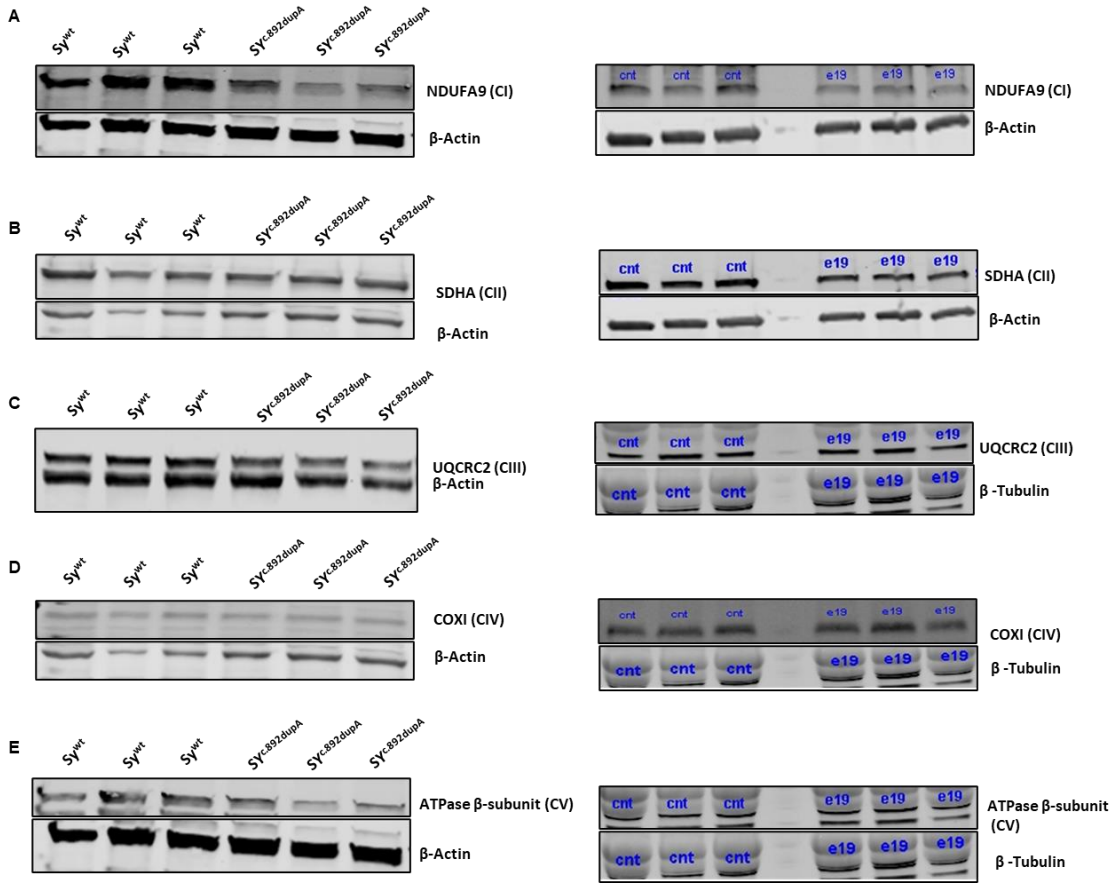


**Fig.19. Mutations in Spartin induces an alteration in the mitochondrial respiratory chain enzymes expression**. (A-E) Western blot analysis for NDUFA9, SDHA, UQCRC2, COXI, and ATPase β-subunit in $SY^{c.892dupA}$ (left panels) and e19 (right panels) versus corresponding control cells. Immunoblotting for the different proteins and β- Actin or β- Tubulin (used as endogenous controls) was performed on the same blot. Cropped images are presented. The immunoblots are representative of at least three independent experiments.

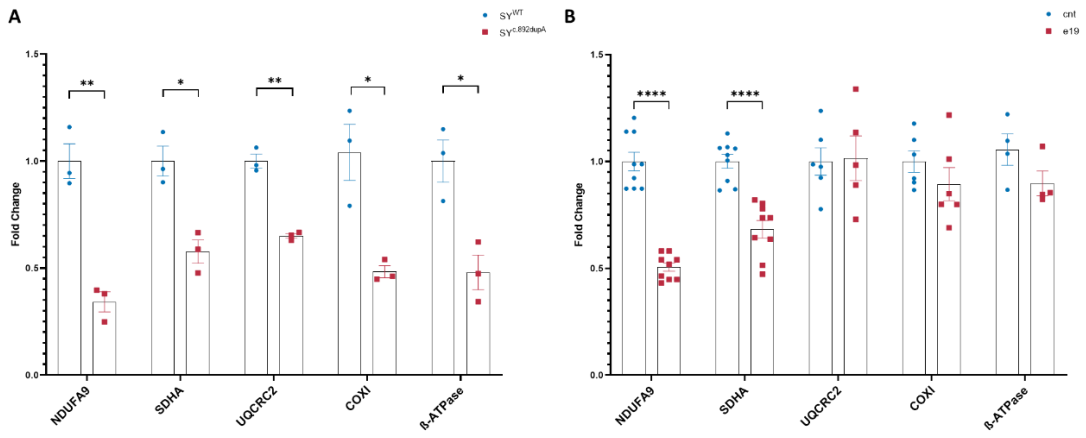


**Fig.20 Mitochondrial respiratory chain enzymes quantification in control fibroblasts, e19, SY$^{WT}$ and SY$^{C.892dupA}$**. (A) Quantification of NDUFA9, SDHA, UQCRC2, COXI, and ATPase β-subunit expression in SY$^{wt}$ (blue dots) and SY$^{c.892dupA}$ (red squares) normalized to β-Actin and β-Tubulin. Three independent experiments were conducted. Data are presented as the mean ± s.e.m, * $p \leq 0.05$; ** $p \leq 0.01$; *** $p \leq 0.001$; **** $p \leq 0.0001$. Statistical analysis was performed using a Multi unpaired t-test. (B) Quantification of NDUFA9, SDHA, UQCRC2, COXI, and ATPase β-subunit expression in cnt (blue dots) and e19 (red squares), normalized to β-Actin and β-Tubulin. An unpaired t-test with Welch's correction demonstrated a significant difference, *P=0.0490 (means ± sem, n=3). At least three independent experiments were conducted. Data are presented as the mean ± s.e.m, * $p \leq 0.05$; ** $p \leq 0.01$; *** $p \leq 0.001$; **** $p \leq 0.0001$. Statistical analysis was performed using a Multi unpaired t-test.

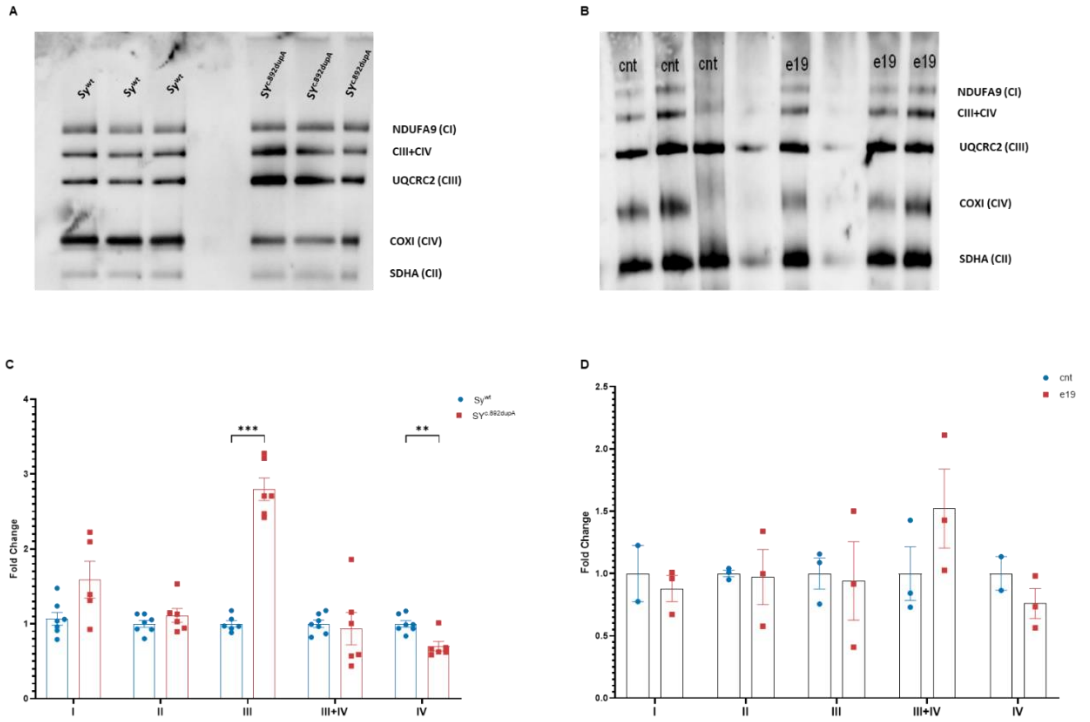


**Fig.21 Evaluation of the mitochondrial respiratory chain enzymes assembly and relative quantification in control fibroblasts, e19, SY$^{WT}$ and SY$^{C.892dupA}$**. (A) Representative immunoblots after 1D BNP-PAGE performed with anti NDUFA9, SDHA, UQCRC2 and COXI in SY$^{wt}$ and SY$^{c.892dupA}$. (B) Representative immunoblots after 1D BNP-PAGE performed with anti NDUFA9, SDHA, UQCRC2 and COXI in cnt and e19. (C) Quantitative immunoblot of mitochondrial respiratory chains subunits in SY$^{wt}$ (blue dots) and SY$^{c.892dupA}$ (red squares) normalized on mitochondrial amount. At least 6 independent experiments were performed. Data are presented as the mean ± s.e.m, * $p \leq 0.05$; ** $p \leq 0.01$; *** $p \leq 0.001$; **** $p \leq 0.0001$. Statistical analysis was performed using a Multi unpaired t-test. (D) Quantitative immunoblot of mitochondrial respiratory chains subunits in cnt (blue dots) and e19 (red squares) normalized on mitochondrial amount. At least 3 independent experiments were performed.

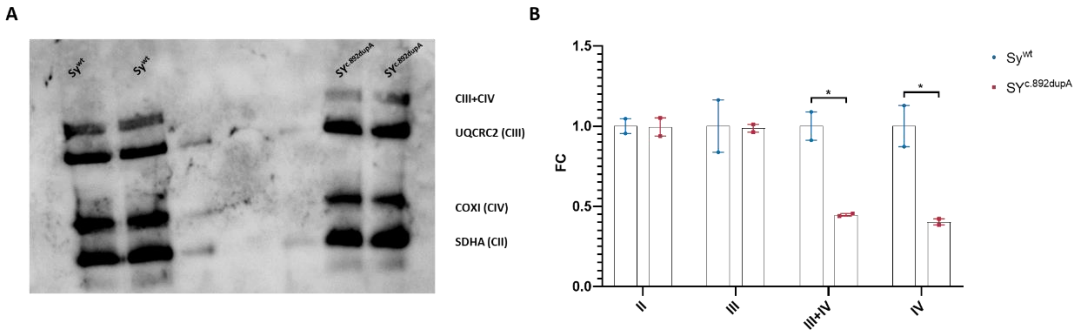


**Fig.22 Evaluation of the mitochondrial respiratory chain enzymes assembly and relative quantification in control fibroblasts SY$^{WT}$ and SY$^{c.892dupA}$ grown for 24 hours in starving conditions.** (A) Representative immunoblots after 1D BNP-PAGE performed with anti NDUFA9, SDHA, UQCRC2 and COXI in SY$^{wt}$ and SY$^{c.892dupA}$. (B) Quantitative immunoblot of mitochondrial respiratory chains subunits in SY$^{wt}$ (blue dots) and SY$^{c.892dupA}$ (red squares) normalized on mitochondrial amount. At least two different experiments were performed.

### *4.10. Loss of function mutation in Spartin affects the transcription of several nuclear and mitochondrial genes*

Spartin is a multifunctional protein localized in various organelles but its main role in the cells is still poorly understood. To identify the overall altered biological pathways due to a loss of function mutation in Spartin and integrate them with the observed mitochondrial dysfunction, we performed a whole transcriptome analysis on SY$^{WT}$ comparing to SY$^{c.892dupA}$. Quantitative analysis performed by Salmon[176] identified 707 genes with differential expression between SY$^{WT}$ and SY$^{c.892dupA}$ at an adjusted Pvalue (padj)<0.05. Compared to control, 342 genes were upregulated whereas 365 genes were downregulated. Gene Ontology (GO) analysis of the RNAseq data was carried out by Enrichr tool[177] using the gene sets derived from the GO Biological Process ontology. In comparison with control cells, we identified 71 downregulated and 38 upregulates biological processes with a padj<0.05 (Tab.2 and 3 respectively). Gene ontology analysis revealed that the top significant downregulated biological pathways were related to transcriptional and translational processes and, notably, the oxidative phosphorylation metabolism (Fig.23A and Tab.2). Indeed, SY$^{c.892dupA}$ showed a lower expression for several nuclear and mitochondrial genes encoding for subunits of the

ETC enzymes (Fig.23B and C) compared to control cells. Trying to confirm the role of Spartin in the transcription of the different genes encoding for the OXPHOS enzymes, we performed qPCR analysis for several MT-ND3 (mitochondrially encoded NADH:ubiquinone oxidoreductase core subunit 3), MT-CO3 (mitochondrially encoded cytochrome c oxidase III) and MT-ATP6 (mitochondrially encoded ATP synthase membrane subunit 6) on SY$^{c.892dupA}$ cells and patient's fibroblasts transiently transfected with a plasmid encoding for a wild type Spartin (pcDNA SPART) and empty vector (Fig.24Band C). The correct transfection was tested through in e19 cells through Western Blot analysis after 48 hours (Fig.24A), as previously described for the SY$^{c.892dupA}$ [154]. As shown in Fig.24B and C, the levels of the downregulated mitochondrial transcripts in e19 and SY$^{c.892dupA}$ were fully restored after the wild type Spartin overexpression. Moreover, the TIMM13 transcript levels, which allows the correct import of TIM23 into the inner mitochondrial membrane[198], were completely recovered in patient's fibroblasts and SY$^{c.892dupA}$ transiently transfected with pcDNA SPART. Taken together, all these data suggest that Spartin modulates the mitochondrial functionality regulating the transcription of the genes involved in the energy production and in the nuclear encoded mitochondrial protein import.

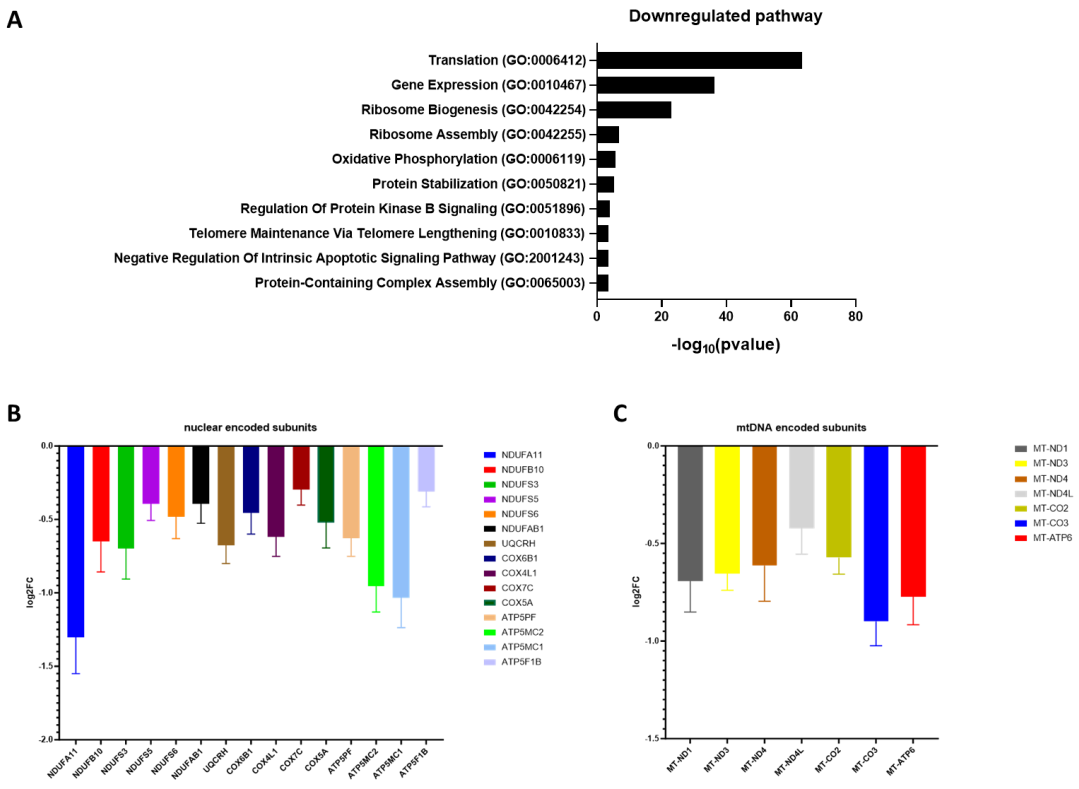


**Fig.23 SY$^{c.892dupA}$ cells exhibited an alteration in the transcriptional process.** (A) Top ten downregulated pathways output by GO Biological Process. (B-C) The log2-fold change values, obtained by transcriptome analysis, represent the expression alterations for 15 genes encoding for nuclear (B) and 7 (C) mitochondrial subunits of the ETC enzymes. The error bars in the figure illustrate the standard error deviation (SD) of the mean of 3 independent experiments (n=3). The log2-fold change values reported in the graphs were significantly different between conditions (padj<0.05).

| Human Gene sets | padj |
|---|---|
| Cytoplasmic Translation (GO:0002181) | 1.08E-60 |
| Macromolecule Biosynthetic Process (GO:0009059) | 8.47E-47 |
| Peptide Biosynthetic Process (GO:0043043) | 9.39E-47 |
| Translation (GO:0006412) | 1.02E-44 |
| Gene Expression (GO:0010467) | 3.49E-34 |
| Ribosome Biogenesis (GO:0042254) | 6.41E-21 |
| Ribonucleoprotein Complex Biogenesis (GO:0022613) | 2.12E-20 |
| Ribosomal Small Subunit Biogenesis (GO:0042274) | 1.66E-16 |
| rRNA Processing (GO:0006364) | 2.97E-13 |
| rRNA Metabolic Process (GO:0016072) | 1.90E-12 |
| ncRNA Processing (GO:0034470) | 1.71E-11 |

| | |
|---|---|
| protein-RNA Complex Assembly (GO:0022618) | 1.44E-07 |
| Proton Motive Force-Driven ATP Synthesis (GO:0015986) | 3.72E-06 |
| Ribosome Assembly (GO:0042255) | 2.63E-05 |
| Ribosomal Small Subunit Assembly (GO:0000028) | 1.91E-04 |
| Oxidative Phosphorylation (GO:0006119) | 3.32E-04 |
| Proton Motive Force-Driven Mitochondrial ATP Synthesis (GO:0042776) | 3.46E-04 |
| Ribosomal Large Subunit Biogenesis (GO:0042273) | 3.97E-04 |
| Aerobic Electron Transport Chain (GO:0019646) | 6.49E-04 |
| Protein Stabilization (GO:0050821) | 7.29E-04 |
| Mitochondrial ATP Synthesis Coupled Electron Transport (GO:0042775) | 8.04E-04 |
| Maturation Of SSU-rRNA From Tricistronic rRNA Transcript (SSU-rRNA, 5.8S rRNA, LSU-rRNA) (GO:0000462) | 9.38E-04 |
| Cellular Respiration (GO:0045333) | 0.001114 |
| ATP Biosynthetic Process (GO:0006754) | 0.002306 |
| mRNA Processing (GO:0006397) | 0.002998 |
| Regulation Of Integrin-Mediated Signaling Pathway (GO:2001044) | 0.004032 |
| Maturation Of SSU-rRNA (GO:0030490) | 0.004973 |
| mRNA Splicing, Via Spliceosome (GO:0000398) | 0.006773 |
| RNA Splicing, Via Transesterification Reactions With Bulged Adenosine As Nucleophile (GO:0000377) | 0.007366 |
| Positive Regulation Of Cell Differentiation (GO:0045597) | 0.007366 |
| Regulation Of Cell Migration (GO:0030334) | 0.007605 |
| Regulation Of Protein Kinase B Signaling (GO:0051896) | 0.008935 |
| Positive Regulation Of Cell Migration (GO:0030335) | 0.009815 |
| Mitochondrial Electron Transport, Cytochrome C To Oxygen (GO:0006123) | 0.015164 |
| Aerobic Respiration (GO:0009060) | 0.018134 |
| Negative Regulation Of Vascular Associated Smooth Muscle Cell Proliferation (GO:1904706) | 0.019463 |
| Telomere Maintenance Via Telomere Lengthening (GO:0010833) | 0.019463 |
| Cellular Response To Cytokine Stimulus (GO:0071345) | 0.019619 |
| Muscle Tissue Development (GO:0060537) | 0.019619 |
| Negative Regulation Of Smooth Muscle Cell Proliferation (GO:0048662) | 0.019619 |
| Negative Regulation Of Intrinsic Apoptotic Signaling Pathway (GO:2001243) | 0.019619 |
| RNA Processing (GO:0006396) | 0.019619 |
| Protein-Containing Complex Assembly (GO:0065003) | 0.019619 |
| Dendritic Cell Migration (GO:0036336) | 0.021672 |
| Axonogenesis (GO:0007409) | 0.024648 |
| Regulation Of Receptor-Mediated Endocytosis (GO:0048259) | 0.024648 |
| Regulation Of Basement Membrane Organization (GO:0110011) | 0.024648 |
| RNA-templated DNA Biosynthetic Process (GO:0006278) | 0.024648 |

| | |
|---|---|
| Telomere Maintenance Via Telomerase (GO:0007004) | 0.024648 |
| Negative Regulation Of RNA Splicing (GO:0033119) | 0.024648 |
| Central Nervous System Neuron Axonogenesis (GO:0021955) | 0.024648 |
| Positive Regulation Of Translation (GO:0045727) | 0.025105 |
| Regulation Of Neuron Differentiation (GO:0045664) | 0.025825 |
| Response To Type II Interferon (GO:0034341) | 0.028067 |
| Positive Regulation Of Hydrolase Activity (GO:0051345) | 0.028888 |
| Positive Regulation Of Integrin-Mediated Signaling Pathway (GO:2001046) | 0.032336 |
| Substantia Nigra Development (GO:0021762) | 0.032336 |
| RNA Splicing (GO:0008380) | 0.035381 |
| Positive Regulation Of Receptor-Mediated Endocytosis (GO:0048260) | 0.036191 |
| Positive Regulation Of Cellular Metabolic Process (GO:0031325) | 0.037152 |
| Noradrenergic Neuron Differentiation (GO:0003357) | 0.038483 |
| Positive Regulation Of Amide Metabolic Process (GO:0034250) | 0.038483 |
| Positive Regulation Of Endothelial Cell Migration (GO:0010595) | 0.038483 |
| Response To Unfolded Protein (GO:0006986) | 0.038483 |
| Regulation Of Translation (GO:0006417) | 0.039998 |
| Positive Regulation Of Cell Motility (GO:2000147) | 0.041188 |
| Positive Regulation Of DNA Binding (GO:0043388) | 0.041897 |
| U2-type Prespliceosome Assembly (GO:1903241) | 0.047154 |
| Positive Regulation Of Cell Population Proliferation (GO:0008284) | 0.047154 |
| Negative Regulation Of Cell Differentiation (GO:0045596) | 0.048668 |

**Tab.2.** Downregulated pathways in $SY^{C.892dupA}$ compare to $SY^{WT}$ obtained by Enrichr

| Human Gene sets | padj |
|---|---|
| Regulation Of Cell Migration (GO:0030334) | 3.12E-04 |
| Regulation Of Integrin-Mediated Signaling Pathway (GO:2001044) | 6.09E-04 |
| Positive Regulation Of Hydrolase Activity (GO:0051345) | 0.001613 |
| Positive Regulation Of Cell Migration (GO:0030335) | 0.002779 |
| Actin Filament Organization (GO:0007015) | 0.00313 |
| Positive Regulation Of Cell Differentiation (GO:0045597) | 0.00313 |
| Regulation Of GTPase Activity (GO:0043087) | 0.006563 |
| Negative Regulation Of Cell Population Proliferation (GO:0008285) | 0.007683 |
| Muscle Tissue Development (GO:0060537) | 0.007683 |
| Negative Regulation Of Smooth Muscle Cell Proliferation (GO:0048662) | 0.007683 |
| Positive Regulation Of Integrin-Mediated Signaling Pathway (GO:2001046) | 0.007683 |
| Regulation Of Basement Membrane Organization (GO:0110011) | 0.00912 |
| Cellular Response To Cytokine Stimulus (GO:0071345) | 0.015274 |
| Positive Regulation Of Muscle Cell Differentiation (GO:0051149) | 0.015983 |
| Positive Regulation Of Cell Motility (GO:2000147) | 0.017827 |
| Positive Regulation Of Protein Modification Process (GO:0031401) | 0.019985 |
| Post-Translational Protein Targeting To Membrane, Translocation (GO:0031204) | 0.021096 |
| Negative Regulation Of Vascular Associated Smooth Muscle Cell Proliferation (GO:1904706) | 0.021096 |
| Regulation Of Protein Phosphorylation (GO:0001932) | 0.024059 |
| Skeletal Muscle Organ Development (GO:0060538) | 0.034244 |
| Regulation Of Cell Population Proliferation (GO:0042127) | 0.035677 |
| Smooth Muscle Tissue Development (GO:0048745) | 0.039707 |
| Regulation Of Neuron Differentiation (GO:0045664) | 0.039968 |
| Response To Type II Interferon (GO:0034341) | 0.04137 |
| Regulation Of G1/S Transition Of Mitotic Cell Cycle (GO:2000045) | 0.042543 |
| Regulation Of Receptor-Mediated Endocytosis (GO:0048259) | 0.042543 |
| Neuron Projection Extension (GO:1990138) | 0.042543 |
| Response To Tumor Necrosis Factor (GO:0034612) | 0.043431 |
| Regulation Of Extracellular Matrix Organization (GO:1903053) | 0.043431 |
| Positive Regulation Of Cell-Substrate Junction Organization (GO:0150117) | 0.043431 |
| Protein Localization To Lysosome (GO:0061462) | 0.046901 |
| Regulation Of Muscle Cell Differentiation (GO:0051147) | 0.048206 |
| Positive Regulation Of GTPase Activity (GO:0043547) | 0.049086 |
| Actin Crosslink Formation (GO:0051764) | 0.049086 |
| Positive Regulation Of Cell Adhesion (GO:0045785) | 0.049086 |
| Positive Regulation Of Cell-Matrix Adhesion (GO:0001954) | 0.049086 |
| Positive Regulation Of Receptor-Mediated Endocytosis (GO:0048260) | 0.049086 |

**Tab.3.** Upregulated pathways in $SY^{C.892dupA}$ compared to $SY^{WT}$ obtained by Enrichr.

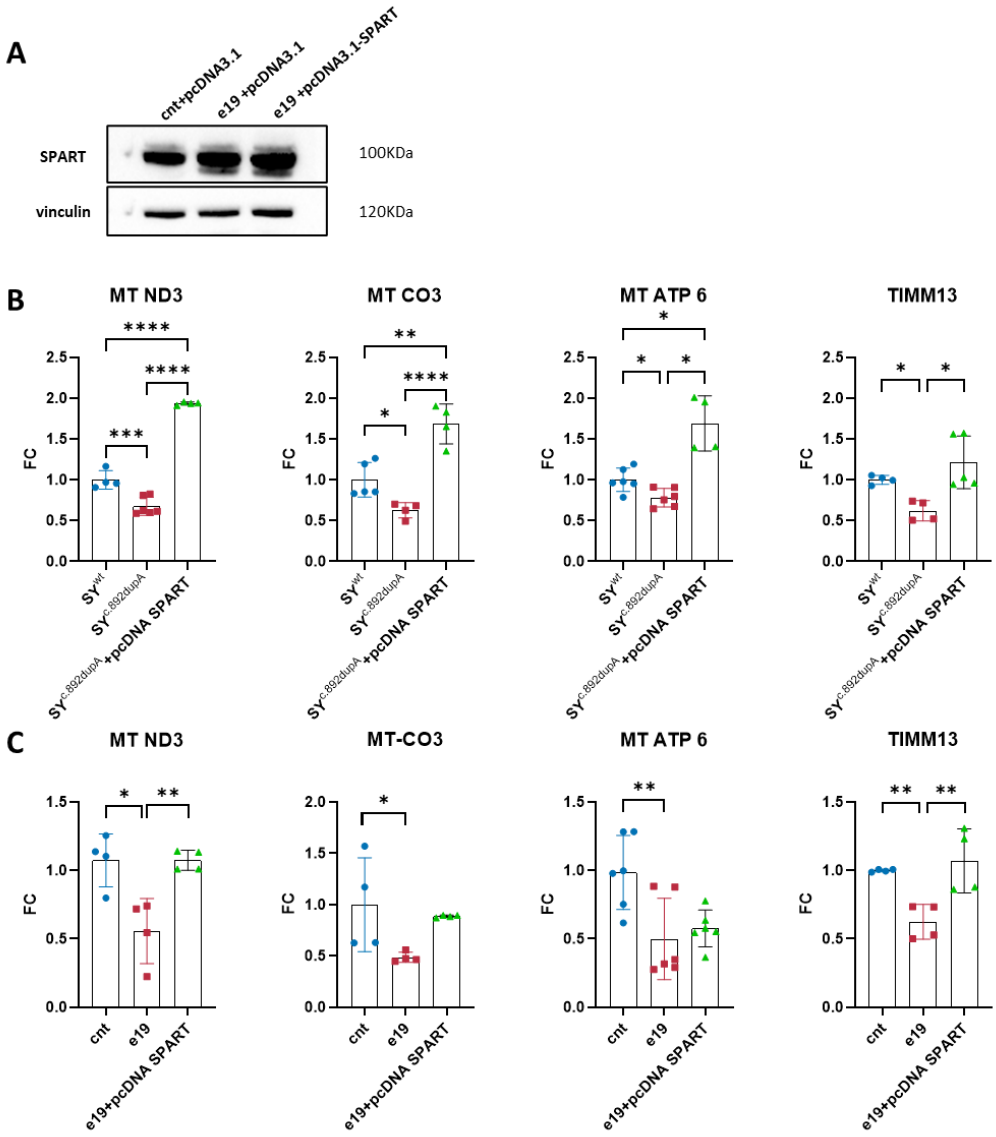


**Fig.24 Wilde type Spartin expression restored the transcript levels in e19 and SY$^{c.892dupA}$ cells.** A) Transcript levels of MT ND3, MT CO3 MT ATP6 and TIMM13 obtained by qPCR on SY$^{wt}$ (blue dots) and SY$^{c.892dupA}$ (red squares) expressed as fold change to SY$^{wt}$. At least 4 independent experiments were performed. Data are presented as the mean ± SD, * $p \leq 0.05$; ** $p \leq 0.01$; *** $p \leq 0.001$; **** $p \leq 0.0001$. Statistical analyses were performed using a Tukey's multiple comparisons test. B) Transcript levels of MT ND3, MT CO3 MT ATP6 and TIMM13 obtained by qPCR on cnt (blue dots) and e19 (red squares) expressed as fold change to SY$^{wt}$. At least 4 independent experiments were performed. Data are presented as the mean ± SD, * $p \leq 0.05$; ** $p \leq 0.01$; *** $p \leq 0.001$; **** $p \leq 0.0001$. Statistical analyses were performed using a Tukey's multiple comparisons test.

### *4.11. Impaired mitochondrial protein import leads to a diminished CoQ10 amount in e19 and SY$^{c.892dupA}$ cells*

Mitochondrial import holds considerable relevance for various mitochondrial protein complexes, including the pivotal 'complex Q,' which orchestrates the final stage of Coenzyme Q (CoQ) biosynthesis. This complex encompasses diverse enzymes, notably COQ7 and COQ9. In our investigation involving mutant cells (e19 and SY$^{c.892dupA}$), we consistently observed a diminished expression of both COQ7 and COQ9 ($p = 0.0250$ for e19, $p = 0.0127$ for SYc$^{.892dupA}$; Fig. 25A; $p = 0.0447$ for e19, $p = 0.0143$ for SY$^{c.892dupA}$; Fig. 25B). Consequently, this reduction in expression corresponded with a significant decrease in CoQ10 content in both e19 and SY892dupA mutant cells when compared to their respective control cells ($p = 0.0455$ for e19, figure 5c; $p = 0.0165$ for SY$^{c.892dupA}$, figure 5d, respectively). These findings underscore the impact of the observed alterations in COQ7 and COQ9 expression on CoQ biosynthesis and content, shedding light on the potential consequences for mitochondrial function and cellular bioenergetics in the context of the studied mutations.

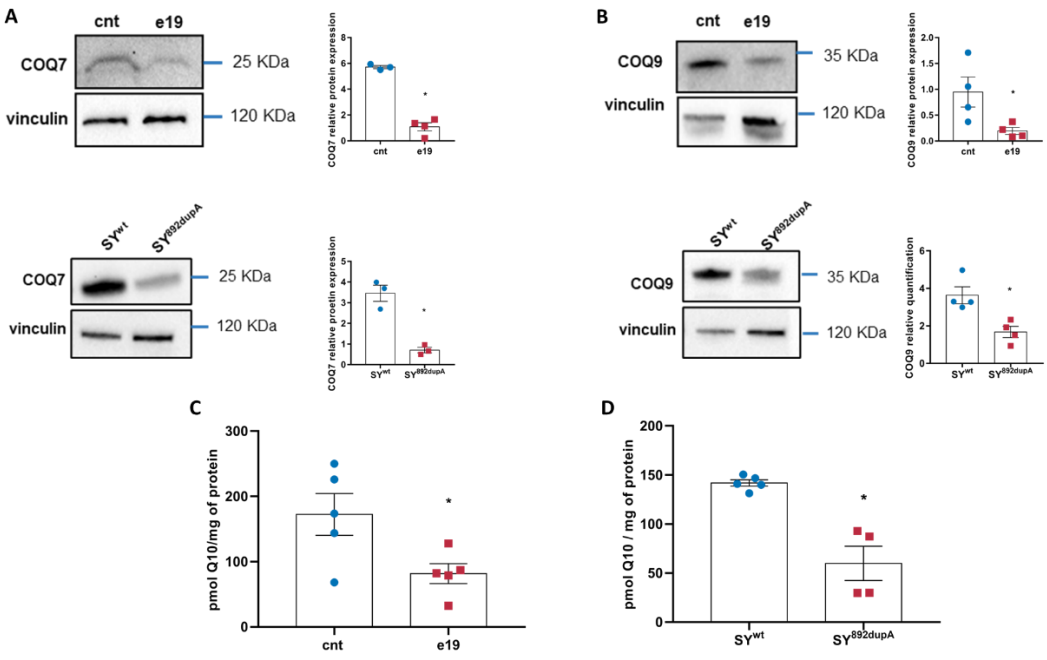

**Fig.25 Mutant Spartin impairs CoQ10 biosynthesis.** A) Western blot analysis and relative quantification for COQ7 proteins in e19 (upper panels) and SY$^{c.892dupA}$ (lower panels) cells versus control (cnt) cell lysates. Immunoblotting for COQ7 and vinculin (endogenous control) was performed on the same blot. Cropped images are reported. The immunoblots are representative of three independent experiments. B) Western blot analysis and relative quantification for COQ9 proteins in e19 (upper panels) and SY$^{c.892dupA}$ (lower panels) cells versus control (cnt) cell lysates. Immunoblotting for COQ9 and vinculin (endogenous control) was performed on the same blot. Cropped images are reported. The immunoblots are representative of three independent experiments (C) Total cellular CoQ10 in control and e19 fibroblasts. At least three independent experiments conducted. Unpaired t-test with Welch's correction, *p = 0.045 (means ± s.e.m.). (D) Total cellular CoQ10 in SY$^{wt}$ and SY$^{c.892dupA}$ cells. At least three independent experiments conducted. Unpaired t-test with Welch's correction, *p = 0.0165 (means ± s.e.m.).

### *4.12. Wild Type Spartin protein expression restored the impaired bioenergetic parameters in patient's fibroblasts and SY$^{C.892dupA}$*

To demonstrate that the biallelic missense variants of Spartin was the main cause of the altered mitochondrial functionality, we evaluated the bioenergetic parameters in e19 cells after transient transfection with pcDNA SPART. Patient's fibroblasts transfected with pcDNA SPART exhibited an ATP/ADP ratio comparable to control cells, contrasting with e19 cells transfected with the empty vector ($p = 0.0288$; Fig.26A). Furthermore, e19 cells transfected with wild-type Spartin displayed a significant recover of intracellular free calcium levels compared to e19 cells transfected with the empty vector (e19-pcDNA3.1 versus e19-pcDNA3.1-SPART, $p < 0.0001$; Fig.26B). Interestingly, the Fluo-3 intensity related to the intracellular free calcium levels completely resembling those measured in control cells (Fig.26B). These results closely mirrored the previously data obtained in SY$^{c.892dupA}$ cells transfected with wild-type SPART, providing additional support for the causative role of the missense changes in eliciting the observed deficits[154].

To further confirm the Spartin involvement in nuclear encoded mitochondrial proteins import, cnt, e19 and e19 expressing wild type Spartin were firstly transfected

with the mitochondrial HyPer7 and then labelled with MitoTarcker RED. The Pearson's coefficient obtained by Imagej software tool showed a completely recover of the merge of the green and red signals, strongly demonstrating the pivotal role of Sartin in the mitochondrial import mechanism.

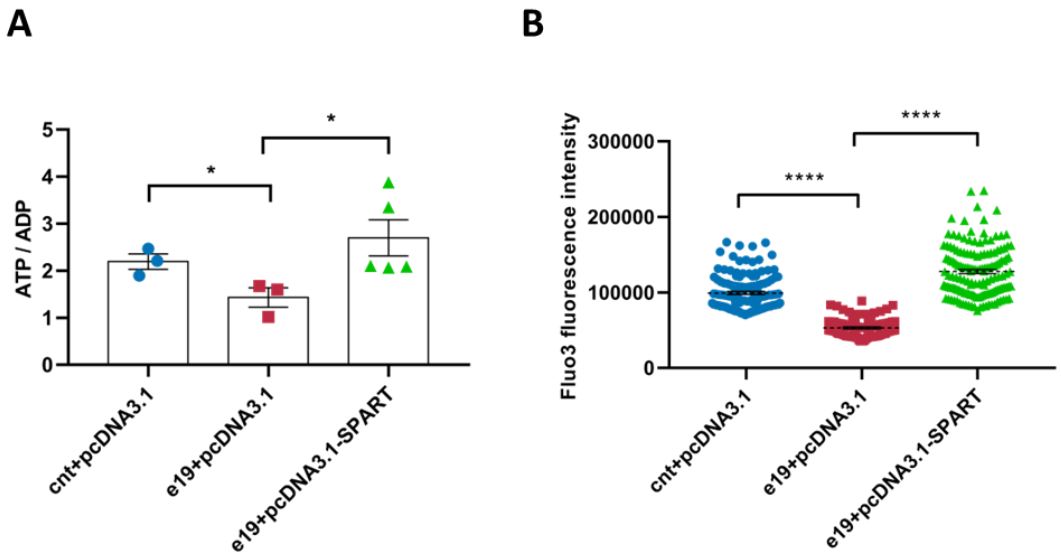


**Fig.26 Wild-type Spartin transient transfection completely rescues the ATP/ADP ratio and the free calcium levels in e19 cells.** A) ATP/ADP ratio in control (cnt-pcDNA3.1, blue dots), e19 mutant (e19-pcDNA3.1, red squares) and e19 mutant cells re-expressing Spartin (e19-pcDNA3.1-SPART, green triangles). At least three independent experiments were conducted. Unpaired t-test with Welch's correction; cnt + pcDNA3.1 versus e19 + pcDNA3.1 *p = 0.0483 (means ± s.e.m.), e19 + pcDNA3.1 versus e19 + pcDNA3.1-SPART *p = 0.0288 (means ± s.e.m.). (B) Intracellular free calcium in live control (cnt-pcDNA3.1, blue dots), mutant (e19-pcDNA3.1, red squares) and mutant cells re-expressing Spartin (e19-pcDNA3.1-SPART, green triangles). At least three independent experiments conducted; Games–Howell's multiple comparisons test, cnt-pcDNA3.1 versus e19-pcDNA3.1, ****p < 0.0001; e19-pcDNA3.1 versus e19-pcDNA3.1-SPART, ****p < 0.0001, (means ± s.e.m.).

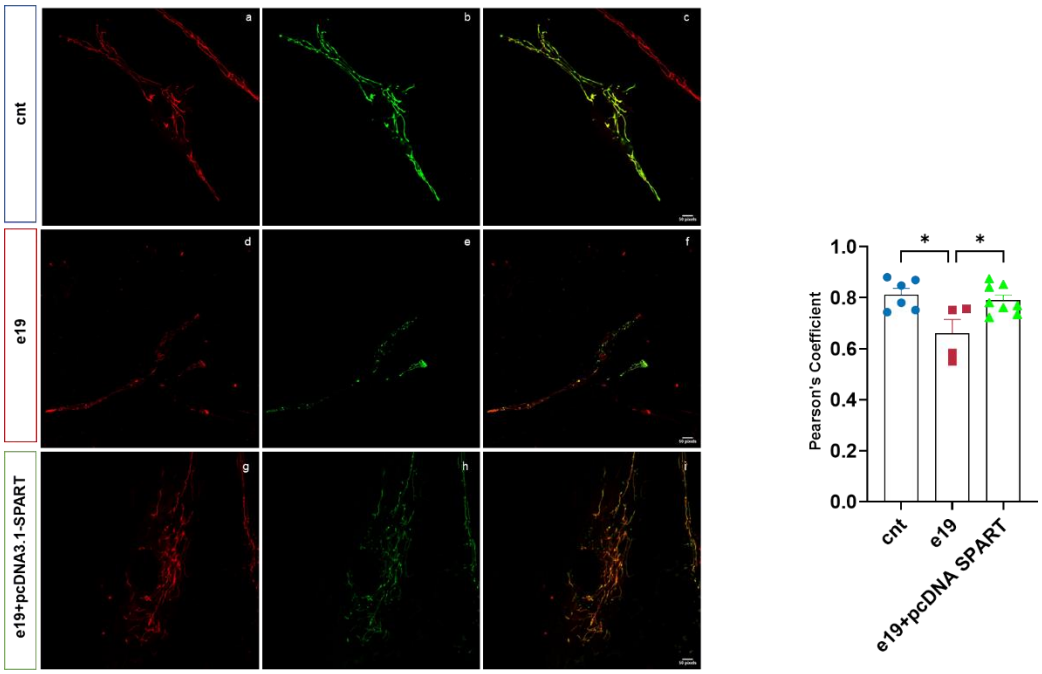


**Fig.27 Wild-type Spartin transient transfection rescues the mitochondrial protein import in e19 cells.** Control fibroblasts, e19 and e19+pcDNA SPART were firstly transfected with a GFP targeting the mitochondria (HyPer7, b, e and h) and then stained with MitoTracker RED (a, d and g). Merged images are shown in panels c, f and h. scale bar representing 50 µm. the Pearson's Coefficient was calculated by ImageJ software tool.

### 4.13. UBQ® treatment partially recovers the mitochondrial functionality in Spartin mutated cells

Considering the identified CoQ10 deficiency across the Spartin mutant cells, we incubated e19, SY$^{c.892dupA}$ and relative controls for 24 hours with 100 nM of UBQ® (Q10) and assessed its impact on growth rate, oxygen consumption, and ATP production. The UBQ® supplementation resulted in an enhanced doubling time for e19 cells, reducing it from 36.82 to 30.33 hours (Fig.28A), while no significant effect was observed in control cells (Fig.28B). Furthermore, incubation with UBQ® restored the ATP/ADP ratio in e19 cells (e19 versus e19 + Q10, p = 0.03; e19 + Q10 versus cnt, p = ns; Fig.28C) and brought the genome edited SY$^{c.892dupA}$ cells back to control levels (SY$^{c.892dupA}$ versus SY$^{c.892dupA}$ + Q10, p = 0.0021; Fig.28D). UBQ® treatment slightly stimulated the integrated activity of Complexes II+III in e19 cells through the electron

transfer capacity of CoQ10 (controls versus e19 + Q10 p = ns; Fig.28E). Additionally, UBQ® treated e19 and SY$^{c.892dupA}$ mutant cells exhibited higher FCCP-induced respiration compared to their respective untreated mutant cells, indicating an improved maximal respiratory capacity for ATP production (Fig.28F and G).

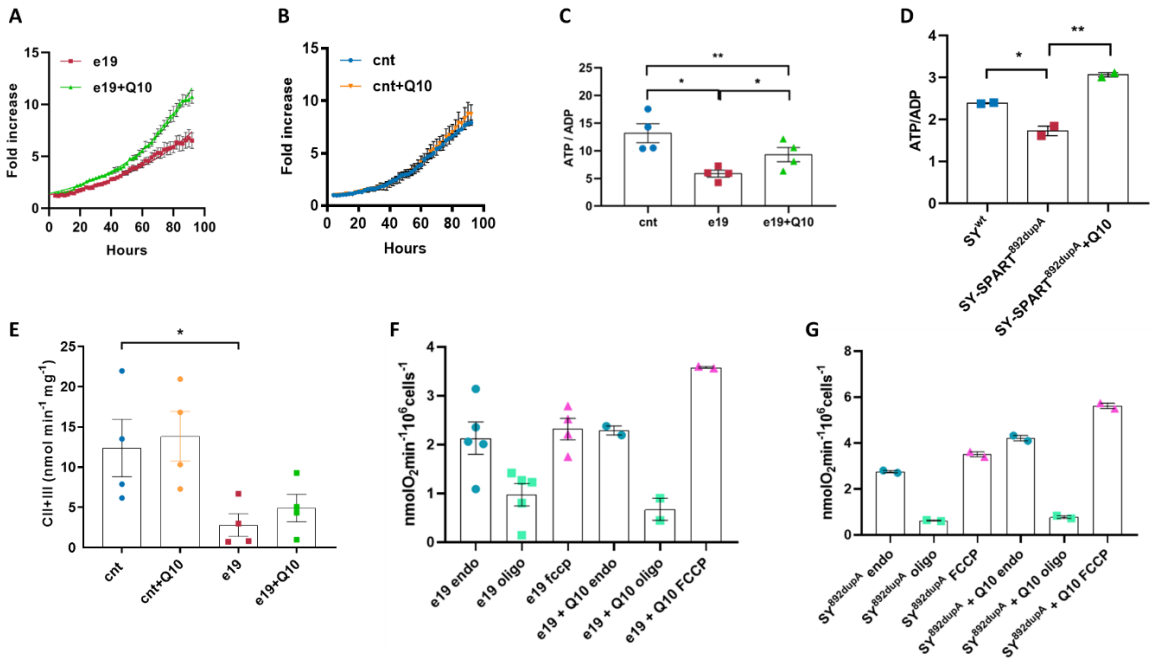


**Fig.28 UBQ® restores the bioenergetic deficiencies in e19 and SY$^{c.892dupA}$ cells.** A) Cell proliferation analysis in mutant cells (e19) incubated with 100nM of UBQ®, imaged and analysed every hour for 96 h. Unpaired t-test with Welch's correction, *p = 0.05 (means ± s.e.m.). (B) Cell proliferation assessment via the IncuCyte Live-Cell Assay. Growth of control cells was not affected by UBQ® (Q10). Untreated control cell, blue dots; Q10-treated control cell, orange triangles. (C) ATP/ADP ratio determination in control (cnt, blue dots), e19 (red squares), and mutant cells supplemented with UBQ® (green triangles). At least three independent experiments were performed. Paired t-test, *p = 0.03 (means ± s.e.m.). (D) ATP/ ADP ratio in control SH-SY5Y cells (SY$^{wt}$, blue dots), SH-SY5Y cells with c.892dupA homozygous change (SY-$^{SPART892dupA}$, red squares) and SY-$^{SPART892dupA}$+ Q10 (green triangles). Tukey's multiple comparisons test, SY-$^{SPART892dupA}$ versus SY–$^{SPART892dupA}$ +Q10, **p = 0.0021 (means ± s.e.m.). (E) Complex II+III activity in control (blue dots) and mutant (red squares) cell lysates with and without treatment with UBQ® for 48 h. Ordinary one-way ANOVA; cnt vs. e19 cells *P =0.0494, (means±sem); cnt vs. e19+Q10, P= 0.1279 (means±sem). (F) Mitochondrial oxygen consumption in endogenous and uncoupled conditions in e19 and e19 cells treated with CoQ (Q10). Respiration was measured in DMEM (basal respiration, petroleum dots), in presence of oligomycin A (non-phosphorylative respiration, green squares) and in presence of FCCP (uncoupled respiration, pink triangles). e19 Q10-treated

fibroblasts showed a significantly increased respiration in presence of FCCP compared to untreated e19. Welch's t test e19 vs. e19+Q10 *P =0.0105 (means±sem). Endo: endogenous basal respiration, oligo: cells treated with oligomycin A. (G) Mitochondrial oxygen consumption in endogenous and uncoupled conditions in $SY^{c.892dupA}$ treated with UBQ® vs. untreated $SY^{c.892dupA}$ cells. Respiration was measured in DMEM (basal respiration, petroleum dots), in presence of oligomycin A (non-phosphorylative respiration, green squares) and in presence of FCCP (uncoupled respiration, pink triangles). $SY^{c.892dupA}$ + Q10-treated fibroblasts showed a significantly increased respiration in presence of FCCP compared to nontreated SY892dupA. Welch's t test $SY^{c.892dupA}$ vs. $SY^{c.892dupA}$ +Q10 *P =0.0058 (means±sem). Endo: endogenous basal respiration, oligo: cells treated with oligomycin A.

# 5. Discussion

## *5.1. Enhanced Coenzyme Q10 Bioavailability and improved mitochondrial functionality in cultured cells through CoQ10 phytosome formulation*

Coenzyme Q10, or CoQ10, is a compound naturally synthetized by every cell in the human body. Due its ubiquitous presence and its quinone structure, CoQ10 is also known as ubiquinone. This red-ox lipid localizes in all cell membranes, but it has been found predominantly in the inner mitochondrial membrane where it plays an essential role in the oxidative phosphorylation carrying the electrons from Complex I and Complex II to Complex III of the mitochondrial respiratory chain. The CoQ10 concentration range differs in organs based on their energy demand. Indeed, CoQ10 is mostly present in heart, skeletal muscle and neurons, underlying its importance in the energy homeostasis. Furthermore, it's the most powerful antioxidant endogenously produced by the cells. It protects against the oxidative-stress-dependent apoptosis promoting the cell survival[199] and prevents the oxidation of several membrane components[200]. Age-related decline and heightened oxidative stress result in reduced tissue concentrations of CoQ10, forming the basis for its clinical recommendation[201,202]. Additionally, a drop in the CoQ10 amount has been reported in several diseases named Primary and Secondary CoQ10 deficiency. Primary CoQ10 deficiency are characterized by mutations in genes directly involved in the CoQ10 biosynthesis, called Primary CoQ10 deficiency. In the Secondary ones the reduction in ubiquinone levels is linked to alterations, both mitochondrial and non-mitochondrial in nature, further highlighting the diverse impact of CoQ10 dysregulation across different pathological conditions. The therapeutic use of CoQ10 gained momentum since its initial application in 1973 for treating congestive heart failure[200]. In fact, it is currently the third most consumed nutritional supplement after fish oil and multivitamins[203]. Due to its robust antioxidant properties and essential physiological role in mitochondrial bioenergetics, CoQ10 has emerged as a promising candidate for treating a spectrum of diseases where oxidative stress prominently

contributes. This includes cardiovascular diseases, neurodegenerative disorders, cancer, and diabetes, all of which rank among the top 10 global causes of death[204,205]. Despite its beneficial role, the CoQ10 shows a hydrophobic proprieties and a substantial molecular weight. These chemical characteristics render it highly water-insoluble, thereby affecting its bioavailability. Consequently, its intestinal absorption is both incomplete and slow. Notably, Hidaka and colleagues collected in a very explicative review a bunch of toxicological studies which they demonstrated that the supplementation of exogenous CoQ10 doesn't influence the endogenous ubiquinone levels and doesn't induce any adverse effects neither[200]. Studies on bioavailability have revealed a non-linear correlation between the amount of CoQ10 supplemented and its plasma concentration. Specifically, it has been noted that as the supplemented dose increases, there is a proportional decrease in the percentage of the dose absorbed. This phenomenon is attributed to the attainment of a maximum plateau level of CoQ10, beyond which further absorption diminishes[206]. So far, various formulations of CoQ10 have been developed and investigated to address its limited bioavailability[97]. For instance, solid dispersion systems[207], nanoparticles[208], cyclodextrin inclusion compounds and microcapsules[209]. However, one of the most auspicious strategies involves the development of nano-liposomes incorporating long-circulating elements. This approach enhances stability, prolongs circulation times, and augments the bioavailability of CoQ10[210]. Furthermore, other formulation developed to enhance the CoQ10 absorption are represented by Self-nanoemulsifying drug delivery systems (SNEDDS)[144], CoQ10-Loaded Oleogels[145] and by the water soluble CoQ10 encapsulated it in β-cyclodextrin inclusion complexes[100,147]. In the first part of this study, we conducted an analysis of the cellular uptake, distribution, and bioenergetic effects of a highly bioavailable food-grade lipid-based CoQ10 formulation known as UBQ® or UBIQSOME. UBQ® comprises a dispersion of CoQ10 in a lecithin matrix[148] and has recently been reported to exhibit improved solubility and enhanced bioavailability in human plasma and muscle tissues [109,148,149]. These findings underscore the need for a comprehensive investigation into the cellular mechanisms to better elucidate the efficiency behind the observed increase in CoQ10 absorption. Utilizing human epithelial intestine cell line (I407) and rat embryonic myoblast cell line (H9c2) as cellular models, our results demonstrated

a substantial improvement in cellular and mitochondrial CoQ10 content induced by UBQ®. Notably, while the uptake of standard CoQ10 was similar in both tested cell lines, the absorption pattern of the CoQ10 phytosome dispersion varied between these cells. This observation suggests that the formulation of CoQ10 may exert a significant impact on the cell-specific uptake of ubiquinone. Since the CoQ10 has antioxidant properties only in its reduced form[211], we assessed the levels of both the reduced ($CoQ_{red}$) and oxidized ($CoQ_{ox}$) forms in our cell lines. Interestingly, the control H9c2 cells exhibited a remarkably predominance of the $CoQ_{ox}$ form over $CoQ_{red}$, whereas the levels of both forms were comparable in I407 cells. Treatment with 100 nM of UBQ in I407 cells equally elevated both CoQ10 forms, providing protection against both endogenous and TBH-induced oxidative stress. Conversely, in H9c2 cells, UBQ® supplementation offered a modest protection against TBH-induced oxidative stress and proved ineffective against endogenous oxidative stress. This lower antioxidant capability in H9c2 could be due to the imbalance in the $CoQ_{ox}/CoQ_{red}$ suggesting that the protection against the oxidant insults by CoQ10 is closely tied to the efficiency of the cells in reducing it, rather than their ability to internalize it at high doses. The present data indicate that an excessive concentration of oxidized CoQ10, in its native unformulated state, not only fails to protect against oxidative stress but may also exhibit a slight pro-oxidant effect[147,212]. These latter observations underscore the significance of a proper CoQ10 formulation, which enhances bioavailability, enabling incubation at lower dosages[213]. This is crucial to prevent nonspecific intracellular accumulation and optimize the therapeutic effectiveness of CoQ10. Furthermore, the treatment with UBQ® protected both cell lines against lipid peroxidation whereas any effect was detected after treatment with native CoQ10 in I407 cell line. Curiously, native CoQ10 treatment as well was able to reduce the lipid peroxidation in H9c2 demonstrating that even a slight accumulation of exogenous CoQ10 is able to defend the cells from this kind of oxidative stress. Remarkably, UBQ® efficiently counteracted ferroptosis, a cell death regulated by iron-dependent peroxidation of lipids[76,214,215]. We identified that UBQ® protected against several oxidative stress and ameliorated bioenergetic parameters. Since mitochondria are involved in the pathogenesis and progression of various diseases such as cancer, neurodegenerative disorders, and cardiovascular diseases, these observed effects

hold significant relevance. The respiration data reported that the spare capacity (the ratio between the oxygen consumption induced by FCCP and Oligomicyn A) was statistically improved by UBQ® treatment in I407 and H9c2 cell lines to sustain the energy demand. Additionally, UBQ® positively impacted cellular ATP and protein content, as well as the mitochondrial transmembrane potential. The increase of intracellular NAD(P)H levels is usually interpreted as a response to a decrease in the OXPHOS[216] and increase in the hypoxia[217]. Contrarily, UBQ treatment led to a decrease in cellular NAD(P)H levels compared to the control, suggesting an enhancement of oxidative metabolism. Has been known from the literature that the mitochondrial biogenesis is prompted in ONH astrocytes by CoQ10 as response to an oxidative stress[218]. Indeed, Noh at al. reported that CoQ10 promoted the expression of mitofilin and peroxisome proliferator-activated receptor-γ coactivator-1 protein indicating a stimulation of mitochondrial biogenesis. Likewise, the UBQ® treatment stimulated the mitochondrial biogenesis in I407 stimulating the citrate synthase (CS) activity, a well-established marker for assessing mitochondrial mass[219]. Conversely, as previously demonstrated, the incubation with crystallin COQ10 didn't show any improvement in all tested bioenergetic parameters[147] underlying the importance of formulation for the CoQ10 treatment. To deeply elucidate the internalization mechanism of UBQ®, we treated our cell models with three different inhibitors for endocytosis. Notably, the macropinocytosis inhibitor amiloride emerged as the most effective in impeding the entry of UBQ®. Macropinocytosis represents a distinctive endocytic pathway marked by the indiscriminate internalization of substantial quantities of extracellular fluid, solutes, and membranes within large endocytic vesicles referred to as macropinosomes[220]. This process plays a pivotal role in various physiological processes, encompassing antigen presentation, nutrient sensing, plasma protein recycling, cellular migration, and signalling. It is plausible that cells leverage macropinocytosis to internalize the CoQ10 phytosome formulation. In fact, it has been reported that MITO-Porter (DF-MITO-Porter) can be absorbed by micropinocytosis through high density of octaarginine (R8)-modified liposome[221]. The treatment with Nile Red allowed us to identify an increase lipid droplet after treatment with both UBQ® and vehicle indicating a challenging intracellular distribution due to the highly lipophilic nature of the molecule. While the oral

distribution is supplementation consistently elevates plasma CoQ10 levels, the tissue distribution of the CoQ10 remains subject of debate[206,222]. Nevertheless, several studies support the accumulation of CoQ10 into the tissue. For example, Drobnic recently identified a slight accumulation of CoQ10 in muscle and plasma of healthy aging athletes supplemented by UBQ®[109]. Furthermore, Bentinger et al., utilizing [3H]CoQ10, demonstrated high uptake in the liver, spleen, and white blood cells, and practically no uptake in muscle, kidney, and the brain[223]. The authors reported that the labelled CoQ10, in the homogenate liver, within organelles but also in the cytosol and transport vesicle suggesting multiple possibilities for intracellular transport. Moreover, the purified mitochondria exhibited a markedly low concentration of [3H]CoQ10, while this lipid was notably enriched in the lysosomal fraction. This distribution can be reasonably explained, as the isoprenoid side chain of CoQ10 likely localizes in the central hydrophobic region of the membrane. The obtained results demonstrated that even in cellular cell model, the CoQ10 supplementation promotes its accumulation in lipid droplets over mitochondria leading to a distinct intracellular distribution, Notably, the two cell lines tested in this study exhibited differential CoQ10 uptake, with lower uptake in the intestinal epithelial cell line (I407) and higher uptake in the embryonal cardiac cell line (H9c2). This supports the notion that intestinal absorption may represent a limiting step in CoQ10 uptake, emphasizing the potential advantages of the phytosome formulation compared to native CoQ10.

### *5.2. Mutations in Spartin affect mitochondrial protein import process leading to an altered bioenergetics reversed by UBQ®*

The expanded availability and the rapid evolution of Next-Generation Sequencing (NGS) brings forth the potential for a heightened diagnostic yield, but concurrently, it elevates the probability of encountering uncertain results. Therefore, The American College of Medical Genetics and Genomics (ACMG) along with the Association for Molecular Pathology (AMP), and the College of American Pathologists revisited and revised standards and guidelines for the interpretation of sequence variants. They recommended a five-tier classification system for interpreting variants: benign, likely benign, variant of uncertain significance (VUS), likely pathogenic, and pathogenic[224]. VUSs denote genetic variants lacking adequate evidence to definitively classify them as benign or pathogenic, and as such, they are not intended to guide clinical decision-making[225]. Attaining a conclusive diagnosis is particularly crucial, especially in scenarios involving prenatal testing or the management of severely affected pediatric patients. Within a routine diagnostic setting, this becomes notably challenging for affected individuals, where comprehensive, unbiased sequencing approaches like Exome Sequencing (ES) or genome sequencing often yield numerous rare missense changes classified as VUS[226]. Nevertheless, ongoing research on these variants may lead to their reclassification, either upgrading them to pathogenic or downgrading them to benign. This underscores the significance of conducting functional studies in the diagnostic variant reclassification process[226]. Herein, we identified a biallelic missense variants in Spartin in a young male patient who manifested clinical phenotype consistent with Troyer syndrome. These features include low normal stature, muscle weakness, impaired walking distance, developmental delay, and MRI findings accordingly with previously reported characteristics of this syndrome[127,128]. Additionally, the presence of epilepsy is considered an extension of the phenotype, as no other causative variants in epilepsy-related genes were detected through Exome Sequencing (ES). Segregation analyses and Carrier testing supported an autosomal recessive mode of inheritance, and the allele frequencies of these changes in both an in-house database and public repositories did not rule out a potential disease-causing

role at the time of the study. To deeply investigate the functional implication and the cellular consequences of the mutations in Spartin, we conducted biochemical and bioenergetics studies on primary fibroblasts derived from the patient (e19) and cell models carrying a loss of function mutation in Spartin ($SY^{c.892dupA}$). Firstly, in silico analysis performed by AlphaFold [186] on fibroblasts derived from patient revealed that the variant p.Lys62Glu was present in the N-terminal MIT domain. According to AlphaFold predictions, the substitution of Lysine 62, located in an exposed region of the MIT-interaction site with Glutamate would likely impact the charge within the domain. The Serine365, instead, was predicted to be an exposed amino acid residue and, particularly, to constitute a terminal point in an alpha helix within a highly flexible region. Consequently, substituting this residue with a Proline would likely induce structural alterations to the alpha helix. Interestingly, Spartin expression seemed to don't be affected suggesting that a putative disruption of the protein folding didn't alter its stability. As reported in our previous results obtained on SH-5SY cells carrying a c.892dupA variant, we observed an altered mitochondrial network organization resulted in a decrease of branch length and a sever bioenergetic deficiency. Specifically, we noted an alteration in the Complex I, Complex II and the integrated activity of the Complex II+III which consequently resulted in an altered ATP-linked respiration and decreased respiratory spare capacity and mitochondrial membrane hyperpolarization (mtΔΨ) versus control fibroblasts. Accordingly with other mitochondrial disorders [170,227], the mitochondrial hyperpolarization led to an increase of the oxidative stress and anion superoxide synthesis. Altogether, these results present compelling evidence for the functional significance of the identified missense variants in Spartin. Indeed, they support the hypothesis that alterations in Spartin functions constitute the molecular defect responsible for the observed disease in the patient. We have previously elucidated the involvement of Spartin in maintaining mitochondrial homeostasis and regulating the free calcium levels[154]. In this study, we conducted a comprehensive analysis of the impact of mutant Spartin on the mitochondrial import of nuclear-encoded proteins and the structure of Mitochondria-Associated Membranes (MAMs), a physical connection between the endoplasmic reticulum (ER) and mitochondria[228]. MAMs, facilitating bidirectional communication between mitochondria and the ER, play crucial roles in fundamental biological

processes such as lipid and calcium homeostasis, mitochondrial dynamics, autophagy, mitophagy, ER stress, inflammation, and apoptosis[195,228,229]. This junction between the ER and mitochondria involves an ER subdomain, the outer mitochondrial membrane (OMM), and over 68 proteins, including those facilitating calcium transport from the ER to the mitochondria [230]. Intriguingly, in mutant cells, we observed a significant reduction in VDAC, GRP75, MCU, TOM70, and TIM23. Additionally, we identified an alteration in calcium levels, specifically rescued by the re-expression of wild-type Spartin. Notably, the mutant cells exhibited insensitivity to the MCU complex inhibitor ruthenium red, further underscoring the role of Spartin in calcium homeostasis. The mitochondrial protein import process plays a crucial role for the survival of eukaryotic cells. The conventional pathway for protein import into the mitochondria is the presequence pathway, as extensively discussed in previous works[231,232]. Over half of all mitochondrial proteins utilize this pathway, wherein the proteins are synthesized as precursors with cleavable amino-terminal extensions known as presequences. These presequences adopt positively charged amphipathic alpha helices and are recognized by receptors within the translocase of the outer mitochondrial membrane (TOM complex)[233,234]. Following translocation through the TOM channel, the cleavable preproteins undergo transfer to the presequence translocase of the inner membrane (TIM23 complex)[235]. TOM70 plays a primary role in facilitating the import of non-cleavable hydrophobic precursors, particularly those such as the metabolite carriers found in the inner membrane[236]. Moreover, TOM70 promotes the ER-mitochondria junctions interacting with the inositol trisphosphates (IP3) receptors sustaining the calcium flux to mitochondria and cell bioenergetics[237]. It has been reported that Spartin localizes on the outer mitochondrial membrane[153] and interacts with the 75-kDA glucose-regulated protein (GRP75)[196]. Since we revealed a decrease in several proteins involved in the MAMs integrity, we speculated that Spartin could regulate the nuclear encoded mitochondrial protein import (Fig.29). To support this thesis, we transfected cells with a mitochondrial-labelled red or green fluorescent protein co-stained using MitoTracker Green or Red dye and we recorded the two fluorescent signals by a confocal microscope. Analysis performed through ImageJ software, clearly demonstrated that the green and red fluorescent signals were overlapped in both control fibroblasts and $SY^{WT}$ while in e19 and

SY$^{c.892dupA}$ the two signals were separated. Surprisingly, patient's fibroblasts transfected with plasmid encoding for a wild-type Spartin displayed an overlapping of the two signals. Moreover, both mutant Spartin displayed an altered TIMM13 expression, an essential transporter for TIM23 in the inner mitochondrial membrane[198], which was fully recovered after wild-type Spartin re-expression. To our knowledge, we reported for the first time an impaired nuclear encoded mitochondrial proteins transport in two Troyer Syndorme cell models attributing to Spartin a pivotal role in this mechanism. The assembly and function of many mitochondrial multiprotein complexes, including OXPHOS, depend on the mitochondrial transport of nuclear-encoded proteins. Indeed, both Spartin mutants showed a significant downregulation of some subunits of the mitochondrial respiratory chain enzymes, especially in SY$^{c.892dupA}$ cells. Notably, as previously reported by Spiegel and collaborators[238], we identified a remarkable decrease of the cytrocome c oxydase subunit 1 (COXI), one component of the cytrocome c oxydase (COX) enzyme. Additionally, SY$^{c.892dupA}$ also showed a diminished assembly of the COX enzyme suggesting that the presence of Spartin is necessary for a correct import of the nuclear subunits of the COX enzyme and their assembly in the inner mitochondrial membrane. Maternal inheritance, predominantly observed in complex forms of HSPs constitute the rarest types of HSP, affecting approximately 1–2% of HSP cases. In specific rare cases of HSP, mutations in the MT-CO3 gene, responsible for encoding Cytochrome c oxidase III (a subunit of respiratory chain complex IV), the MT-T1 gene associated with Isoleucine transfer RNA, and the MT-ND4 and MT-ATP6 genes encoding Complex V, ATP synthase, and subunit ATPase 6 (components of respiratory chain complex V) have been linked to manifestations such as mental retardation, cerebellar ataxias, loss of hearing, chronic progressive external ophthalmoplegia, and neuropathy[239,240]. Therefore, we performed a whole transcriptomic analysis to identify a possible alteration in the genes encoding for the mitochondrial subunit of the ETC enzymes. Obtained results, confirmed by further qPCR analysis, revealed that the gene expression of several mitochondrial subunits for the OXPHOS enzymes was statistically decreased in patient's fibroblasts and SY$^{c.892dupA}$ cells in comparison to controls. Surprisingly, the transfection of Wild Type Spartin was able to completely recover the expression of MT-ND1 and MT-CO3 in both mutated Spartin cells and MT-

ATP6 only in SY$^{c.892dupA}$ cells indicating that Spartin could regulate the correct internalization of the mitochondrial transcription factor TFAM allowing the transcription of the genes encoding the mitochondrial subunits of the ETC enzymes. The mitochondrial protein import plays a crucial role in the cell bioenergetics also allowing the biosynthesis of the CoQ10. Indeed, proteins involved in CoQ synthesis are firstly transcribed in the nucleus and then imported into the mitochondria where they assemble themselves forming the "Complex Q"[141]. We identified a lower expression of COQ7 and COQ9 proteins, involved in the last stages of the CoQ10 biosynthesis[52], in e19 and SY$^{c.892dupA}$ cells compared to related controls followed by a consequent drop in the CoQ10 levels. The decrease of the CoQ10 amount in mutant cells might have profound implications for the bioenergetics and redox homeostasis of Spartin-mutant cells, as CoQ10 serves as an essential electron carrier in ETC and functions as a lipophilic antioxidant[241]. Notably, we successfully restored the growth rate and ATP levels of mutant cells in vitro through the addition of a pythosome formulation of CoQ10 (UBQ®). The recovery of ATP levels with UBQ® supplementation was comparable to that observed in mutant cells transfected with wild-type Spartin. Concordantly with the recovery in the growth rate and ATP production, the UBQ® incubation improved the maximal respiration and, slightly, the Complex II+III integrated activity in both mutants. The primary cause of mitochondrial dysfunction resulting from Spartin mutations could be attributed to OXPHOS defects ROS production. This could arise from impaired proteins import leading to the loss of respiratory complex assembly or the absence of ubiquinone-producing enzymes. As the CoQ10 supplementation was beneficial for several bioenergetic defects in both Troyer Syndrome cell models, we can strongly support the latter proposed mechanism. In fact, CoQ10 treatment may contribute to improved cell growth by alleviating the severe mitochondrial oxidative stress observed in mutant cells, as indicated by elevated mitochondrial superoxide production and reduced glutathione levels[141]. Notably, the CoQ10 supplementation has been reported as an efficient therapeutical approach for neurological and neurodegenerative disorders with defective mitochondrial function, as well as mitochondrial disorders characterized by multisystemic involvement, particularly affecting high-energy demanding cells such as neurons and muscle cells[242,243]. Furthermore, it is well known that the

administration of CoQ10 has no contraindications and very rare adverse effects, with fewer than 1% of patients experiencing mild dose-related gastrointestinal discomfort[244]. Considering the crucial role of mitochondrial impairment in Troyer Syndrome and the beneficial role of the CoQ10 treatment we propose that patients affected by this disease may take advantage from a similar therapeutic approach.

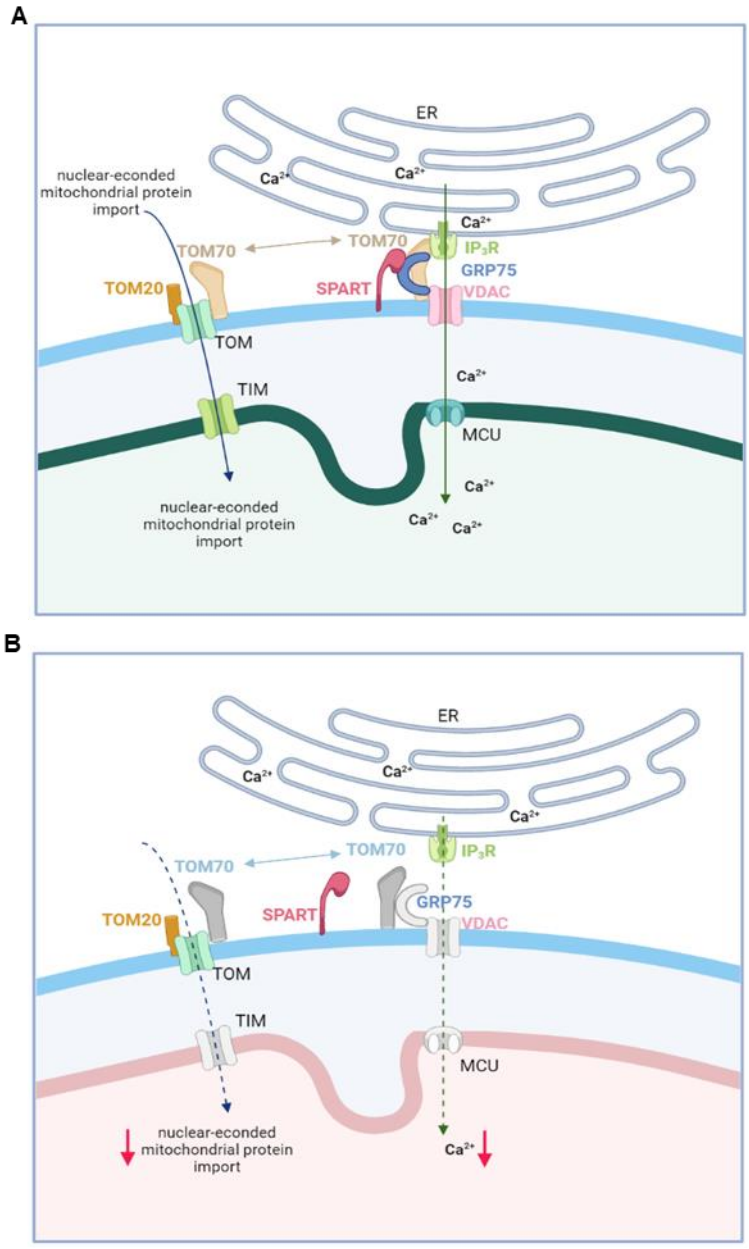


**Fig.29 Model for the molecular role of wild-type and mutant Spartin at the MAMs.** A) *Wild-type Spartin*. The protein core complex mediating the calcium transport from the ER to the mitochondria comprehends IP3R (green), located in the ER, VDAC (light pink), located in the OMM and mediating the uptake of Ca2+ into mitochondria, GRP75 (blue), which forms a bridge between IP3R and VDAC, and the mitochondrial calcium uniporter (MCU, turquoise), the calcium channel localized in the inner

mitochondrial membrane. Spartin (red) localizes to the OMM and binds to GRP75. TOM70 shifts between the nuclear-encoded mitochondrial protein import complex and the ER-mitochondria contacts, recruiting IP3R, and promoting inter-organelle calcium transfer, bioenergetics, and cell proliferation. (B) *Absent or misfolded Spartin*. When Spartin is mutated/absent, there is a reduced expression of VDAC, GRP75, MCU, TOM70 and TIM23, part of the TIM complex and an altered calcium transport leading to defects in the import of nuclear-encoded mitochondrial proteins, with an impaired metabolism and altered mitochondrial functions as final effects. Figures created with Biorender.com.

## 6. Conclusions

In conclusion, our results from two distinct studies underscore the critical role of tailored Coenzyme Q10 (CoQ10) formulations in influencing cellular bioenergetics and their therapeutic potential. Initially, we observed that the food-grade formulation UBQ® effectively elevated cellular and mitochondrial CoQ10 content, resulting in improved cellular bioenergetic parameters in in vitro models. Importantly, the antioxidant benefits of CoQ10 were intricately linked to the formulation's efficiency, emphasizing the necessity of achieving correct intracellular distribution for optimal cellular reduction. Furthermore, our investigations revealed that the mechanism of macropinocytosis is responsible for the cellular internalization of the phytosome formulation, offering valuable insights into CoQ10 uptake. Both studies emphasized the pivotal role of a suitable CoQ10 formulation in enhancing bioenergetic parameters while mitigating nonspecific cellular accumulation associated with high-dose supplementation. The integration of Next-Generation Sequencing (NGS) with molecular phenotyping, demonstrated in the second study, enabled us to attribute functional relevance and diagnostic potential to variants initially classified as of unknown significance. Notably, we demonstrated for the first time the crucial role of Spartin in the mitochondrial import of nuclear-encoded proteins. This led us to speculate that mutations in Spartin may disrupt this mechanism, causing alterations in the mitochondrial import of key components involved in sustaining oxidative phosphorylation, such as nuclear-encoded subunits of ETC enzymes, transcription factors for mitochondrial genes encoding for the respiratory complexes, and key enzymes of the “Complex Q”. This innovative approach, particularly in identifying

druggable altered pathways like CoQ10 biosynthesis, opens avenues for targeted in vivo treatments for rare yet severe conditions such as Troyer Syndrome. In essence, our collective findings underscore the importance of CoQ10 formulations and the potential of advanced molecular techniques in comprehending and addressing complex genetic disorders.

## 7. Bibliography


1. Crane, F. L., Widmer, C., Lester, R. L., Hatefi, Y. & Fechner, W. Studies on the electron transport system: XV. Coenzyme Q (Q275) and the succinoxidase activity of the electron transport particle. *Biochim. Biophys. Acta* **31**, 476–489 (1959).

2. Stefely, J. A. & Pagliarini, D. J. Biochemistry of Mitochondrial Coenzyme Q Biosynthesis. *Trends Biochem. Sci.* **42**, 824–843 (2017).

3. OLSON, R. E. *et al.* BENZOATE DERIVATIVES AS INTERMEDIATES IN THE BIOSYNTHESIS OF COENZYME Q. *J. Biol. Chem.* **238**, 3146–3148 (1963).

4. Gloor, U. & Wiss, O. On the biosynthesis of ubiquinone (50). *Arch. Biochem. Biophys.* **83**, 216–222 (1959).

5. Kaymak, I. *et al.* Mevalonate Pathway Provides Ubiquinone to Maintain Pyrimidine Synthesis and Survival in p53-Deficient Cancer Cells Exposed to Metabolic Stress. *Cancer Res.* **80**, 189–203 (2020).

6. Bloch, K. The biological synthesis of cholesterol. *Science* **150**, 19–28 (1965).

7. Bentley, R., Ramsey, V. G., Springer, C. M., Dialameh, G. H. & Olson, R. E. The origin of the benzoquinone ring of coenzyme Q9 in the rat. *Biochem. Biophys. Res. Commun.* **5**, 443–446 (1961).

8. Booth, A. N. *et al.* Urinary Phenolic Acid Metabolites of Tyrosine. *J. Biol. Chem.* **235**, 2649–2652 (1960).

9. Morgan, P. N., Gibson, M. I. & Gibson, F. Conversion of Shikimic Acid to Aromatic Compounds. *Nature* **194**, 1239–1241 (1962).

10. Pierrel, F. *et al.* Involvement of Mitochondrial Ferredoxin and Para-Aminobenzoic Acid in Yeast Coenzyme Q Biosynthesis. *Chem. Biol.* **17**, 449–459 (2010).

11. Gin, P. & Clarke, C. F. Genetic Evidence for a Multi-subunit Complex in Coenzyme Q Biosynthesis in Yeast and the Role of the Coq1 Hexaprenyl Diphosphate Synthase*. *J. Biol. Chem.* **280**, 2676–2681 (2005).

12. He, C. H., Xie, L. X., Allan, C. M., Tran, U. C. & Clarke, C. F. Coenzyme Q supplementation or over-expression of the yeast Coq8 putative kinase stabilizes multi-subunit Coq polypeptide complexes in yeast coq null mutants. *Biochim. Biophys. Acta BBA - Mol. Cell Biol. Lipids* **1841**, 630–644 (2014).

13. Okada, K. *et al.* Polyprenyl diphosphate synthase essentially defines the length of the side chain of ubiquinone. *Biochim. Biophys. Acta BBA - Lipids Lipid Metab.* **1302**, 217–223 (1996).

14. Structural Insights into Ubiquinone Biosynthesis in Membranes | Science. https://www.science.org/doi/10.1126/science.1246774.

15. Mugoni, V. *et al.* Ubiad1 Is an Antioxidant Enzyme that Regulates eNOS Activity by CoQ10 Synthesis. *Cell* **152**, 504–518 (2013).

16. Pagliarini, D. J. *et al.* A Mitochondrial Protein Compendium Elucidates Complex I Disease Biology. *Cell* **134**, 112–123 (2008).

17. Proteomic Mapping of Mitochondria in Living Cells via Spatially Restricted Enzymatic Tagging | Science. https://www.science.org/doi/10.1126/science.1230593.

18. Coenzyme Q Biosynthesis: Coq6 Is Required for the C5-Hydroxylation Reaction and Substrate Analogs Rescue Coq6 Deficiency - ScienceDirect. https://www.sciencedirect.com/science/article/pii/S1074552111002407.

19. Identification of 3,4-dihydroxy-5-hexaprenylbenzoic acid as an intermediate in the biosynthesis of ubiquinone-6 by Saccharomyces cerevisiae | Biochemistry. https://pubs.acs.org/doi/abs/10.1021/bi00517a041.

20. ubiI, a New Gene in Escherichia coli Coenzyme Q Biosynthesis, Is Involved in Aerobic C5-hydroxylation - ScienceDirect. https://www.sciencedirect.com/science/article/pii/S0021925820457163.

21. Clarke, C. F., Williams, W. & Teruya, J. H. Ubiquinone biosynthesis in Saccharomyces cerevisiae. Isolation and sequence of COQ3, the 3,4-dihydroxy-5-hexaprenylbenzoate methyltransferase gene. *J. Biol. Chem.* **266**, 16636–16644 (1991).

22. Scopus - Document details - Complementation of coq3 mutant yeast by mitochondrial targeting of the Escherichia coli UbiG polypeptide: Evidence that UbiG catalyzes both O- methylation steps in ubiquinone biosynthesis. https://www.scopus.com/record/display.uri?eid=2-s2.0-0029745317&origin=inward.

23. Cox, G. B., Young, I. G., McCann, L. M. & Gibson, F. Biosynthesis of Ubiquinone in Escherichia coli K-12: Location of Genes Affecting the Metabolism of 3-Octaprenyl-4-hydroxybenzoic Acid and 2-Octaprenylphenol. *J. Bacteriol.* **99**, 450–458 (1969).

24. Pathway for Ubiquinone Biosynthesis in Escherichia coli K-12: Gene-Enzyme Relationships and Intermediates | Journal of Bacteriology. https://journals.asm.org/doi/10.1128/jb.114.1.42-52.1973.

25. Barkovich, R. J. *et al.* Characterization of the COQ5 Gene from Saccharomyces cerevisiae EVIDENCE FOR A C-METHYLTRANSFERASE IN UBIQUINONE BIOSYNTHESIS*. *J. Biol. Chem.* **272**, 9182–9188 (1997).

26. Dibrov, E., Robinson, K. M. & Lemire, B. D. The COQ5 Gene Encodes a Yeast Mitochondrial Protein Necessary for Ubiquinone Biosynthesis and the Assembly of the Respiratory Chain*. *J. Biol. Chem.* **272**, 9175–9181 (1997).

27. Ewbank, J. J. *et al.* Structural and functional conservation of the Caenorhabditis elegans timing gene clk-1. *Science* **275**, 980–983 (1997).

28. Yeast Clk-1 Homologue (Coq7/Cat5) Is a Mitochondrial Protein in Coenzyme Q Synthesis - ScienceDirect. https://www.sciencedirect.com/science/article/pii/S002192581893735X.

29. The COQ7 Gene Encodes a Protein in Saccharomyces cerevisiae Necessary for Ubiquinone Biosynthesis - ScienceDirect. https://www.sciencedirect.com/science/article/pii/S002192581897969X.

30. Stenmark, P. *et al.* A New Member of the Family of Di-iron Carboxylate Proteins. *J. Biol. Chem.* **276**, 33297–33300 (2001).

31. The Aging-Associated Enzyme CLK-1 Is a Member of the Carboxylate-Bridged Diiron Family of Proteins | Biochemistry. https://pubs.acs.org/doi/10.1021/bi101475z.

32. Aging-Associated Enzyme Human Clock-1: Substrate-Mediated Reduction of the Diiron Center for 5-Demethoxyubiquinone Hydroxylation | Biochemistry. https://pubs.acs.org/doi/10.1021/bi301674p.

33. Characterization and Genetic Analysis of Mutant Strains of Escherichia coli K-12 Accumulating the Ubiquinone Precursors 2-Octaprenyl-6-Methoxy-1,4-Benzoquinone and 2-Octaprenyl-3-Methyl-6-Methoxy-1,4-Benzoquinone | Journal of Bacteriology. https://journals.asm.org/doi/10.1128/jb.105.3.769-778.1971.

34. Lee, P. T., Hsu, A. Y., Ha, H. T. & Clarke, C. F. A C-methyltransferase involved in both ubiquinone and menaquinone biosynthesis: isolation and identification of the Escherichia coli ubiE gene. *J. Bacteriol.* **179**, 1748–1754 (1997).

35. Pelosi, L. *et al.* Evolution of Ubiquinone Biosynthesis: Multiple Proteobacterial Enzymes with Various Regioselectivities To Catalyze Three Contiguous Aromatic Hydroxylation Reactions. *mSystems* **1**, 10.1128/msystems.00091-16 (2016).

36. Marbois, B. *et al.* Coq3 and Coq4 Define a Polypeptide Complex in Yeast Mitochondria for the Biosynthesis of Coenzyme Q*. *J. Biol. Chem.* **280**, 20231–20238 (2005).

37. The yeast Coq4 polypeptide organizes a mitochondrial protein complex essential for coenzyme Q biosynthesis - ScienceDirect. https://www.sciencedirect.com/science/article/pii/S138819810800190X.

38. Hayashi, K. *et al.* Functional Conservation of Coenzyme Q Biosynthetic Genes among Yeasts, Plants, and Humans. *PLOS ONE* **9**, e99038 (2014).

39. Biosynthesis of coenzyme Q in eukaryotes | Bioscience, Biotechnology, and Biochemistry | Oxford Academic. https://academic.oup.com/bbb/article/80/1/23/5939105?login=true.

40. Tauche, A., Krause-Buchholz, U. & Rödel, G. Ubiquinone biosynthesis in Saccharomyces cerevisiae: the molecular organization of O-methylase Coq3p depends on Abc1p/Coq8p. *FEMS Yeast Res.* **8**, 1263–1275 (2008).

41. Expression of the human atypical kinase ADCK3 rescues coenzyme Q biosynthesis and phosphorylation of Coq polypeptides in yeast coq8 mutants - ScienceDirect. https://www.sciencedirect.com/science/article/pii/S1388198111000199.

42. Lagier-Tourenne, C. *et al.* ADCK3, an ancestral kinase, is mutated in a form of recessive ataxia associated with coenzyme Q10 deficiency. *Am. J. Hum. Genet.* **82**, 661–672 (2008).

43. Johnson, A. *et al.* COQ9, a New Gene Required for the Biosynthesis of Coenzyme Q in Saccharomyces cerevisiae*. *J. Biol. Chem.* **280**, 31397–31404 (2005).

44. Hsieh, E. J. *et al.* Saccharomyces cerevisiae Coq9 polypeptide is a subunit of the mitochondrial coenzyme Q biosynthetic complex. *Arch. Biochem. Biophys.* **463**, 19–26 (2007).

45. Dysfunctional Coq9 protein causes predominant encephalomyopathy associated with CoQ deficiency | Human Molecular Genetics | Oxford Academic. https://academic.oup.com/hmg/article/22/6/1233/584009.

46. Lohman, D. C. *et al.* Mitochondrial COQ9 is a lipid-binding protein that associates with COQ7 to enable coenzyme Q biosynthesis. *Proc. Natl. Acad. Sci.* **111**, E4697–E4705 (2014).

47. The Saccharomyces cerevisiae COQ10 Gene Encodes a START Domain Protein Required for Function of Coenzyme Q in Respiration - ScienceDirect. https://www.sciencedirect.com/science/article/pii/S0021925819478678.

48. Allan, C. M. *et al.* A conserved START domain coenzyme Q-binding polypeptide is required for efficient Q biosynthesis, respiratory electron transport,

and antioxidant function in Saccharomyces cerevisiae. *Biochim. Biophys. Acta BBA - Mol. Cell Biol. Lipids* **1831**, 776–791 (2013).

49. Loiseau, L. *et al.* The UbiK protein is an accessory factor necessary for bacterial ubiquinone (UQ) biosynthesis and forms a complex with the UQ biogenesis factor UbiJ. *J. Biol. Chem.* **292**, 11937–11950 (2017).

50. Coenzyme Q biosynthetic proteins assemble in a substrate-dependent manner into domains at ER–mitochondria contacts | Journal of Cell Biology | Rockefeller University Press. https://rupress.org/jcb/article/218/4/1353/61880/Coenzyme-Q-biosynthetic-proteins-assemble-in-a.

51. Eisenberg-Bord, M. *et al.* The Endoplasmic Reticulum-Mitochondria Encounter Structure Complex Coordinates Coenzyme Q Biosynthesis. *Contact* **2**, 2515256418825409 (2019).

52. Guerra, R. M. & Pagliarini, D. J. Coenzyme Q biochemistry and biosynthesis. *Trends Biochem. Sci.* **48**, 463–476 (2023).

53. Hernansanz-Agustín, P. & Enríquez, J. A. Functional segmentation of CoQ and cyt c pools by respiratory complex superassembly. *Free Radic. Biol. Med.* **167**, 232–242 (2021).

54. Baschiera, E., Sorrentino, U., Calderan, C., Desbats, M. A. & Salviati, L. The multiple roles of coenzyme Q in cellular homeostasis and their relevance for the pathogenesis of coenzyme Q deficiency. *Free Radic. Biol. Med.* **166**, 277–286 (2021).

55. Olsen: Clear relationship between ETF/ETFDH genotype... - Google Scholar. https://scholar.google.com/scholar_lookup?title=Clear%20relationship%20between%20ETFETFDH%20genotype%20and%20phenotype%20in%20patients%20with%20multiple%20acyl-CoA%20dehydrogenation%20deficiency&publication_year=2003&author=R.K.%20Olsen&author=B.S.%20Andresen&author=E.%20Christensen&author=P.%20Bross&author=F.%20Skovby&author=N.%20Gregersen.

56. Henriques: Electron transfer flavoprotein and its... - Google Scholar. https://scholar.google.com/scholar_lookup?title=Electron%20transfer%20flavoprotein%20and%20its%20role%20in%20mitochondrial%20energy%20metabolism%20in%20health%20and%20disease&publication_year=2021&author=B.J.%20Henriques&author=R.%20Katrine%20Jentoft%20Olsen&author=C.M.%20Gomes&author=P.%20Bross.

57. Minet, M., Dufour, M.-E. & Lacroute, F. Cloning and sequencing of a human cDNA coding for dihydroorotate dehydrogenase by complementation of the corresponding yeast mutant. *Gene* **121**, 393–396 (1992).

58. Three enzymatic activities catalyze the oxidation of sulfide to thiosulfate in mammalian and invertebrate mitochondria - Hildebrandt - 2008 - The FEBS Journal -

Wiley Online Library. https://febs.onlinelibrary.wiley.com/doi/10.1111/j.1742-4658.2008.06482.x.

59. Mráček, T., Drahota, Z. & Houštěk, J. The function and the role of the mitochondrial glycerol-3-phosphate dehydrogenase in mammalian tissues. *Biochim. Biophys. Acta BBA - Bioenerg.* **1827**, 401–410 (2013).

60. Servet, C., Ghelis, T., Richard, L., Zilberstein, A. & Savoure, A. Proline dehydrogenase: a key enzyme in controlling cellular homeostasis. *Front. Biosci.-Landmark* **17**, 607–620 (2012).

61. Banerjee, R., Purhonen, J. & Kallijärvi, J. The mitochondrial coenzyme Q junction and complex III: biochemistry and pathophysiology. *FEBS J.* **289**, 6936–6958 (2022).

62. Jarmuszkiewicz, W., Dominiak, K., Budzinska, A., Wojcicki, K. & Galganski, L. Mitochondrial Coenzyme Q Redox Homeostasis and Reactive Oxygen Species Production. *Front. Biosci.-Landmark* **28**, 61 (2023).

63. Mellors, A. & Tappel, A. The Inhibition of Mitochondrial Peroxidation by Ubiquinone and Ubiquinol. *J. Biol. Chem.* **241**, 4353–6 (1966).

64. Turunen, M., Olsson, J. & Dallner, G. Metabolism and function of coenzyme Q. *Biochim. Biophys. Acta BBA - Biomembr.* **1660**, 171–199 (2004).

65. New developments on the functions of coenzyme Q in mitochondria - Genova - 2011 - BioFactors - Wiley Online Library. https://iubmb.onlinelibrary.wiley.com/doi/full/10.1002/biof.168.

66. Beyer, R. E. *et al.* The role of DT-diaphorase in the maintenance of the reduced antioxidant form of coenzyme Q in membrane systems. *Proc. Natl. Acad. Sci.* **93**, 2528–2532 (1996).

67. Ross, D. & Siegel, D. Functions of NQO1 in Cellular Protection and CoQ10 Metabolism and its Potential Role as a Redox Sensitive Molecular Switch. *Front. Physiol.* **8**, (2017).

68. Liebler, D. C. The Role of Metabolism in the Antioxidant Function of Vitamin E. *Crit. Rev. Toxicol.* **23**, 147–169 (1993).

69. Siegel, D. *et al.* NAD(P)H:Quinone Oxidoreductase 1: Role as a Superoxide Scavenger. *Mol. Pharmacol.* **65**, 1238–1247 (2004).

70. The Highly Expressed and Inducible Endogenous NAD(P)H:quinone Oxidoreductase 1 in Cardiovascular Cells Acts as a Potential Superoxide Scavenger | Cardiovascular Toxicology. https://link.springer.com/article/10.1007/s12012-007-9001-z.

71. Pink, J. J. *et al.* NAD(P)H:Quinone Oxidoreductase Activity Is the Principal Determinant of β-Lapachone Cytotoxicity *. *J. Biol. Chem.* **275**, 5416–5424 (2000).

72. Bello, R. I. *et al.* Hydrogen Peroxide- and Cell-Density-Regulated Expression of NADH-Cytochrome b5 Reductase in HeLa Cells. *J. Bioenerg. Biomembr.* **35**, 169–179 (2003).

73. Villalba, J. M. *et al.* Role of cytochrome b5 reductase on the antioxidant function of coenzyme Q in the plasma membrane. *Mol. Aspects Med.* **18**, 7–13 (1997).

74. Dixon, S. J. *et al.* Ferroptosis: An Iron-Dependent Form of Nonapoptotic Cell Death. *Cell* **149**, 1060–1072 (2012).

75. Jiang, X., Stockwell, B. R. & Conrad, M. Ferroptosis: mechanisms, biology and role in disease. *Nat. Rev. Mol. Cell Biol.* **22**, 266–282 (2021).

76. Bersuker, K. *et al.* The CoQ oxidoreductase FSP1 acts parallel to GPX4 to inhibit ferroptosis. *Nature* **575**, 688–692 (2019).

77. Pallotti, F., Bergamini, C., Lamperti, C. & Fato, R. The Roles of Coenzyme Q in Disease: Direct and Indirect Involvement in Cellular Functions. *Int. J. Mol. Sci.* **23**, 128 (2021).

78. López-Lluch, G., Hernández-Camacho, J. D., Fernández-Ayala, D. J. M. & Navas, P. Mitochondrial dysfunction in metabolism and ageing: shared mechanisms and outcomes? *Biogerontology* **19**, 461–480 (2018).

79. Pagano, G. *et al.* Aging-Related Disorders and Mitochondrial Dysfunction: A Critical Review for Prospect Mitoprotective Strategies Based on Mitochondrial Nutrient Mixtures. *Int. J. Mol. Sci.* **21**, 7060 (2020).

80. Haas, R. H. Mitochondrial Dysfunction in Aging and Diseases of Aging. *Biology* **8**, 48 (2019).

81. Döring, F., Schmelzer, C., Lindner, I., Vock, C. & Fujii, K. Functional connections and pathways of coenzyme Q10-inducible genes: An in-silico study. *IUBMB Life* **59**, 628–633 (2007).

82. Moreno Fernández-Ayala, D. J., Navas, P. & López-Lluch, G. Age-related mitochondrial dysfunction as a key factor in COVID-19 disease. *Exp. Gerontol.* **142**, 111147 (2020).

83. Alcázar-Fabra, M., Trevisson, E. & Brea-Calvo, G. Clinical syndromes associated with Coenzyme Q10 deficiency. *Essays Biochem.* **62**, 377–398 (2018).

84. Mutations in COQ2 in Familial and Sporadic Multiple-System Atrophy. *N. Engl. J. Med.* **369**, 233–244 (2013).

85. Horvath, R. *et al.* Adult-onset cerebellar ataxia due to mutations in CABC1/ADCK3. *J. Neurol. Neurosurg. Psychiatry* **83**, 174–178 (2012).

86. Cerebellar ataxia and severe muscle CoQ10 deficiency in a patient with a novel mutation in ADCK3 - Barca - 2016 - Clinical Genetics - Wiley Online Library. https://onlinelibrary.wiley.com/doi/10.1111/cge.12742.

87. Atmaca, M. *et al.* Follow-up results of patients with ADCK4 mutations and the efficacy of CoQ10 treatment. *Pediatr. Nephrol.* **32**, 1369–1375 (2017).

88. Navas, P. *et al.* Secondary CoQ10 deficiency, bioenergetics unbalance in disease and aging. *BioFactors* **47**, 551–569 (2021).

89. Secondary coenzyme Q10 deficiencies in oxidative phosphorylation (OXPHOS) and non-OXPHOS disorders - ScienceDirect. https://www.sciencedirect.com/science/article/pii/S1567724916300848?via%3Dihub.

90. Coenzyme Q – Biosynthesis and functions - ScienceDirect. https://www.sciencedirect.com/science/article/pii/S0006291X10003815?via%3Dihub.

91. González-Mariscal, I. *et al.* Regulation of coenzyme Q biosynthesis in yeast: A new complex in the block. *IUBMB Life* **66**, 63–70 (2014).

92. Sacconi, S. *et al.* Coenzyme Q10 is frequently reduced in muscle of patients with mitochondrial myopathy. *Neuromuscul. Disord.* **20**, 44–48 (2010).

93. Trevisson, E., DiMauro, S., Navas, P. & Salviati, L. Coenzyme Q deficiency in muscle. *Curr. Opin. Neurol.* **24**, 449 (2011).

94. Desbats, M. A., Lunardi, G., Doimo, M., Trevisson, E. & Salviati, L. Genetic bases and clinical manifestations of coenzyme Q10 (CoQ10) deficiency. *J. Inherit. Metab. Dis.* **38**, 145–156 (2015).

95. Cordero, M. D. *et al.* Mitochondrial dysfunction and mitophagy activation in blood mononuclear cells of fibromyalgia patients: implications in the pathogenesis of the disease. *Arthritis Res. Ther.* **12**, R17 (2010).

96. Mantle, D. & Dybring, A. Bioavailability of Coenzyme Q10: An Overview of the Absorption Process and Subsequent Metabolism. *Antioxidants* **9**, 386 (2020).

97. IJMS | Free Full-Text | Coenzyme Q10: Novel Formulations and Medical Trends. https://www.mdpi.com/1422-0067/21/22/8432.

98. Suárez-Rivero, J. M. *et al.* Coenzyme Q10 Analogues: Benefits and Challenges for Therapeutics. *Antioxidants* **10**, 236 (2021).

99. Pravst, I. *et al.* Comparative Bioavailability of Different Coenzyme Q10 Formulations in Healthy Elderly Individuals. *Nutrients* **12**, 784 (2020).

100. Yang, H. & Song, J. [Inclusion of coenzyme Q10 with beta-cyclodextrin studied by polarography]. *Yao Xue Xue Bao* **41**, 671–674 (2006).

101. Pesini, A., Hidalgo-Gutierrez, A. & Quinzii, C. M. Mechanisms and Therapeutic Effects of Benzoquinone Ring Analogs in Primary CoQ Deficiencies. *Antioxidants* **11**, 665 (2022).

102. Pierrel, F. Impact of chemical analogs of 4-hydroxybenzoic acid on coenzyme Q biosynthesis: From inhibition to bypass of coenzyme Q deficiency. *Front. Physiol.* **8**, (2017).

103. Freyer, C. *et al.* Rescue of primary ubiquinone deficiency due to a novel COQ7 defect using 2,4–dihydroxybensoic acid. *J. Med. Genet.* **52**, 779–783 (2015).

104. Kelso, G. F. *et al.* Selective Targeting of a Redox-active Ubiquinone to Mitochondria within Cells: ANTIOXIDANT AND ANTIAPOPTOTIC PROPERTIES*. *J. Biol. Chem.* **276**, 4588–4596 (2001).

105. Sena Ozbay, H. *et al.* Mitochondria-targeted CoQ10 loaded PLGA-b-PEG-TPP nanoparticles: Their effects on mitochondrial functions of COQ8B-/- HK-2 cells. *Eur. J. Pharm. Biopharm.* **173**, 22–33 (2022).

106. Yamada, Y. *et al.* MITO-Porter: A liposome-based carrier system for delivery of macromolecules into mitochondria via membrane fusion. *Biochim. Biophys. Acta BBA - Biomembr.* **1778**, 423–432 (2008).

107. Wang, Y. & Hekimi, S. Micellization of coenzyme Q by the fungicide caspofungin allows for safe intravenous administration to reach extreme supraphysiological concentrations. *Redox Biol.* **36**, 101680 (2020).

108. Rizzardi, N. *et al.* Coenzyme Q10 Phytosome Formulation Improves CoQ10 Bioavailability and Mitochondrial Functionality in Cultured Cells. *Antioxidants* **10**, 927 (2021).

109. Drobnic, F. *et al.* Efficient muscle distribution reflects the positive influence of coenzyme Q10 Phytosome in healthy aging athletes after stressing exercise. (2020).

110. Marcheggiani, F. *et al.* CoQ10Phytosomes Improve Cellular Ubiquinone Uptake in Skeletal Muscle Cells: An Ex Vivo Study Using CoQ10-Enriched Low-Density Lipoproteins Obtained in a Randomized Crossover Study. *Antioxidants* **12**, 964 (2023).

111. Parenti, I., Rabaneda, L. G., Schoen, H. & Novarino, G. Neurodevelopmental Disorders: From Genetics to Functional Pathways. *Trends Neurosci.* **43**, 608–621 (2020).

112. Alazami, A. M. *et al.* Accelerating novel candidate gene discovery in neurogenetic disorders via whole-exome sequencing of prescreened multiplex consanguineous families. *Cell Rep.* **10**, 148–161 (2015).

113. Salinas, S., Proukakis, C., Crosby, A. & Warner, T. T. Hereditary spastic paraplegia: clinical features and pathogenetic mechanisms. *Lancet Neurol.* **7**, 1127–1138 (2008).

114. Ae, H. Hereditary ‘pure’ spastic paraplegia: a clinical and genetic study of 22 families. *J. Neurol. Neurosurg. Psychiatry* **44**, (1981).

115. Tallaksen, C. M. E., Dürr, A. & Brice, A. Recent advances in hereditary spastic paraplegia. *Curr. Opin. Neurol.* **14**, 457 (2001).

116. Schüle, R. *et al.* Hereditary spastic paraplegia: Clinicogenetic lessons from 608 patients. *Ann. Neurol.* **79**, 646–658 (2016).

117. Harding, A. E. CLASSIFICATION OF THE HEREDITARY ATAXIAS AND PARAPLEGIAS. *The Lancet* **321**, 1151–1155 (1983).

118. Finsterer, J. *et al.* Hereditary spastic paraplegias with autosomal dominant, recessive, X-linked, or maternal trait of inheritance. *J. Neurol. Sci.* **318**, 1–18 (2012).

119. Tesson, C., Koht, J. & Stevanin, G. Delving into the complexity of hereditary spastic paraplegias: how unexpected phenotypes and inheritance modes are revolutionizing their nosology. *Hum. Genet.* **134**, 511–538 (2015).

120. Cross, H. E. & McKusick, V. A. The Troyer syndrome. A recessive form of spastic paraplegia with distal muscle wasting. *Arch. Neurol.* **16**, 473–485 (1967).

121. Liang, H. *et al.* Dwarfism in Troyer syndrome: a family with SPG20 compound heterozygous mutations and a literature review. *Ann. N. Y. Acad. Sci.* **1462**, 118–127 (2020).

122. Proukakis, C. *et al.* Troyer syndrome revisited. *J. Neurol.* **251**, 1105–1110 (2004).

123. Bizzari, S. *et al.* Novel SPG20 mutation in an extended family with Troyer syndrome. *Metab. Brain Dis.* **32**, 2155–2159 (2017).

124. Farag, T. I., El-Badramany, M. H. & Al-Sharkawy, S. Troyer Syndrome: report of the first ‘non-Amish’ sibship and review. *Am. J. Med. Genet.* **53**, 383–385 (1994).

125. Tawamie, H. *et al.* Recurrent null mutation in SPG20 leads to Troyer syndrome. *Mol. Cell. Probes* **29**, 315–318 (2015).

126. Butler, S. *et al.* Three cases of Troyer syndrome in two families of Filipino descent. *Am. J. Med. Genet. A.* **170**, 1780–1785 (2016).

127. Dardour, L. *et al.* SPG20 mutation in three siblings with familial hereditary spastic paraplegia. *Cold Spring Harb. Mol. Case Stud.* **3**, a001537 (2017).

128. Manzini, M. C. *et al.* Developmental and degenerative features in a complicated spastic paraplegia. *Ann. Neurol.* **67**, 516–525 (2010).

129. Auer-Grumbach, M. *et al.* Troyer syndrome: a combination of central brain abnormality and motor neuron disease? *J. Neurol.* **246**, 556–561 (1999).

130. Patel, H. *et al.* SPG20 is mutated in Troyer syndrome, an hereditary spastic paraplegia. *Nat. Genet.* **31**, 347–348 (2002).

131. Zhi, X. & Chen, C. WWP1: a versatile ubiquitin E3 ligase in signaling and diseases. *Cell. Mol. Life Sci.* **69**, 1425–1434 (2012).

132. Bakowska, J. C., Jenkins, R., Pendleton, J. & Blackstone, C. The Troyer syndrome (SPG20) protein spartin interacts with Eps15. *Biochem. Biophys. Res. Commun.* **334**, 1042–1048 (2005).

133. Ciccarelli, F. D. *et al.* The identification of a conserved domain in both spartin and spastin, mutated in hereditary spastic paraplegia. *Genomics* **81**, 437–441 (2003).

134. Ring, J. *et al.* Mitochondrial energy metabolism is required for lifespan extension by the spastic paraplegia-associated protein spartin. *Microb. Cell Graz Austria* **4**, 411–422 (2017).

135. Eastman, S. W., Yassaee, M. & Bieniasz, P. D. A role for ubiquitin ligases and Spartin/SPG20 in lipid droplet turnover. *J. Cell Biol.* **184**, 881–894 (2009).

136. Bakowska, J. C., Jupille, H., Fatheddin, P., Puertollano, R. & Blackstone, C. Troyer Syndrome Protein Spartin Is Mono-Ubiquitinated and Functions in EGF Receptor Trafficking. *Mol. Biol. Cell* **18**, 1683–1692 (2007).

137. Edwards, T. L. *et al.* Endogenous spartin (SPG20) is recruited to endosomes and lipid droplets and interacts with the ubiquitin E3 ligases AIP4 and AIP5. *Biochem. J.* **423**, 31–39 (2009).

138. Dulak, A. M. *et al.* Exome and whole-genome sequencing of esophageal adenocarcinoma identifies recurrent driver events and mutational complexity. *Nat. Genet.* **45**, 478–486 (2013).

139. van't Veer, M. B. *et al.* The predictive value of lipoprotein lipase for survival in chronic lymphocytic leukemia. *Haematologica* **91**, 56–63 (2006).

140. Wei, K.-L. *et al.* Methylomics analysis identifies a putative STAT3 target, SPG20, as a noninvasive epigenetic biomarker for early detection of gastric cancer. *PLOS ONE* **14**, e0218338 (2019).

141. Littarru, G. P. & Tiano, L. Bioenergetic and Antioxidant Properties of Coenzyme Q10: Recent Developments. *Mol. Biotechnol.* **37**, 31–37 (2007).

142. Potgieter, M., Pretorius, E. & Pepper, M. S. Primary and secondary coenzyme Q10 deficiency: the role of therapeutic supplementation. *Nutr. Rev.* **71**, 180–188 (2013).

143. Yamada, Y. *et al.* Mitochondrial delivery of Coenzyme Q10 via systemic administration using a MITO-Porter prevents ischemia/reperfusion injury in the mouse liver. *J. Controlled Release* **213**, 86–95 (2015).

144. Self-Nanoemulsifying Drug Delivery System of Coenzyme (Q10) with Improved Dissolution, Bioavailability, and Protective Efficiency on Liver Fibrosis | AAPS PharmSciTech. https://link.springer.com/article/10.1208/s12249-016-0632-x.

145. Masotta, N. E., Martinefski, M. R., Lucangioli, S., Rojas, A. M. & Tripodi, V. P. High-dose coenzyme Q10-loaded oleogels for oral therapeutic supplementation. *Int. J. Pharm.* **556**, 9–20 (2019).

146. Gokce, E. H. *et al.* A comparative evaluation of coenzyme Q10-loaded liposomes and solid lipid nanoparticles as dermal antioxidant carriers. *Int. J. Nanomedicine* **7**, 5109–5117 (2012).

147. Bergamini, C., Moruzzi, N., Sblendido, A., Lenaz, G. & Fato, R. A Water Soluble CoQ10 Formulation Improves Intracellular Distribution and Promotes Mitochondrial Respiration in Cultured Cells. *PLoS ONE* **7**, e33712 (2012).

148. Petrangolini, G. *et al.* A New Food-grade Coenzyme Q10 Formulation Improves Bioavailability: Single and Repeated Pharmacokinetic Studies in Healthy Volunteers. *Curr. Drug Deliv.* **16**, 759–767 (2019).

149. Paredes-Fuentes, A. J. *et al.* Coenzyme Q10 Treatment Monitoring in Different Human Biological Samples. *Antioxidants* **9**, 979 (2020).

150. Yubero, D. *et al.* Secondary coenzyme Q10 deficiencies in oxidative phosphorylation (OXPHOS) and non-OXPHOS disorders. *Mitochondrion* **30**, 51–58 (2016).

151. Sacconi: Coenzyme Q10 is frequently reduced in muscle... - Google Scholar. https://scholar.google.com/scholar_lookup?hl=en&volume=20&publication_year=2010&pages=44&journal=Neuromuscul+Disord&author=S+Sacconi&author=E+Trevisson&author=L+Salviati&author=S+Aym%C3%A9&author=O+Rigal&author=AG+Redondo&title=Coenzyme+Q10+is+frequently+reduced+in+muscle+of+patients+with+mitochondrial+myopathy.

152. Quinzii, C. M. & Hirano, M. Primary and secondary CoQ10 deficiencies in humans. *BioFactors* **37**, 361–365 (2011).

153. Joshi, D. C. & Bakowska, J. C. SPG20 Protein Spartin Associates with Cardiolipin via Its Plant-Related Senescence Domain and Regulates Mitochondrial Ca2+ Homeostasis. *PLOS ONE* **6**, e19290 (2011).

154. Diquigiovanni, C. *et al.* A novel mutation in SPART gene causes a severe neurodevelopmental delay due to mitochondrial dysfunction with complex I impairments and altered pyruvate metabolism. *FASEB J. Off. Publ. Fed. Am. Soc. Exp. Biol.* **33**, 11284–11302 (2019).

155. Falb, R. J. *et al.* Bi-allelic loss-of-function variants in KIF21A cause severe fetal akinesia with arthrogryposis multiplex. *J. Med. Genet.* **60**, 48–56 (2023).

156. Cicero, A., Fogacci, F., Giovannini, M., Tocci, G. & Borghi, C. EFFECT OF COENZYME Q10 ON MUSCULAR STRENGTH IN ELDERLY PATIENTS WITH STATIN-ASSOCIATED ASTHENIA: A DOUBLE-BLIND, RANDOMIZED, PLACEBO-CONTROLLED CLINICAL TRIAL. *J. Hypertens.* **41**, e152 (2023).

157. Liparulo, I. *et al.* Coenzyme Q biosynthesis inhibition induces HIF-1α stabilization and metabolic switch toward glycolysis. *FEBS J.* **288**, 1956–1974 (2021).

158. Takada, M., Ikenoya, S., Yuzuriha, T. & Katayama, K. [17] Simultaneous determination of reduced and oxidized ubiquinones. in *Methods in Enzymology* vol. 105 147–155 (Academic Press, 1984).

159. Spinazzi, M., Casarin, A., Pertegato, V., Salviati, L. & Angelini, C. Assessment of mitochondrial respiratory chain enzymatic activities on tissues and cultured cells. *Nat. Protoc.* **7**, 1235–1246 (2012).

160. Lowry, O. H., Rosebrough, N. J., Farr, A. L. & Randall, R. J. Protein measurement with the Folin phenol reagent. *J. Biol. Chem.* **193**, 265–275 (1951).

161. Quantification of reduced and oxidized coenzyme Q10 in supplements and medicines by HPLC-UV - Analytical Methods (RSC Publishing). https://pubs.rsc.org/en/content/articlelanding/2020/AY/D0AY00683A.

162. Bartolomé, F. & Abramov, A. Y. Measurement of Mitochondrial NADH and FAD Autofluorescence in Live Cells. in *Mitochondrial Medicine: Volume I, Probing Mitochondrial Function* (eds. Weissig, V. & Edeas, M.) 263–270 (Springer, New York, NY, 2015). doi:10.1007/978-1-4939-2257-4_23.

163. Jones, D. P. Determination of pyridine dinucleotides in cell extracts by high-performance liquid chromatography. *J. Chromatogr. B. Biomed. Sci. App.* **225**, 446–449 (1981).

164. Bioenergetic markers in skin fibroblasts of sporadic amyotrophic lateral sclerosis and progressive lateral sclerosis patients - Kirk - 2014 - Annals of Neurology - Wiley Online Library. https://onlinelibrary.wiley.com/doi/10.1002/ana.24244.

165. Greenspan, P., Mayer, E. P. & Fowler, S. D. Nile red: a selective fluorescent stain for intracellular lipid droplets. *J. Cell Biol.* **100**, 965–973 (1985).

166. Pap, E. h. w. *et al.* Ratio-fluorescence microscopy of lipid oxidation in living cells using C11-BODIPY581/591. *FEBS Lett.* **453**, 278–282 (1999).

167. Plummer, E. M. & Manchester, M. Endocytic uptake pathways utilized by CPMV nanoparticles. *Mol. Pharm.* **10**, 26–32 (2013).

168. Dutta, D. & Donaldson, J. G. Search for inhibitors of endocytosis: Intended specificity and unintended consequences. *Cell. Logist.* **2**, 203–208 (2012).

169. Vercauteren, D. *et al.* The Use of Inhibitors to Study Endocytic Pathways of Gene Carriers: Optimization and Pitfalls. *Mol. Ther.* **18**, 561–569 (2010).

170. Bonora, E. *et al.* Biallelic variants in LIG3 cause a novel mitochondrial neurogastrointestinal encephalomyopathy. *Brain J. Neurol.* **144**, 1451–1466 (2021).

171. Valente, A. J., Maddalena, L. A., Robb, E. L., Moradi, F. & Stuart, J. A. A simple ImageJ macro tool for analyzing mitochondrial network morphology in mammalian cell culture. *Acta Histochem.* **119**, 315–326 (2017).

172. Krohn, A. J., Wahlbrink, T. & Prehn, J. H. Mitochondrial depolarization is not required for neuronal apoptosis. *J. Neurosci. Off. J. Soc. Neurosci.* **19**, 7394–7404 (1999).

173. Ultrasensitive Genetically Encoded Indicator for Hydrogen Peroxide Identifies Roles for the Oxidant in Cell Migration and Mitochondrial Function - ScienceDirect. https://www.sciencedirect.com/science/article/pii/S1550413120300620.

174. Protocol for the Analysis of Yeast and Human Mitochondrial Respiratory Chain Complexes and Supercomplexes by Blue Native Electrophoresis. https://star-protocols.cell.com/protocols/177.

175. Anders, S., Pyl, P. T. & Huber, W. HTSeq—a Python framework to work with high-throughput sequencing data. *Bioinformatics* **31**, 166–169 (2015).

176. Patro, R., Duggal, G., Love, M. I., Irizarry, R. A. & Kingsford, C. Salmon provides fast and bias-aware quantification of transcript expression. *Nat. Methods* **14**, 417–419 (2017).

177. Kuleshov, M. V. *et al.* Enrichr: a comprehensive gene set enrichment analysis web server 2016 update. *Nucleic Acids Res.* **44**, W90–W97 (2016).

178. Sivandzade, F., Bhalerao, A. & Cucullo, L. Analysis of the Mitochondrial Membrane Potential Using the Cationic JC-1 Dyeas a Sensitive Fluorescent Probe. *Bio-Protoc.* **9**, e3128 (2019).

179. Mogensen, M., Bagger, M., Pedersen, P. K., Fernström, M. & Sahlin, K. Cycling efficiency in humans is related to low UCP3 content and to type I fibres but not to mitochondrial efficiency. *J. Physiol.* **571**, 669–681 (2006).

180. Larsen, S. *et al.* Biomarkers of mitochondrial content in skeletal muscle of healthy young human subjects. *J. Physiol.* **590**, 3349–3360 (2012).

181. McLennan, H. R. & Degli Esposti, M. The contribution of mitochondrial respiratory complexes to the production of reactive oxygen species. *J. Bioenerg. Biomembr.* **32**, 153–162 (2000).

182. Arslanbaeva, L. *et al.* UBIAD1 and CoQ10 protect melanoma cells from lipid peroxidation-mediated cell death. *Redox Biol.* **51**, 102272 (2022).

183. Bello, R. I. *et al.* Enhanced anti-oxidant protection of liver membranes in long-lived rats fed on a coenzyme Q10-supplemented diet. *Exp. Gerontol.* **40**, 694–706 (2005).

184. Ratio-fluorescence microscopy of lipid oxidation in living cells using C11-BODIPY581/591 - Pap - 1999 - FEBS Letters - Wiley Online Library.

https://febs.onlinelibrary.wiley.com/doi/full/10.1016/S0014-5793%2899%2900696-1.

185. Drummen, G. P. C., van Liebergen, L. C. M., Op den Kamp, J. A. F. & Post, J. A. C11-BODIPY581/591, an oxidation-sensitive fluorescent lipid peroxidation probe: (micro)spectroscopic characterization and validation of methodology. *Free Radic. Biol. Med.* **33**, 473–490 (2002).

186. Jumper, J. *et al.* Highly accurate protein structure prediction with AlphaFold. *Nature* **596**, 583–589 (2021).

187. Manfredi, M., Savojardo, C., Martelli, P. L. & Casadio, R. DeepREx-WS: A web server for characterising protein–solvent interaction starting from sequence. *Comput. Struct. Biotechnol. J.* **19**, 5791–5799 (2021).

188. Mukhopadhyay, P., Rajesh, M., Yoshihiro, K., Haskó, G. & Pacher, P. Simple quantitative detection of mitochondrial superoxide production in live cells. *Biochem. Biophys. Res. Commun.* **358**, 203–208 (2007).

189. Yu, T., Robotham, J. L. & Yoon, Y. Increased production of reactive oxygen species in hyperglycemic conditions requires dynamic change of mitochondrial morphology. *Proc. Natl. Acad. Sci.* **103**, 2653–2658 (2006).

190. Angelova, P. R. & Abramov, A. Y. Role of mitochondrial ROS in the brain: from physiology to neurodegeneration. *FEBS Lett.* **592**, 692–702 (2018).

191. Esteras, N., Rohrer, J. D., Hardy, J., Wray, S. & Abramov, A. Y. Mitochondrial hyperpolarization in iPSC-derived neurons from patients of FTDP-17 with 10+16 MAPT mutation leads to oxidative stress and neurodegeneration. *Redox Biol.* **12**, 410–422 (2017).

192. Lee, S.-J., Zhang, J., Choi, A. M. K. & Kim, H. P. Mitochondrial Dysfunction Induces Formation of Lipid Droplets as a Generalized Response to Stress. *Oxid. Med. Cell. Longev.* **2013**, e327167 (2013).

193. Talari, N. K. *et al.* Lipid-droplet associated mitochondria promote fatty-acid oxidation through a distinct bioenergetic pattern in male Wistar rats. *Nat. Commun.* **14**, 766 (2023).

194. Giorgi, C., Marchi, S. & Pinton, P. The machineries, regulation and cellular functions of mitochondrial calcium. *Nat. Rev. Mol. Cell Biol.* **19**, 713–730 (2018).

195. Marchi, S. *et al.* Mitochondrial and endoplasmic reticulum calcium homeostasis and cell death. *Cell Calcium* **69**, 62–72 (2018).

196. Milewska, M., McRedmond, J. & Byrne, P. C. Identification of novel spartin-interactors shows spartin is a multifunctional protein. *J. Neurochem.* **111**, 1022–1030 (2009).

197. Gomkale, R. *et al.* Mapping protein interactions in the active TOM-TIM23 supercomplex. *Nat. Commun.* **12**, 5715 (2021).

198. Paschen, S. A. *et al.* The role of the TIM8–13 complex in the import of Tim23 into mitochondria. *EMBO J.* **19**, 6392–6400 (2000).

199. Gómez-Díaz, C., Barroso, M. P. & Navas, P. Plasma membrane coenzyme Q10 and growth control. *Protoplasma* **214**, 19–23 (2000).

200. Hidaka, T., Fujii, K., Funahashi, I., Fukutomi, N. & Hosoe, K. Safety assessment of coenzyme Q10 (CoQ10). *BioFactors* **32**, 199–208 (2008).

201. Nutrients | Free Full-Text | The Paradox of Coenzyme Q10 in Aging. https://www.mdpi.com/2072-6643/11/9/2221.

202. Lass, A., Kwong, L. & Sohal, R. S. Mitochondrial coenzyme Q content and aging. *BioFactors Oxf. Engl.* **9**, 199–205 (1999).

203. Kapoor: Coenzyme Q10-a novel molecule - Google Scholar. https://scholar.google.com/scholar_lookup?hl=en&volume=14&publication_year=2013&pages=37-45&journal=JIACM&author=P.+Kapoor&author=A.+K.+Kapoor&title=Coenzyme+Q10%E2%80%90A+novel+molecule.

204. Dhanasekaran, M. & Ren, J. The emerging role of coenzyme Q-10 in aging, neurodegeneration, cardiovascular disease, cancer and diabetes mellitus. *Curr. Neurovasc. Res.* **2**, 447–459 (2005).

205. Villalba, J. M., Parrado, C., Santos-Gonzalez, M. & Alcain, F. J. Therapeutic use of coenzyme Q10 and coenzyme Q10-related compounds and formulations. *Expert Opin. Investig. Drugs* **19**, 535–554 (2010).

206. Bhagavan, H. N. & Chopra, R. K. Coenzyme Q10: Absorption, tissue uptake, metabolism and pharmacokinetics. *Free Radic. Res.* **40**, 445–453 (2006).

207. Novel solid self-emulsifying drug delivery system of coenzyme Q10 with improved photochemical and pharmacokinetic behaviors - ScienceDirect. https://www.sciencedirect.com/science/article/pii/S0928098712001698.

208. Zhou: Novel lipid-free nanoformulation for improving... - Google Scholar. https://scholar.google.com/scholar_lookup?title=Novel+lipid-free+nanoformulation+for+improving+oral+bioavailability+of+coenzyme+Q10&author=Zhou,+H.&author=Liu,+G.&author=Zhang,+J.&author=Sun,+N.&author=Duan,+M.&author=Yan,+Z.&author=Xia,+Q.&publication_year=2014&journal=BioMed+Res.+Int.&volume=2014&doi=10.1155/2014/793879.

209. Beg: Bioavailability enhancement of coenzyme Q10:... - Google Scholar. https://scholar.google.com/scholar_lookup?title=Bioavailability+enhancement+of+coenzyme+Q10:+An+extensive+review+of+patents&author=Beg,+S.&author=Javed,+S.&author=Kohli,+K.&publication_year=2010&journal=Recent+Patents+Drug+Deliv.+

Formul.&volume=4&pages=245%E2%80%93255&doi=10.2174/187221110793237565.

210. Li: Preparation and quality evaluation of coenzyme... - Google Scholar. https://scholar.google.com/scholar_lookup?title=Preparation+and+quality+evaluation+of+coenzyme+Q10+long-circulating+liposomes&author=Li,+H.&author=Chen,+F.&publication_year=2017&journal=Saudi+J.+Biol.+Sci.&volume=24&pages=797%E2%80%93802&doi=10.1016/j.sjbs.2015.10.025.

211. Ernster, L. & Forsmark-Andrée, P. Ubiquinol: an endogenous antioxidant in aerobic organisms. *Clin. Investig.* **71**, S60–S65 (1993).

212. James, A. M., Smith, R. A. J. & Murphy, M. P. Antioxidant and prooxidant properties of mitochondrial Coenzyme Q. *Arch. Biochem. Biophys.* **423**, 47–56 (2004).

213. Zaki, N. M. Strategies for oral delivery and mitochondrial targeting of CoQ10. *Drug Deliv.* **23**, 1868–1881 (2016).

214. Lipid Peroxidation-Dependent Cell Death Regulated by GPx4 and Ferroptosis | SpringerLink. https://link.springer.com/chapter/10.1007/82_2016_508.

215. Emerging Mechanisms and Disease Relevance of Ferroptosis: Trends in Cell Biology. https://www.cell.com/trends/cell-biology/fulltext/S0962-8924(20)30054-4.

216. Wang: Coenzyme Q depletion reshapes MCF-7 cells metabolism - Google Scholar. https://scholar.google.com/scholar_lookup?title=Coenzyme+Q+depletion+reshapes+MCF-7+cells+metabolism&author=Wang,+W.&author=Liparulo,+I.&author=Rizzardi,+N.&author=Bolignano,+P.&author=Calonghi,+N.&author=Bergamini,+C.&author=Fato,+R.&publication_year=2020&journal=Int.+J.+Mol.+Sci.&volume=22&pages=198&doi=10.3390/ijms22010198&pmid=33379147.

217. Frezza: Metabolic profiling of hypoxic cells revealed... - Google Scholar. https://scholar.google.com/scholar_lookup?title=Metabolic+profiling+of+hypoxic+cells+revealed+a+catabolic+signature+required+for+cell+survival&author=Frezza,+C.&author=Zheng,+L.&author=Tennant,+D.A.&author=Papkovsky,+D.B.&author=Hedley,+B.A.&author=Kalna,+G.&author=Watson,+D.G.&author=Gottlieb,+E.&publication_year=2011&journal=PLoS+ONE&volume=6&pages=e24411&doi=10.1371/journal.pone.0024411.

218. Inhibition of oxidative stress by coenzyme Q10 increases mitochondrial mass and improves bioenergetic function in optic nerve head astrocytes | Cell Death & Disease. https://www.nature.com/articles/cddis2013341.

219. Renner: Changes of mitochondrial respiration, mitochondri... - Google Scholar.

https://scholar.google.com/scholar_lookup?title=Changes+of+mitochondrial+respiration,+mitochondrial+content+and+cell+size+after+induction+of+apoptosis+in+leukemia+cells&author=Renner,+K.&author=Amberger,+A.&author=Konwalinka,+G.&author=Kofler,+R.&author=Gnaiger,+E.&publication_year=2003&journal=Biochim.+Biophys.+Acta+Mol.+Cell+Res.&volume=1642&pages=115%E2%80%93123&doi=10.1016/S0167-4889(03)00105-8.

220. Lin, X. P., Mintern, J. D. & Gleeson, P. A. Macropinocytosis in Different Cell Types: Similarities and Differences. *Membranes* **10**, 177 (2020).

221. Apostolova, N. & Victor, V. M. Molecular Strategies for Targeting Antioxidants to Mitochondria: Therapeutic Implications. *Antioxid. Redox Signal.* **22**, 686–729 (2015).

222. Miles: The uptake and distribution of coenzyme Q (10) - Google Scholar. https://scholar.google.com/scholar_lookup?title=The+uptake+and+distribution+of+coenzyme+Q(10)&author=Miles,+M.V.&publication_year=2007&journal=Mitochondrion&volume=7&pages=S72%E2%80%93S77&doi=10.1016/j.mito.2007.02.012.

223. Bentinger: Distribution and breakdown of labeled... - Google Scholar. https://scholar.google.com/scholar_lookup?title=Distribution+and+breakdown+of+labeled+coenzyme+Q10+in+rat&author=Bentinger,+M.&author=Dallner,+G.&author=Chojnacki,+T.&author=Swiezewska,+E.&publication_year=2003&journal=Free+Radic.+Biol.+Med.&volume=34&pages=563%E2%80%93575&doi=10.1016/S0891-5849(02)01357-6.

224. Richards, S. *et al.* Standards and guidelines for the interpretation of sequence variants: a joint consensus recommendation of the American College of Medical Genetics and Genomics and the Association for Molecular Pathology. *Genet. Med.* **17**, 405–423 (2015).

225. Patient perspectives on variant reclassification after cancer susceptibility testing - Halverson - 2020 - Molecular Genetics & Genomic Medicine - Wiley Online Library. https://onlinelibrary.wiley.com/doi/full/10.1002/mgg3.1275.

226. Ali-Khan, S. E., Daar, A. S., Shuman, C., Ray, P. N. & Scherer, S. W. Whole Genome Scanning: Resolving Clinical Diagnosis and Management Amidst Complex Data. *Pediatr. Res.* **66**, 357–363 (2009).

227. Hirano, M. *et al.* Mitochondrial neurogastrointestinal encephalomyopathy (MNGIE): Position paper on diagnosis, prognosis, and treatment by the MNGIE International Network. *J. Inherit. Metab. Dis.* **44**, 376–387 (2021).

228. Perrone, M. *et al.* Chapter Four - The role of mitochondria-associated membranes in cellular homeostasis and diseases. in *International Review of Cell and Molecular Biology* (eds. Kepp, O. & Galluzzi, L.) vol. 350 119–196 (Academic Press, 2020).

229. Mitochondria-associated membranes (MAMs) and inflammation | Cell Death & Disease. https://www.nature.com/articles/s41419-017-0027-2.

230. Hung, V. *et al.* Proteomic mapping of cytosol-facing outer mitochondrial and ER membranes in living human cells by proximity biotinylation. *eLife* **6**, e24463 (2017).

231. Neupert: Translocation of proteins into mitochondria - Google Scholar. https://scholar.google.com/scholar_lookup?title=Translocation%20of%20proteins%20into%20mitochondria&publication_year=2007&author=W.%20Neupert&author=J.M.%20Herrmann.

232. Chacinska: Importing mitochondrial proteins: machineries... - Google Scholar. https://scholar.google.com/scholar_lookup?title=Importing%20mitochondrial%20proteins%3A%20machineries%20and%20mechanisms&publication_year=2009&author=A.%20Chacinska&author=C.M.%20Koehler&author=D.%20Milenkovic&author=T.%20Lithgow&author=N.%20Pfanner.

233. Saitoh: Tom20 recognizes mitochondrial presequences... - Google Scholar. https://scholar.google.com/scholar_lookup?title=Tom20%20recognizes%20mitochondrial%20presequences%20through%20dynamic%20equilibrium%20among%20multiple%20bound%20states&publication_year=2007&author=T.%20Saitoh&author=M.%20Igura&author=T.%20Obita&author=T.%20Ose&author=R.%20Kojima&author=K.%20Maenaka&author=T.%20Endo&author=D.%20Kohda.

234. Meisinger: Protein import channel of the outer mitochondr... - Google Scholar. https://scholar.google.com/scholar_lookup?title=Protein%20import%20channel%20of%20the%20outer%20mitochondrial%20membrane%3A%20a%20highly%20stable%20Tom40-Tom22%20core%20structure%20differentially%20interacts%20with%20preproteins%2C%20small%20tom%20proteins%2C%20and%20import%20receptors&publication_year=2001&author=C.%20Meisinger&author=M.T.%20Ryan&author=K.%20Hill&author=K.%20Model&author=J.H.%20Lim&author=A.%20Sickmann&author=H.%20M%C3%BCller&author=H.E.%20Meyer&author=R.%20Wagner&author=N.%20Pfanner.

235. Martin: Role of an energized inner membrane in mitochondr... - Google Scholar. https://scholar.google.com/scholar_lookup?title=Role%20of%20an%20energized%20inner%20membrane%20in%20mitochondrial%20protein%20import.%20%20psi%20drives%20the%20movement%20of%20presequences&publication_year=1991&author=J.%20Martin&author=K.%20Mahlke&author=N.%20Pfanner.

236. Young: Molecular chaperones Hsp90 and Hsp70 deliver... - Google Scholar. https://scholar.google.com/scholar_lookup?title=Molecular%20chaperones%20Hsp90%20and%20Hsp70%20deliver%20preproteins%20to%20the%20mitochondrial%2

0import%20receptor%20Tom70&publication_year=2003&author=J.C.%20Young&author=N.J.%20Hoogenraad&author=F.U.%20Hartl.

237. Filadi, R. *et al.* TOM70 Sustains Cell Bioenergetics by Promoting IP3R3-Mediated ER to Mitochondria Ca2+ Transfer. *Curr. Biol.* **28**, 369-382.e6 (2018).

238. Spiegel, R. *et al.* Novel Homozygous Missense Mutation in SPG20 Gene Results in Troyer Syndrome Associated with Mitochondrial Cytochrome c Oxidase Deficiency. *JIMD Rep.* **33**, 55–60 (2017).

239. Murala, S., Nagarajan, E. & Bollu, P. C. Hereditary spastic paraplegia. *Neurol. Sci.* **42**, 883–894 (2021).

240. Meyyazhagan, A. & Orlacchio, A. Hereditary Spastic Paraplegia: An Update. *Int. J. Mol. Sci.* **23**, 1697 (2022).

241. Enriquez, J. A. & Lenaz, G. Coenzyme Q and the Respiratory Chain: Coenzyme Q Pool and Mitochondrial Supercomplexes. *Mol. Syndromol.* **5**, 119–140 (2014).

242. Rinninella: Nutritional support in mitochondrial... - Google Scholar. https://scholar.google.com/scholar_lookup?hl=en&volume=22&publication_year=2018&pages=4288-4298&journal=Eur.+Rev.+Med.+Pharmacol.+Sci.&author=E+Rinninella&author=M+Pizzoferrato&author=M+Cintoni&author=S+Servidei&author=MC+Mele&title=Nutritional+support+in+mitochondrial+diseases%3A+the+state+of+the+art.

243. Coenzyme Q10 a mitochondrial restorer for various brain disorders | Naunyn-Schmiedeberg's Archives of Pharmacology. https://link.springer.com/article/10.1007/s00210-021-02161-8.

244. Shults: Coenzyme Q10 in neurodegenerative diseases - Google Scholar. https://scholar.google.com/scholar_lookup?hl=en&volume=10&publication_year=2003&pages=1917-1921&journal=Curr.+Med.+Chem.&author=CW+Shults&title=Coenzyme+Q10+in+neurodegenerative+diseases.